ALPHA FOUNDATION FOR THE IMPROVEMENT OF MINE SAFETY AND HEALTH

Final Technical Report

Project Title: A Holistic Approach to Reducing Coal Worker's Pneumoconiosis (CWP) using Integrated Monitoring and Response Systems for Respirable Dust in Surface Mines and Facilities

Grant Number: AFC417-39

Organization: The Pennsylvania State University, University Park, PA, 16802

Principal Investigator: William A. Groves, PhD, MPH, CIH, CSP

Contact Information : 223 Hosler Building
University Park, PA 16802
814-863-1618
wag10@psu.edu

Period of Performance: 12/1/17 – 12/31/21

Acknowledgement/Disclaimer: This study was sponsored by the Alpha Foundation for the Improvement of Mine Safety and Health, Inc. (ALPHA FOUNDATION). The views, opinions and recommendations expressed herein are solely those of the authors and do not imply any endorsement by the ALPHA FOUNDATION, its Directors and staff.

1.0 Executive Summary

The goal of this project was to contribute toward the reduction of coal workers' pneumoconiosis (CWP) in miners through the development of a continuous wireless real-time monitoring system for respirable dust in surface mines and support facilities. The specific aims of the project were to develop, assemble, and test in the laboratory, a portable wireless dust sensing system capable of monitoring respirable dust concentrations using affordable optical sensors, and to deploy and evaluate the performance of an integrated network of dust sensors capable of real-time detection and reporting of respirable dust concentrations to cloud-based data management and monitoring services.

In the first phase of the study, the performance of three inexpensive optical dust sensors (Shinyei PPD42NS, Sharp GP2Y1010AU0F, and Laser SEN0177) was evaluated using reference aerosol monitors including a DustTrak DRX and traditional gravimetric respirable dust samplers. Test atmospheres spanning a concentration range of approximately 0.15-3.0 mg/m^3 respirable dust were prepared using ISO Fine (A2) Arizona Road Dust (ARD) in an aerosol test chamber. Sensor responses were calibrated against reference aerosol instruments and performance was found to be similar with linear response and good agreement with reference measurements.

The Sharp sensor was selected for further study based upon low cost and power consumption and was subsequently calibrated for ISO Ultrafine (A1), Fine (A2), and Medium (A3) ARD, and a fine coal dust. Baseline corrected Sharp sensor responses were highly linear (r^2=0.89-0.98) with slopes ranging from 0.92-1.01 (volt/mg/m^3 respirable dust) for A1, A2, and A3 ARD, and 0.58 (volt/mg/m3 respirable dust) for coal dust. A combined calibration for ARD and coal dust with a slope of 0.92 volt/mg/m3 respirable dust (r2=0.94) was used in subsequent field studies comparing wireless dust sensor performance to a reference DustTrak DRX instrument at a coal loadout facility and a surface mine.

Photovoltaic-based systems were designed to provide remote power for individual sensing nodes and LoRaWAN gateways, and subsequent field testing demonstrated that reliable power could be provided over a period of several months. Results showed that a 14-node network of prototype wireless dust sensors successfully transmitted data over distances greater than 2 km to the LoRaWAN gateway for cloud-based display and storage. Sensor responses (15-min TWA) were highly correlated with reference instrument respirable dust measurements with average absolute errors ranging from 22-34%.

These results demonstrate the great potential of inexpensive dust sensors coupled with long-range low-power wireless transmission protocols such as LoRa and cloud-based data management and storage for monitoring respirable dust exposures in surface mining and support operations. The use of wireless sensing systems and interconnected devices (Internet of Things or IoT) is expanding rapidly, and the system demonstrated in this project provides a flexible platform that can be used with a growing number of wireless transducers available for sensing parameters relevant to occupational and environmental exposure monitoring including temperature, humidity, illumination, particulate matter, oxygen, carbon dioxide, carbon monoxide, and many other toxic gases.

2.0 Problem Statement and Objective

The overall goal of this research is to reduce the occurrence of coal workers' pneumoconiosis (CWP) in miners through the development of continuous wireless real-time monitoring systems for respirable dust. The proposed research will address the problem of CWP, or black lung disease, in the coal mining industry. While the problem is associated with both surface and underground operations, this project focuses on surface mining and addresses Topical Area 1) Health and Safety Interventions with a specific emphasis on exposure assessment and control interventions related to the MSHA 1.5 mg/m^3 respirable dust standard. This work is directly relevant to Alpha Foundation Priority Areas 1) Dust and Toxic Substance Control - Prevention of health risks due to generation of dust or other toxic substances, and 2) Monitoring Systems and Integrated Control Technologies - Recognition of and intervention to prevent the escalation of conditions that lead to health and safety risks before they reach hazardous levels.

Coal workers' pneumoconiosis (CWP) is a chronic occupational lung disease caused by the inhalation of respirable dust that results in potentially irreversible damage to the alveoli of the lungs (CDC, 2012). The severity of CWP can range from simple to advanced, with the most severe forms being referred to as progressive massive fibrosis (PMF). Advanced types of CWP can be debilitating and are often fatal, and it has been estimated that CWP has been the cause or contributing factor in the deaths of more than 76,000 miners since 1968 (MSHA, 2014).

The Coal Mine Health and Safety Act of 1969 established federal exposure limits for respirable dust (2.0 mg/m^3) in underground and surface mines in order to prevent the occurrence of CWP, and surveillance data indicates that the prevalence of CWP among underground coal miners decreased from 11% in the early 1970s to 2% in the mid- to late-1990s (CDC, 2012). However, more recent surveillance results have shown that the prevalence of CWP has increased over the past decade, and NIOSH estimates that the prevalence of the most severe form of CWP (PMF) has reached the highest levels since the early 1970s (CDC, 2012; Blackley, 2014). Miners continue to be diagnosed with CWP (including younger workers) with more than 1,000 workers identified as having the disease (from more than a dozen different states) based on recent 10-year surveillance data. It is estimated that approximately $45 billion in federal compensation benefits have been paid to those affected by CWP with more than $5 billion paid out to approximately 7,000 affected miners over a 10-year period prior to 2014 (MSHA, 2014).

In response to this upsurge in the prevalence of CWP, in 2009 MSHA initiated the "End Black Lung – Act Now!" campaign which featured a proposed new rule to lower miners' exposure to respirable coal mine dust. The resulting final rule which was implemented in phases over the period of 2014-2016 included a reduction in the limit for respirable dust concentrations from 2.0 to 1.5 mg/m^3, and also requires the use of a direct-reading instrument - the continuous personal dust monitor (CPDM) - for providing real-time estimates of workers' exposure to respirable dust. The new rule also extends medical surveillance activities to include surface miners, a group excluded from previous surveillance requirements.

Although it is generally assumed that exposure to respirable dust is lower in surface mining compared with underground mines, the prevalence of CWP within surface miners has not been well characterized due to the exclusion of this group from required medical surveillance under previous standards. A study by NIOSH (CDC, 2012; Halldin, 2015) found that 46 (2%) of 2,257 miners working at surface mines during 2010-2011 had CWP based on chest x-rays, and that approximately 80% (36) of these individuals had no history of working underground. In addition, 9 of the 36 workers (25%) had the most severe form of CWP – progressive massive fibrosis (PMF). The researchers concluded that significant exposures to respirable dust must occur in surface mining operations and MSHA air sampling results for several occupations in surface mining confirm this (Table 1). Results indicate that more than 10% of the exposures to respirable dust are expected to exceed the new 1.5 mg/m^3 standard for fine coal plant operators, cleaning plant operators, crusher attendants, utility men, and welders (non-shop). In addition, studies of surface mine haul roads have reported that overexposure rates for truck drivers and road grader operators ranged from 5-10% and 3-29%, respectively, based on the MSHA database of respirable dust samples containing silica (Reed, 2005; Reed, 2007).

Table 2.1 Summary of MSHA 2008-2009 respirable dust data for surface mines and facilities

Occupation	Mean Conc. (n), mg/m^3	Percentage > 1.5 mg/m^3
Fine Coal Plant Operator	0.84 (177)	14
Cleaning Plant Operator	0.75 (175)	13
Crusher Attendant	0.62 (104)	12
Utility Man	0.71 (188)	12
Welder (non-shop)	0.69 (188)	10

Federal Register, Final Rule, 79 FR 24869

In summarizing the relevant factors that influence the problem of CWP in surface mining it is useful to employ a source - pathway - receptor framework. The main advantage of employing this approach lies in the intuitive nature of the resulting process for identifying and controlling exposures. The causative agent in CWP is dust that arises from a source. The dust becomes airborne as a result of operations and then can travel via various pathways to the workers who are exposed through inhalation. Control strategies then focus on the elimination, reduction, or mitigation of relevant factors thereby reducing exposure to acceptable levels.

Sources of respirable dust in surface mining operations have been well characterized and consist largely of mobile earth moving equipment including drag lines, excavators, bulldozers, front-end loaders, haul-trucks, and drills (Organiscak, 1999; Organiscak, 2004; Organiscak, 2010a; Organiscak, 2010b; Reed, 2005; Reed, 2007; Reed, 2014; Lashgari, 2016). It is recognized that sources of dust in surface mining can often be noted visually and that these observations can be helpful both in identifying sources and diagnosing malfunctioning engineering controls. However, the presence of respirable dust is not always visually apparent, for example when filtration systems are missing or not functioning properly, and these scenarios highlight the importance of air sampling and monitoring of respirable dust concentrations in order to identify potentially hazardous exposures and take corrective action.

CWP is a respiratory disease and the relevant route of exposure, or pathway, is inhalation. Most sources of respirable dust in surface mining produce a range of particle sizes with corresponding differences in settling velocities which makes factors such as proximity, prevailing air currents, and surrounding structure very influential with regard to exposure pathways. Studies of haul road dust (Reed, 2014) for example have shown that there is a dust dissipation effect that reduces respirable dust concentrations as elapsed time and distance from the passing trucks increases; however, other factors also have a significant impact on dust concentrations including haul truck speed, spacing of trucks, and the type and condition of the roadway material.

Factors affecting the source and exposure pathways are also relevant to the receptor which is the miner. Operators of the various types of earth moving equipment represent the most obvious category of receptor for the problem of CWP and exposures to these workers are determined by the types of equipment being operated, the nature and composition of the material being handled, proximity to other sources and pathways, and control strategies in place. Workers engaged in support activities also have significant potential exposure as evidenced by the job titles listed in Table 1 including coal plant operators, cleaning plant operators, crusher attendants, utility men, and welders.

Factors that are likely to complicate solutions directed toward the problem of CWP in surface mining include the transient nature of respirable dust concentrations and mine operations (temporal and spatial variability of dust concentrations), the continuous and relatively harsh production environment that can contribute to the often undetected deterioration or failure of control systems (e,g, staging curtains at dumping hoppers, cab filtration systems, water spray suppression systems), a lack of clear visual indicators for many respirable dust exposures, and the very limited medical surveillance data available for surface miners.

A number of researchers have been engaged in efforts to identify and control sources of respirable dust in underground and surface mines (Cecala, 2013; Colinet, 2010; Haas, 2016; Lashgari, 2016; Organiscak, 1999; Organiscak, 2004; Organiscak, 2010; Reed, 2005; Reed, 2007; Reed, 2014). NIOSH scientists have been particularly active in this area and have prepared several guidance documents and presentations specific to controlling respirable dust at surface mines (Organiscak, 1999, Organiscak, 2004; Organiscak, 2010; Reed, 2014). The work of these researchers has led to a good characterization of many sources of respirable dust exposure, identification of factors influencing the pathways of exposure, and different job categories (receptors) that appear likely to have significant exposure.

Equipment and operations identified as significant sources of respirable dust include drilling, operation of earth-moving equipment including drills, bulldozers, and haul trucks, haul road dust, and crusher hopper dump points. Controls described for these different sources include wet and dry drilling dust controls, maintaining proper drill shroud integrity, proper maintenance of dust collector systems, enclosed cab filtration systems, water and alternative treatments for haul roads, partial enclosure of hopper dump points, and use of water sprays (Organiscak, 2010; Reed, 2014).

Given that the effectiveness of these types of controls has been demonstrated in field and laboratory studies, and further that many have been available for years, the recent rise in CWP prevalence among underground miners and the significant number of surface miners identified as having CWP with no previous underground mining exposure is especially troubling and indicates that additional actions are necessary. The recent development of the Enhanced Video Analysis of Dust Exposures (EVADE) system by NIOSH scientists (Cecala, 2013; Cecala, 2014) is an example of the application of newer technologies to the ongoing problem of identifying and characterizing how miners are exposed to respirable dust, and which results in a video exposure record that can also be used in the training of miners to potentially modify behaviors and reduce exposure (Haas, 2016).

There have been recent reports describing the potential use of small inexpensive dust sensors to monitor dust concentrations after blasting at open pit mine sites (Alvarado, 2015) and for environmental monitoring at construction sites (Carbonari, 2014). The study by Alvarado focused on the development of a sensor system for use on an unmanned aerial vehicle (UAV), or "drone", while the Carbonari study described the early evaluation of two different types of optical dust sensor for eventual deployment in a wireless dust sensor network and included a limited field study. The Alvarado study has little relevance to the proposed project given the very different sampling platform employed (UAV) and the sampling approach which involved flying a drone equipped with a dust sensor in close proximity to plumes created by blasting. The Carbonari study is more relevant to this project and the results provide a useful starting point for identifying the types and brands of dust sensors to be evaluated, and also describe one type of framework for integrating the network of sensors.

The goal of the proposed research is to reduce the occurrence of CWP through the development and deployment of an integrated monitoring and response system for respirable dust. The system employs an integrated network of fixed- and mobile-wireless dust sensors capable of continuous real-time detection and reporting of respirable dust concentrations to a centralized monitoring and control station. This work expands the solution space by developing and demonstrating a new capability for continuous real-time measurement of respirable dust concentrations in surface mines using new technologies that make integrated monitoring systems much more affordable. The intended outcomes of the project are directly relevant to the problem of CWP in mining, and the approach employs an interdisciplinary approach to address the most important factors identified as having impeded progress towards CWP solutions.

The system enables rapid response to detected elevations in respirable dust concentrations including actions such as the dispatch of water trucks to reduce dust on haulage roads, use of water sprays at digging and loading benches and for dumping at the crushing facility, the repair or adjustment of existing control (e.g., ventilation) systems, or the investigation of previously unidentified sources or variables of exposure. The ability to measure exposure to respirable dust in real-time allows for an immediate and proactive control response to what can often be very transient exposure scenarios, and for which traditional sampling and analysis approaches are ineffective.

Therefore, the Specific Aims of the project were to:

1) Develop, assemble, and test in the laboratory, a portable wireless dust sensing system capable of monitoring respirable dust concentrations using affordable optical sensors.

2) Deploy and evaluate the performance of an integrated network of fixed- and mobile-wireless dust sensors capable of continuous real-time detection and reporting of respirable dust concentrations to a centralized location

3.0 Research Approach

Specific Aims for the project are accomplished through achievement of supporting Research Objectives and the associated individual research tasks as described in the following sections. Methodology and experimental methods are described in more detail by individual research tasks where appropriate.

Specific Aim 1 - Develop, assemble, and test in the laboratory, a portable wireless dust sensing system capable of monitoring respirable dust concentrations using affordable optical sensors.

Research Objective 1: Evaluate candidate dust sensor technologies and monitoring software systems for the connection, integration, and relay of data from wireless monitors to a centralized system.

Task 1.1 - Identify "off the shelf" enterprise instrumentation capable of wireless sensing of respirable dust concentrations with centralized monitoring.

After reviewing available enterprise or “turnkey” dust monitoring packages including versions available from TSI and RAE Systems, the decision was made to proceed with the purchase of the TSI system as described below. While the systems considered generally had similar capabilities and components, the TSI system could be implemented using the DustTrak DRX instrument which was already included in the project as one of the reference instruments needed to calibrate the dust sensors in the experimental and field studies. The use of the DustTrak DRX as the central dust measuring component of the system required an environmental enclosure (TSI DustTrak™ Environmental Enclosure 8535), internal battery system with charger (DustTrak™ II ESP Internal Battery System P/N 801807), a GMS/GPS modem (Thiamis 1000 Cloud Data Management System P/N 801905), and a cloud-based subscription service for uploading, storage, display, and remote access to real-time data (Netronix Environet).

Task 1.2 - Identify available combinations of compatible inexpensive dust sensors, microprocessors, wireless communication hardware, batteries, and software options for monitoring. Select best candidate combinations of technology to be evaluated in the laboratory.

While there are several different manufacturers of inexpensive dust sensors and programmable microprocessors, based on a review of the literature, two commonly cited dust sensors are the Shinyei PPD42NS and the Sharp GP2Y1010AU0F. In addition to the Sharp and Shinyei sensors, a laser-based optical dust sensor was included in preliminary studies (DFRobot Gravity: PM2.5 Air Quality Sensor).

The most commonly cited microprocessor platforms for dust sensing applications are the Arduino (e.g., Uno R3) and Rasberry Pi. The Arduino platform was selected for the project with various prototypes employing several different versions of Arduino LoRa compatible devices including the Arduino Uno R3 with Dragino 915-MHz LoRa Shield, The Things

Network Uno (The Things Industries P/N TTN-UN-915) which is an Arduino Leonardo-based microprocessor board with integrated LoRa modem, a low- power Arduino-compatible microprocessor with integrated radio module (Adafruit Feather M0 – 900 MHz P/N 3178), and Arduino MKRWAN 1300 and 1310 boards which are low-power LoRa/LoRaWAN compatible microprocessors.

Task 1.3 - Purchase and assemble the required components for the reference dust sensing node and candidate inexpensive wireless sensing nodes.

The reference "enterprise" dust sensing system was purchased from TSI, Incorporated, Shoreview, MN. Components for dust sensing nodes were purchased from several different vendors including the following:

- DFRobot (https://www.dfrobot.com/): Sharp dust sensor (SEN0144) and interface module (DFR0280), Gravity: PM2.5 Air Quality Sensor (SEN0177), Solar Panels / Solar Power Manager (DFR0559-1), IO Expansion Shield for Arduino (DFR0265), Solar LiPo Charger (DFR0264).
- Adafruit (https://www.adafruit.com/): Assembled Data Logging Shield for Arduino (P/N 1141), Adafruit Feather M0 with RFM95 LoRa Radio - 900MHz - RadioFruit (P/N 3178), Lithium-Ion Battery - 3.7v 2000mAh (P/N 2011).
- Robot Shop (https://www.robotshop.com/en/): Shinyei (Grove or Amphenol Dust Sensor) (P/N RB-See-552), Dragino LoRa Gateway 915 MHz USA (P/N drt-10).
- Connected Things (https://connectedthings.store/gb/): The Things Outdoor Gateway - US 915 Mhz.
- Newark Electronics (https://www.newark.com/): The Things Network Indoor Gateway US 915 MHz (discontinued), The Things Network Arduino UNO (P/N TTN-UN-915), Arduino MKR1300 IoT Development Board US-915 MHz, SERPAC A27 Two-Piece Project Enclosure Box (P/N 24K3968).
- Mouser Electronics (https://www.mouser.com/): Flanged Weatherproof Enclosure With PG-7 Cable Glands (P/N 485-3931).
- Digi-Key (https://www.digikey.com/): Battery Lithium 3.7v 2Ah (P/N 1528-1857-ND), Feather M0 LoRa Board RFM95 900MHz (P/N 1528-1705-ND), Simple Spring Antenna 915 MHz (P/N 1528-4269-ND).

Task 1.4 - Conduct preliminary dust chamber studies to establish operation and function of the reference enterprise node and candidate dust sensing node.

Dust chamber studies were conducted using a test chamber (Figure 3.1) located in the mineral processing laboratory. The dust chamber has been used previously in research conducted as part of a NIOSH-funded respirable dust center (Marple, 1978; Marple, 1983). The chamber is approximately 2.4 m high with an inside diameter of 1.2 m. Dust is produced by a TSI Fluidized Bed Aerosol Generator (Model 3400) and after being mixed in a dilution air stream passes through a charge neutralizer and honeycomb flow straightening structure before entering the chamber, The chamber was specifically designed for the testing and calibration of aerosol sampling instrumentation and provides flow rates of approximately 80-300 L/min, with dust concentrations ranging from less than 0.5 mg/m^3 to greater than 3 mg/m^3 depending on the dust feed rate of the fluidized bed generator. The fluidized bed aerosol generator was replaced by a new TSI Dust Aerosol Generator Model 3410U for later calibration studies.

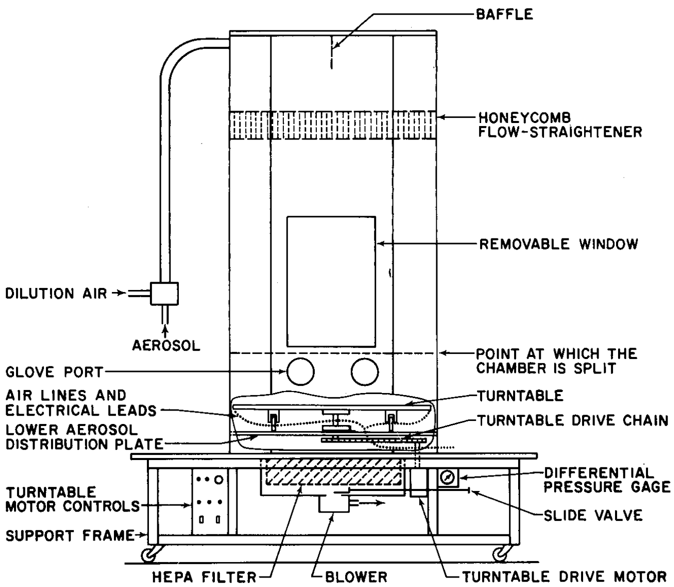

a)

b)

Figure 3.1. a) Aerosol chamber for instrument evaluation and calibration, with b) TSI Fluidized Bed Aerosol Generator (Model 3400). ISO Fine Arizona Road Dust was used to generate respirable dust concentrations in the chamber for instrument evaluation and testing.

Experiments consisted of placing the candidate dust sensors with attached microprocessor, data logging cards, and connecting modules (Figure 3.2), into the dust chamber (Figure 3.3) along with reference aerosol measurement instrumentation including a Thermo PDM 3700, TSI DustTrak DRX, Thermo PDR 1500, and personal sampling pump/cyclone, to yield estimates of respirable dust concentration. Gravimetric samples for respirable dust were collected using SKC AirChek TOUCH sampling pumps (SKC, Inc., P/N 220-5000TC) calibrated with a Mesa Labs Defender 510 Electronic Flowmeter (laboratory) or SKC Precision Rotameter (SKC, Inc., P/N 396-0650). Samples were collected on pre-weighed 37-mm 5-um PVC filters using a 10-mm Dorr-Oliver type cyclone (Zefon International, P/N 10044015) at flow rates of either 1.7 or 2.0 lpm (MSHA Standard specifies 2.0 lpm flow rate while other organizations specify 1.7 lpm flowrate for respirable dust sampling with Dorr-Oliver cyclone). Filters were weighed post-sampling using a microbalance with 0.1 ug resolution.

July 25-26, 2018, Site Visit: The first field evaluation of the three candidate dust sensor platforms was conducted at the Pax Loadout location. Three each of the Sharp, Shinyei, and Laser PM 2.5 sensing nodes, and the TSI DustTrak reference system were placed adjacent to a rail car loading process (Figure 3.4). Individual sensor responses were logged by each sensing node using SD cards with the data subsequently uploaded to a computer for post-processing and analysis and comparison with the results from the DustTrak instrument.

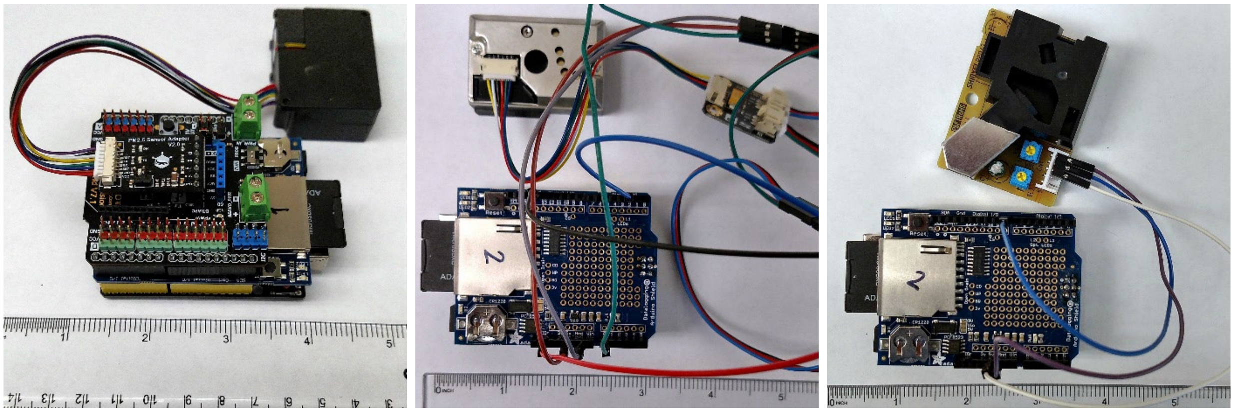

a) b) c)

Figure 3.2. Dust sensor assemblies developed for this project showing microprocessors (Arduino Uno 3) with data logging cards and connecting wires / modules for the a) Laser PM2.5, b) Sharp, and c) Shinyei sensors.

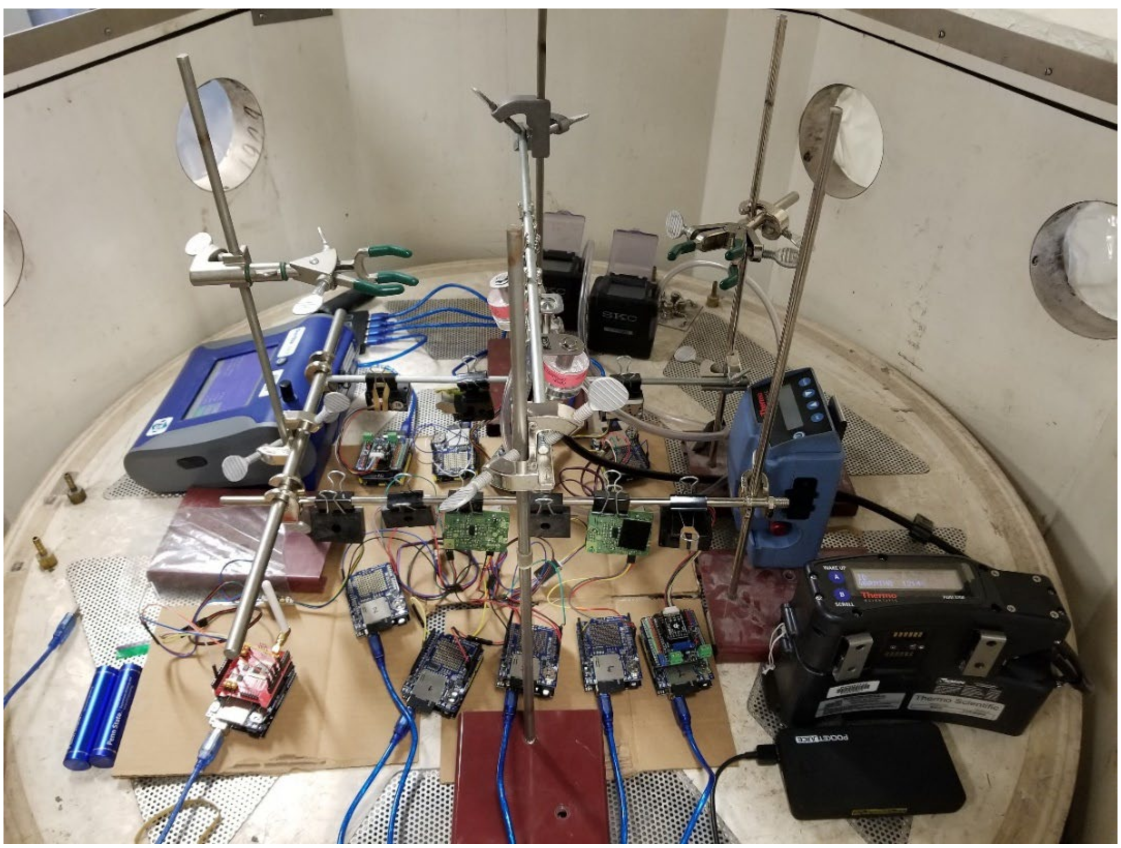

Figure 3.3. Experimental arrangement in dust chamber showing TSI Dusttrak DRX, Thermo-Science PDR 1500, Thermo-Science PDM 3700, personal sampling pumps with 10-mm Dorr-Oliver cyclone, and dusts sensors (three each of Sharp, Shinyei, and Laser PM2.5 sensors).

Figure 3.4. Pax Loadout field evaluation of reference dust sensing system (TSI DustTrak and Environet Data Service) and candidate dust sensors (Sharp, Shinyei, and Laser PM 2.5).

Task 1.5 - Select the brand and model of dust sensor and microprocessor to be used for a prototype sensing node.

Based on the results of preliminary performance studies the Sharp GP2Y1010AU0F dust sensor and The Things Network UNO (The Things Industries P/N TTN-UN-915) were selected for use in the first prototype dust sensing nodes. The selection was based upon a review of size, power requirements, cost, and simplicity and reliability of the sensor interface circuitry for connection with a microprocessor, and the performance of the devices in the laboratory and field studies.

Task 1.6 - Establish the calibration curve for the dust sensors using dust chamber studies.

Experiments generally consist of placing the candidate dust sensors with attached microprocessor, data logging cards, and connecting modules, into the dust chamber (Figure 3.3) along with reference instruments including the PDM 3700, DustTrak DRX, PDR 1500, and personal sampling pump/cyclone, to yield estimates of respirable dust concentration. The primary reference measures of respirable dust are the PDM 3700 and personal sampling pump with cyclone, both of which yield gravimetric estimates of the respirable dust concentration. The DustTrak DRX and PDR-1500 data is corrected using the reference gravimetric results. The PDM 3700 also logs a 15 min TWA (moving) measure of respirable dust concentration to which dust sensor output can be compared.

The target concentration range for experimental runs was approximately 0.15 – 3.0 mg/m^3 respirable dust which represents a range of approximately 0.1-2x the exposure limit of 1.5 mg/m^3. The chamber concentrations were controlled by varying the air flow rate and dust feed rates into the TSI fluidized bed dust generator that supplies the chamber. Although it is difficult to precisely control concentrations, the intent is to vary concentrations over the range of interest several times over the course of an experimental run (Figure 3.5).

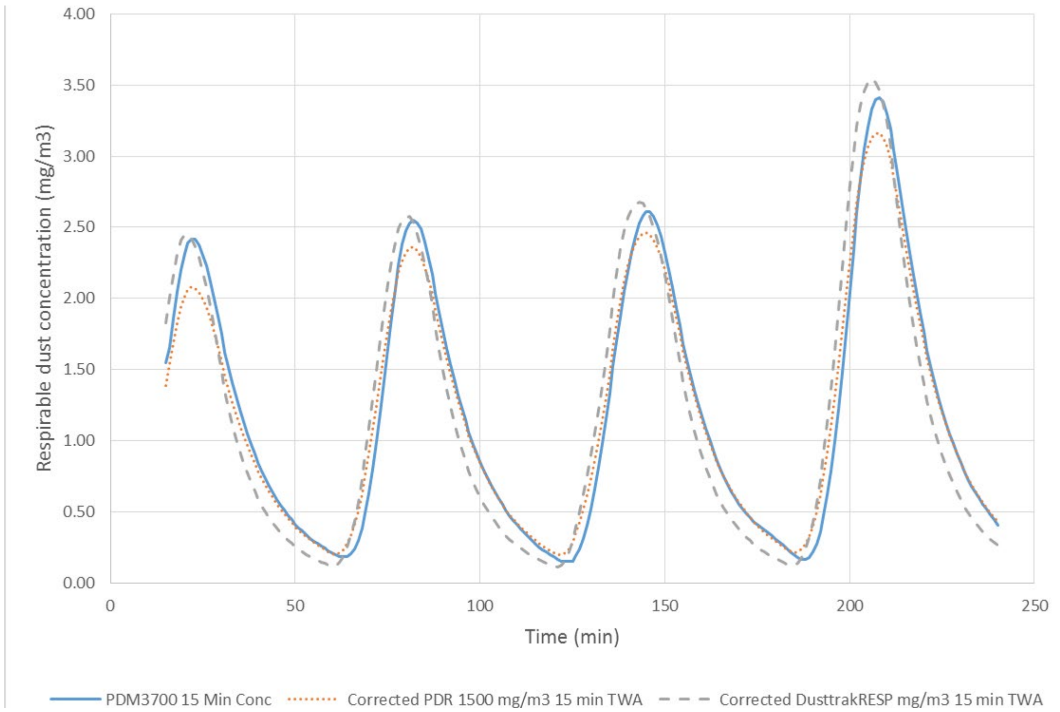

Figure 3.5. Comparison of direct reading instruments for measurement of respirable dust concentrations – 15 min TWA for PDM 3700, corrected PDR 1500, and corrected Dusttrak DRX.

Task 1.7 - Establish the performance characteristics of dust sensors.

Calibration accuracy and precision, cost, size, power requirements, and interface circuitry were summarized for comparison and selection. Calibration performance and sensor characteristics were evaluated based upon the results of the laboratory and field studies described in Tasks 1.4 and 1.6.

Task 1.8 - Identify and evaluate candidate infrastructure for wireless sensor communication.

Consideration was given to Cellular, Bluetooth, Wi-Fi, and proprietary and open-source Radio Modem infrastructures. Based upon information gathered during the first site visit, it was determined that the terrain and distances between likely sampling locations presented challenges with regard to range, and the availability of cellular service. The cost of individual cell service plans for multiple sensing nodes was also a consideration. These factors potentially eliminate Cellular, Bluetooth and Wi-Fi approaches, while favoring long distance, low power radio-based protocols. It was determined that LoRa-based wireless networks (low power wide area networks) which are specifically designed for use with low power, long range, low bandwidth, sensing networks, offered the best performance characteristics for the project.

LoRa is a low power long range networking protocol designed to wirelessly connect devices to the internet (LoRa Alliance). The LoRaWAN® network architecture employs a star topology which uses a gateway to relay messages between end-devices (e.g., dust sensors) and a central network server. LoRa Gateways are connected to the network server using ethernet, Wi-Fi, or cellular service, and act as a bridge for converting RF packets to IP packets for transmission.

A wireless LoRa wide area network (LoRaWAN) requires several components to function including a LoRaWAN gateway server, network server (identity server, join server), and an application server or console (Figure 3.6). These functions can be performed by multiple devices or separate service providers, or in some cases a single hardware component can have several of the functions embedded within the operating system. For example, some LoRaWAN gateways can function as the gateway server as well as the LoRa network server, identity server, and join server. Other services distribute these functions over cloud-based providers. In addition, many services provide a way to pass data to third-party cloud-based data management and display functions or private servers. These services are usually accessed through integration tools that are often available for established vendors such as Amazon Web Services (AWS) or Microsoft Azure. While many of the services are available for free on a limited scale or for short durations, most require a subscription to access all features.

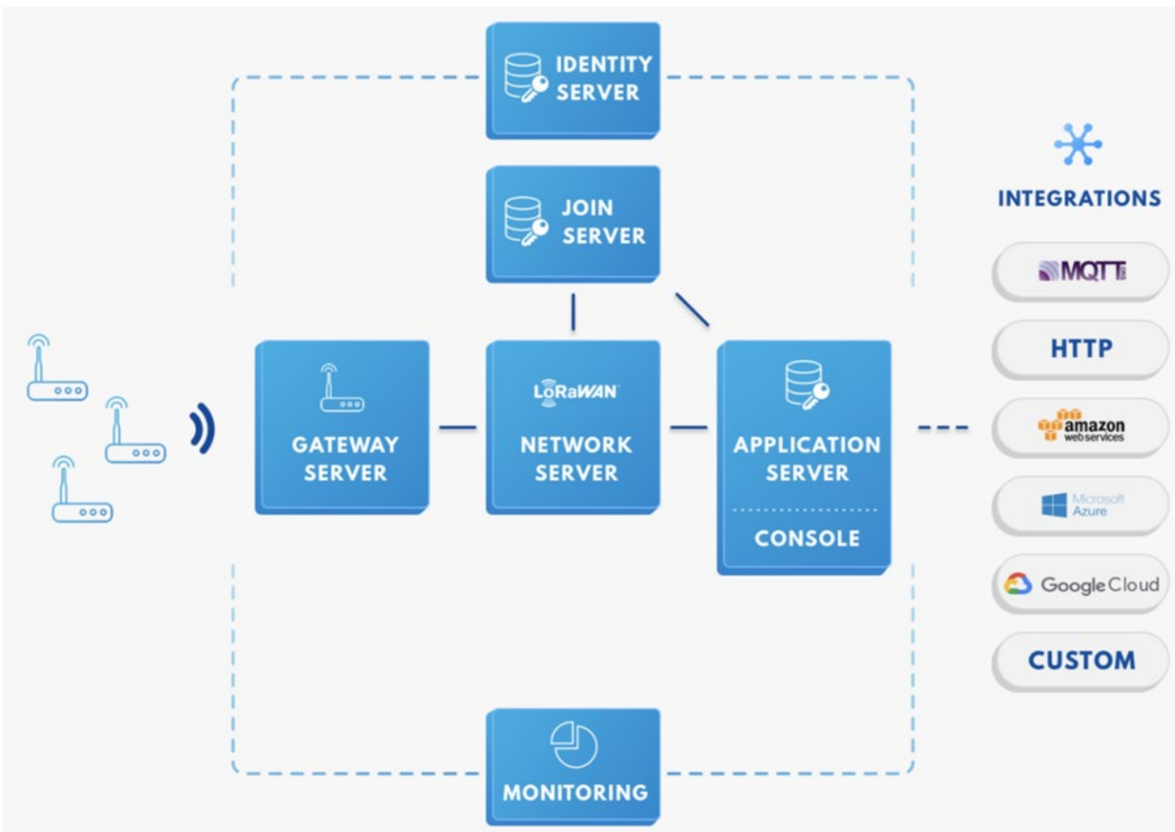

Figure 3.6. Typical LoRaWAN architecture / components.

After reviewing various no-fee LoRa service providers, The Things Network (TTN) (https://www.thethingsnetwork.org/) was identified as the best option for the project based on the availability of compatible LoRa hardware, relatively user-friendly interfaces for the gateway server, network server, and application server, and established integrations for passing data to third party data management and display as well as the option to use HTTP and MQTT for passing and storing data on cloud-based or local servers. For this project an integration was used to pass data from The Things Network to Cayenne in order to create data display dashboards, alarms, or triggers:

- Cayenne https://developers.mydevices.com/cayenne/features/

Research Objective 2: Characterize respirable dust exposures by occupation and operation at partnering mine location(s) using continuous personal dust monitors (CPDM), aerosol monitors, helmet-cam (video), and the EVADE software system.

Task 2.1 - Preliminary identification of primary sources of respirable dust exposure.

The Pax Loadout location was identified as the first field site based upon the nature of the activities which include regular operations, significant potential sources of respirable dust associated with the transport, crushing, and loading of coal onto rail cars, and the availability of a centralized office location that would facilitate the development and testing of the first prototype wireless dust networks. Mine personnel provided site plans as well as previous respirable dust exposure monitoring results that were used to identify areas of interest for locating wireless dust sensors. A tour of operations was provided by mine personnel and likely sources of dust exposure were identified.

Task 2.2 - Characterization of personal respirable dust exposure for each job category.

Personal gravimetric monitoring for respirable dust was conducted at the Pax Loadout Facility for occupations identified as having likely exposure to respirable dust including the sweeper operator, Bobcat operator/utility worker, loader operator, and dozer operator. In addition, area sampling was conducted on the loadout platform during rail car loading. Helmet-Cam surveys were conducted for the scale house operator, utility worker, dozer operator, and loadout operator.

Task 2.3 - Characterization of personal respirable dust exposure using Helmet-Cam with EVADE software for synchronizing video with logged dust concentrations.

Video studies were conducted according to published guidelines (Reed, 2014a) with the modification that the camera was worn on the chest of the worker rather than attached to the helmet (Figure 3.7). Respirable dust sampling and data-logging was performed with either the pDR-1500 or the PDM 3700. A GoPro Hero4 camera was used to record video and the NIOSH Evade software was used for post-sampling analysis of respirable dust exposures.

Figure 3.7. Video and respirable dust exposure monitoring for analysis using EVADE software system.

Specific Aim 2 - Deploy and evaluate the performance of an integrated network of fixed- and mobile-wireless dust sensors capable of continuous real-time detection and reporting of respirable dust concentrations to a centralized location.

Research Objective 3: Design and deploy an integrated wireless respirable dust sensing network with centralized monitoring capability.

Task 3.1 - Fabricate one complete wireless respirable dust sensing node / unit and confirm performance in the dust chamber.

The first complete dust sensing node (Prototype-1) was fabricated using:

- Sharp dust sensor (SEN0144) and interface module (DFR0280)
- Custom designed / 3D-printed sensor mounting fixture
- The Things Network Arduino UNO (P/N TTN-UN-915)
- SERPAC A-27 Two-Piece Project Enclosure Box (P/N 24K3968)

The sensing node could be powered by a 9-volt battery (4-6 hours of operation) or an external USB battery pack (hours of operation determined by capacity of battery pack).

A second prototype (Prototype-2) was developed based on improvements identified during laboratory and field testing of Prototype-1. The second prototype was based on a smaller, low power microprocessor (3.3V logic) with integrated LoRa chip and was designed to be supplied by solar power in the field for extended operation. Prototype-2 dust sensing nodes were based upon the following main components and packaging:

- Sharp dust sensor (SEN0144) and interface module (DFR0280)
- Custom designed / 3D-printed sensor mounting fixture
- Adafruit Feather M0 with RFM95 LoRa Radio - 900MHz - RadioFruit (P/N 3178)
- Lithium-Ion Battery - 3.7v 2000mAh (P/N 2011)
- Semi Flexible Monocrystalline Solar Panel (5V, 1A, 5W)
- 5V Solar Power Manager (DFR0559-1)
- Flanged Weatherproof Enclosure With PG-7 Cable Glands (P/N 485-3931)

Task 3.2 - Develop finalized code for control of the dust sensing node, data-logging, and transfer of data, and confirm performance in laboratory and at local field/remote settings.

Code used to control dust sensing nodes and for data logging was developed using the Arduino Integrated Development Environment (https://www.arduino.cc/en/software). Prototype sensing nodes were programmed to send the average analog voltage from the Sharp dust sensor each minute. These numbers are then baseline-corrected (each sensor has a non-zero output voltage even when dust concentrations are below the detection limit), and the pooled calibration result for Arizona Road Dust (A1 Ultrafine, A2 Fine, and A3 Medium) and coal were used to convert the baseline-corrected voltage to a respirable dust concentration. The resulting firmware was uploaded to the microprocessor and used to operate the device during subsequent laboratory and field testing. Examples of source code are provided in an Appendix.

Field performance was first demonstrated for the Prototype-1 dust sensing node which was based on The Things Network (TTN) Uno microprocessor (Arduino Leonardo). A LoRaWAN gateway device (The Things Industries Indoor Gateway) and Verizon Jetpack 4G LTE Mobile Hotspot were implemented for wireless reception of dust sensing node data and transmission to cloud-based display and storage applications (Figure 3.8).

Figure 3.8. The Things Network (TTN) LoRa Gateway, Verizon Jetpack 4G LTE Mobile Hotspot 8800L, and three prototype dust sensing nodes consisting of TTN Uno Microprocessor (Arduino Leonardo) with Sharp GP2Y1010AU0F dust sensor powered by 9-volt Lithium battery.

Task 3.3 - Fabricate ten fully functional sensing nodes and conduct performance testing in the dust chamber and in a local field performance demonstration.

Fourteen Prototype-1 dust sensing nodes were fabricated and tested in the dust chamber and in local field performance evaluations. Calibration runs were conducted as described previously in Tasks 1.4 and 1.6.

Task 3.4 - Deploy 5-10 dust sensing nodes at the partnering surface mine location and demonstrate performance.

June 12-14, 2019, Site Visit: Performance evaluation of Prototype-1wireless dust sensing nodes placed at the Pax loadout Coal Crusher/Sizer Building Level 2 (Figure 3.9). Two Prototype-1 units were placed in close proximity to the inlet of the reference dust sensing node (TSI DustTrak DRX with environmental enclosure, Thiamis GSM/GPS Modem, and Environet data service) and a gravimetric respirable dust sampler. The DustTrak DRX was connected wirelessly via cellular modem to the Environet data service for display and storage of respirable dust concentrations.

Figure 3.9. Sampling position at Crusher Building Level 2 showing Dusttrak DRX with environmental enclosure, two prototype dust sensing nodes, and a gravimetric respirable dust sampler (10-mm Dorr-Oliver cyclone with pre-weighed 37-mm 5-um PVC filter).

The prototype sensing nodes were connected wirelessly to a LoRa gateway located in the main office of the Pax Loadout facility (Figure 3.10). Data received from the prototype respirable dust sensing nodes was recorded and compared with data sent by the reference DustTrak DRX instrument.

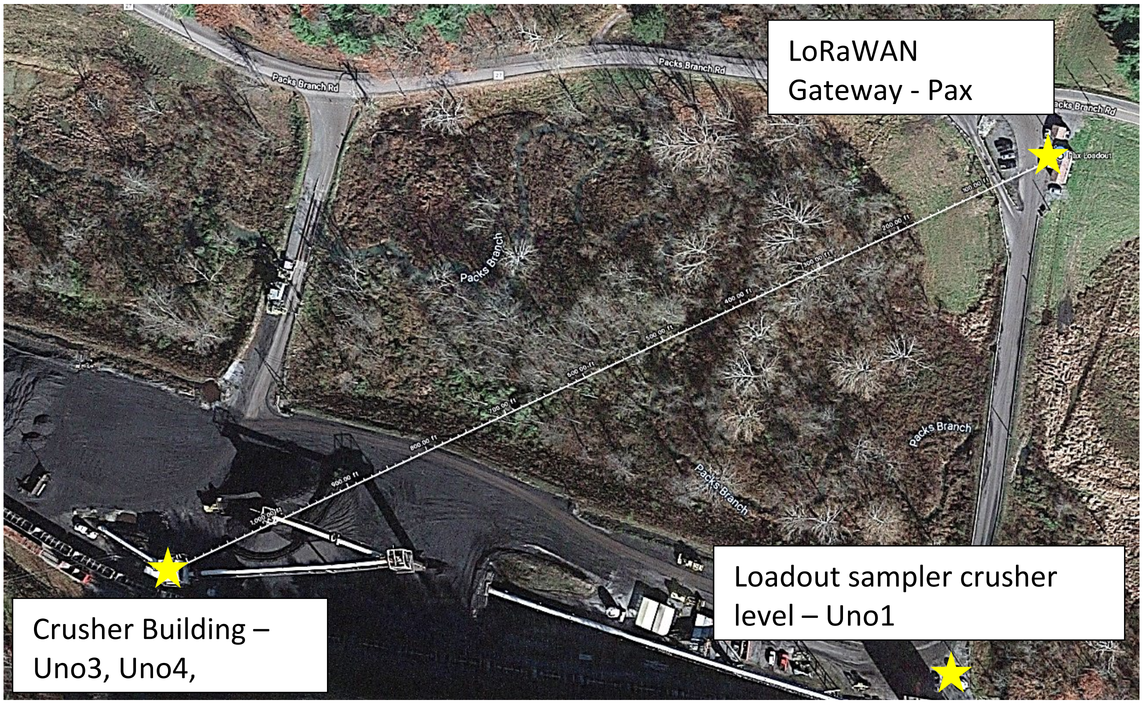

Figure 3.10. Satellite photo showing the sampling location at the Crusher Building and the location of the LoRa gateway at the Office approximately 340 meters away.

October 10-11, 2019, Site Visit: Seven of the Prototype-1 dust sensing nodes were deployed at the Pax South Surface Mine to evaluate transmission over longer distances compared with those at the Pax Loadout Facility. A Things Network Outdoor Gateway was deployed at the Substation South location on the first day (Figure 3.11) and at the Radio Repeater location on the second day. Dust sensing nodes were placed at eight different locations to determine whether connections between nodes and gateway could be established with successful transmission of data packets. Node locations included the South Field Office, North Field Office, LP1806, LP1802, 34 Marker-25 Haul Road, Repeater Station, and Little Eagle South, with distance between nodes and gateways ranging from approximately 0.5-2.2 km.

Figure 3.11. LoRa Gateway at South Substation location and a pair of dust sensing nodes temporarily located along a haul road.

May 19-21, 2021, Site Visit: Deployed six each of the Prototype-1 and Prototype-2 sensing nodes at the Pax Loadout Facility to evaluate wireless dust sensing network performance including data transmission using a new gateway located on top of the loadout (Figure 3.12), and to compare dust sensor measured concentrations to reference direct-reading instruments (PDM 3700, Dusttrak DRX, and PDR 1500) and gravimetric sample results for respirable dust. Reference direct-reading instruments were placed at three locations expected to have the highest respirable dust concentrations based on previous site visits: 1) Crusher / Sizer, 2) Clean Coal Stacker Belt, and 3) Truck Dump Belt. One each of the v1 (Uno) and v2 (m0) nodes and a gravimetric sample were also placed at each location. An additional three sampling locations were selected to span the area of the loadout facility to evaluate data transmission (Figure 3.13).

Figure 3.12. Pax gateway position a) on top of loadout structure, and b) DustTrak DRX, Uno and m0 nodes, and gravimetric sampler at Crusher / Sizer – Pax Loadout 5/20/21.

Figure 3.13. Pax locations for air samples, sensor nodes, and LoRaWAN gateway – 5/20/21.

Task 3.5 - Deploy the full integrated wireless dust monitoring and response system for respirable dust (20-25 sensing nodes).

June 10, 2021, Site Visit: 13 second-generation dust sensing nodes (Prototype-2) and a LoRa gateway were deployed at the Workman Creek North (WCN) surface mine for more extensive and long-term testing of: transmission/reception range, durability of dust sensing nodes, reliability of solar power and battery management modules, and the functionality of cloud-based data management and display applications. Sensor nodes were placed in portable sampling stations that were fabricated by WCN personnel to secure respirable dust monitoring equipment (Figure 3.14). The gateway placement is shown in Figure 3.15. The number of sensing nodes that could be placed was limited to the number of available sampling stations (14 in total). Sensors were deployed for approximately one month from June 10-July 15 at which time the devices were retrieved and returned to the lab for post-calibration.

Figure 3.14. Portable respirable dust sampling station used to secure equipment with closeup showing sensing node and gravimetric respirable dust sample – WCN June 10, 2021.

Figure 3.15. Solar-powered LoRa gateway deployed June 10 – July 15, 2021.

September 29, 2021, Site Visit: In a return visit to the WCN surface mine, 14 Prototype-2 dust sensing nodes were redeployed to evaluate the effect of the placement of inlet screens over the dust sensor openings and to install a permanent LoRa Gateway at the WCN Field Office (Figure 3.16). Results from the previous June-July 2021 deployment at WCN indicated that fog, heavy dust loading, and insects potentially contributed to decreased sensor performance including reversible full scale-response, irreversible full-scale response, and significant baseline shift. In preparation for this visit, a stainless-steel screen (120-mesh) was installed over the sensor inlets on seven of the dust sensors while the remaining seven sensors remained open to the air. Screened and unscreened sensors were calibrated in the laboratory. Dust nodes were then placed at seven sampling stations, pairing one screened sensing node with one unscreened sensing node at each location (Figure 3.17) and performance was compared.

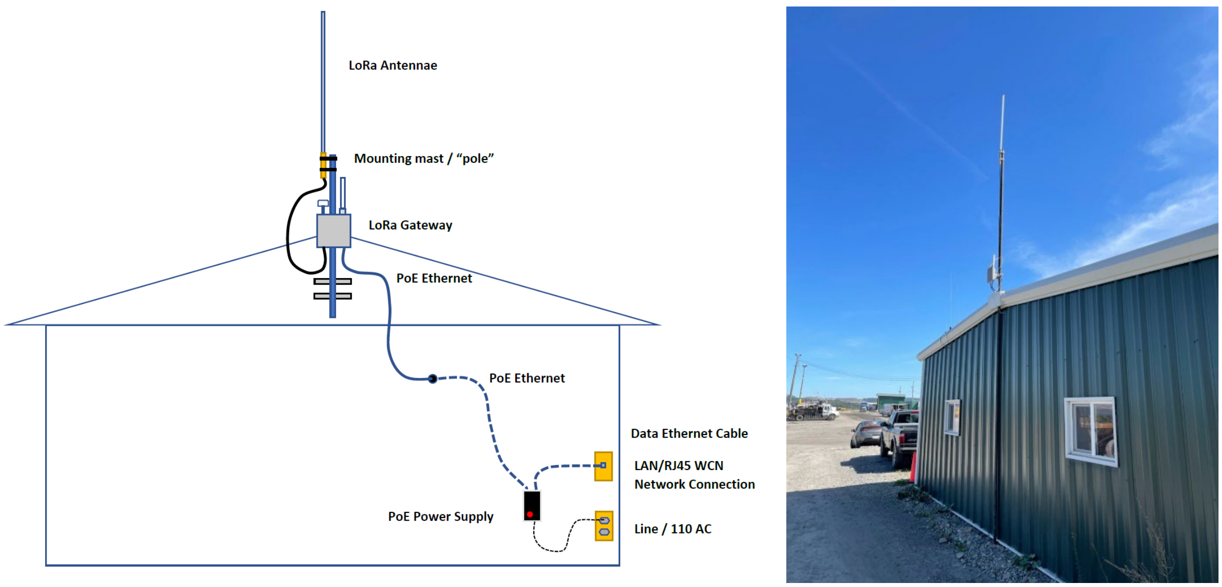

Figure 3.16. Permanent LoRa Gateway installation at WCN Field Office

a) b)

Figure 3.17. a) Sampling station with screened and un-screened dust nodes – near WCN Coal Handling Facility, and b) 40-mesh (left) and 120-mesh (right) inlet screen materials.

October 27, 2021, Site Visit: A return trip to WCN surface mine was conducted to repair or replace five of the 14 sensors that were deployed during the September 29 Site Visit. Two sensing nodes had lost power, two displayed a fixed full-scale output, and one sensor was showing a significantly shifting baseline. Upon examining the two full-scale sensors, it was apparent that insects had nested within the sensor body (both sensors were unscreened) so the decision was made to place 40-mesh screens on all of the unscreened sensors to reduce the likelihood of insects disrupting the sensing function for the remainder of the study. Solar panels were replaced on the two sensors that had lost power – one cable appeared to have been damaged by animals and was completely severed while the second node's solar panel cable showed signs of being crushed by the sample station access door. Both nodes functioned normally after the solar panels were replaced. The sensing node with the shifting baseline was equipped with a new dust sensor. The 14 sensing nodes continued to function until equipment was retrieved on December 9, 2021, and post calibrations were performed in the laboratory.

Research Objective 4: Evaluate the overall performance of the integrated wireless monitoring and response system for respirable dust.

Task 4.1 - Prepare final performance summary comparing the integrated wireless sensor system to results for the enterprise sensing node, PDM 3700, and traditional gravimetric methods for respirable dust monitoring.

No separate research approach or methods required for this task.

Task 4.2 - Prepare summary of the costs of the integrated monitoring system with comparison to an equivalent turnkey or enterprise type system.

Estimated costs for the enterprise "turnkey" system are based upon the purchase price for the TSI DustTrak and associated environmental enclosure, accessories, and subscription data service. Costs for the prototype dust sensing nodes and LoRaWAN network components are itemized and totaled for each version examined for the project.

Task 4.3 - Summarize feedback from the partnering mine on performance of the monitoring system including strengths, weaknesses, and future needs.

At the completion of the project a survey will be developed and administered using Survey Monkey to solicit feedback from the partnering mine personnel. Specific questions and prompts will be included to gauge the strengths and weaknesses of the integrated respirable dust sensing network, solicit suggested improvements, and itemize priority areas for future developments in dust sensing technologies from the perspective of the industry.

4.0 Research Findings and Accomplishments

Specific Aim 1 - Develop, assemble, and test in the laboratory, a portable wireless dust sensing system capable of monitoring respirable dust concentrations using affordable optical sensors.

Research Objective 1: Evaluate candidate dust sensor technologies and monitoring software systems for the connection, integration, and relay of data from wireless monitors to a centralized system.

An extensive review of the literature, manufacturers' product information, and online development communities was conducted to identify candidate microprocessors, dust sensors, and associated hardware and software packages. While there are a number of different options available, and the prevalence of various technologies can vary internationally, far and away the most common microprocessor systems employed were found to be the Arduino and Raspberry Pi line of products. The most frequently cited inexpensive dust sensors were the Shinyei PPD42 (sometime referred to as the Grove or Amphenol sensor) and Sharp GP2Y1010AU0F. These are both optical (LED) based sensors that produce an output as a result of the LED light reflecting from dust particles on to a photodetector. The devices are usually employed in circuitry that produces pulses that can be quantified and related to airborne dust concentrations.

More recently several different versions of laser-based dust sensors have become available. These devices are also based on the reflection of light (laser) from the dust particles with a photodetector-based response. While representing a higher price point than the Shinyei and Sharp sensors (~ $45 each for laser sensors versus ~$10 each for Sharp or Shinyei), the laser-sensors often have a fan included in the packaging and are designed to provide estimates of dust concentrations in different size ranges (PM1, PM2.5, PM10, etc.). While the precision and accuracy of the size selective measurement has not been verified and is probably questionable given that this is a $40 device, it was decided to include this type of sensor in the pool of candidate technologies to be evaluated for use in the wireless sensor networks since the inclusion of a fan potentially improves response time (several projects describing the use of Sharp and Shinyei sensors included the addition of fans to improve dynamic performance, and in fact the Shinyei sensor includes a heater resistor to create a convective current to move air and dust through the sensing zone).

The Sharp, Shinyei, and laser sensors are each capable of providing output at one-second intervals, while the Dusttrak DRX and PDR 1500 instruments record average concentrations for each minute, and the PDM 3700 provides a 15-min TWA concentration that is updated each minute. Although the dust sensors can be sampled at a higher frequency, there is little value in reporting data every second given the typical highly variable nature of airborne concentrations, the relevant time-frame of interest for exposure monitoring and response, and in some cases the noise inherent in the dust sensors themselves. In particular it was found that noise can be significant for the Sharp and Shinyei sensors when the output is sampled at 1-second intervals. This is demonstrated for the Sharp sensor in Figure 4.1a which shows the output recorded each second (voltage) and a 60s moving average. The figure clearly demonstrates the noise inherent in the data sampled at a higher frequency versus the smoothed waveform that results from averaging the output over 60 seconds.

Alternatively, the laser sensor output (Fig. 4.1b) is not nearly as noisy when sampled each second, but also benefits from the smoothing that occurs with one-minute averaging.

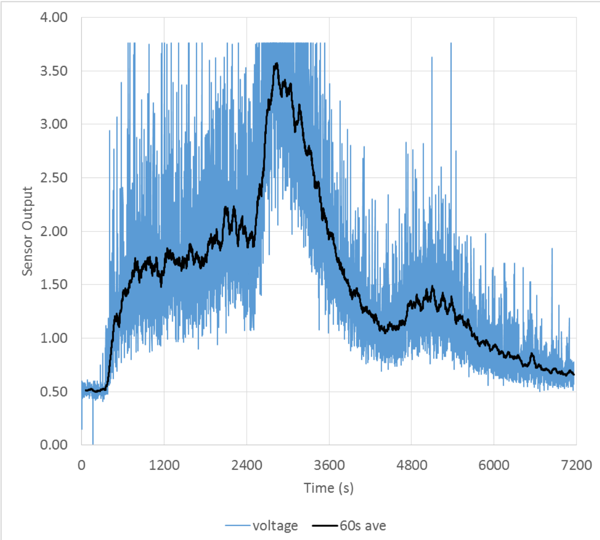

a)

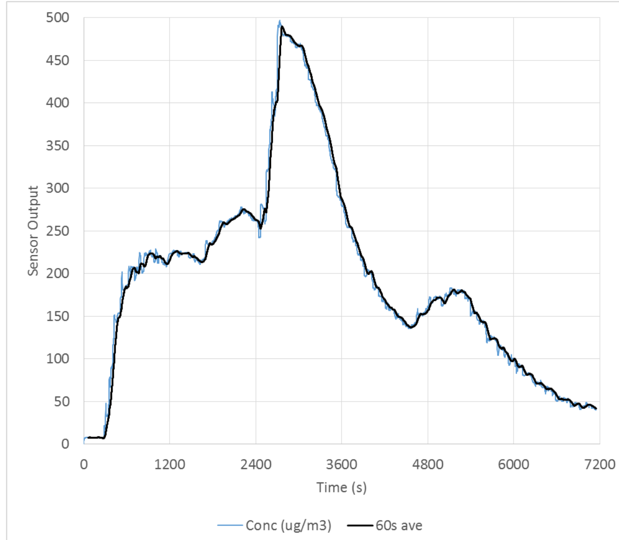

b)

Figure 4.1. Effect of averaging time on sensor response for a) Sharp and b) PM2.5 laser sensors – 1 sec response versus 60s average response for 120 min (7200s) experimental run.

Given that the reference direct reading instruments record 1-minute averaged data, and that realistic monitoring and response systems are unlikely to be based on sampling frequencies greater than one minute, the decision was made to average sensor responses over a period of 60 seconds and to log the resulting value for each minute. This will also have the effect of significantly reducing the storage requirements for the data logging systems as well as the throughput required for transmission of data for the integrated wireless sensor networks.

A representative plot of the 15-min TWA output from a Shinyei sensor versus the reference PDM 3700 instrument is presented in Figure 4.2. The PDM 3700 records respirable dust concentration in units of mg/m^3 while the output from the Shinyei sensor is displayed as low pulse occupancy time (LPO%) which is a measure of the amount of reflected light detected by the sensor in a given measurement period and that is proportional to dust concentration as can be seen by the close tracking of the PDM 3700 output over a four-hour experimental run. Calibration of the Shinyei sensor was required to establish the quantitative relationship between LPO% and respirable dust concentration and these calibrations were completed for each of the three sensors considered.

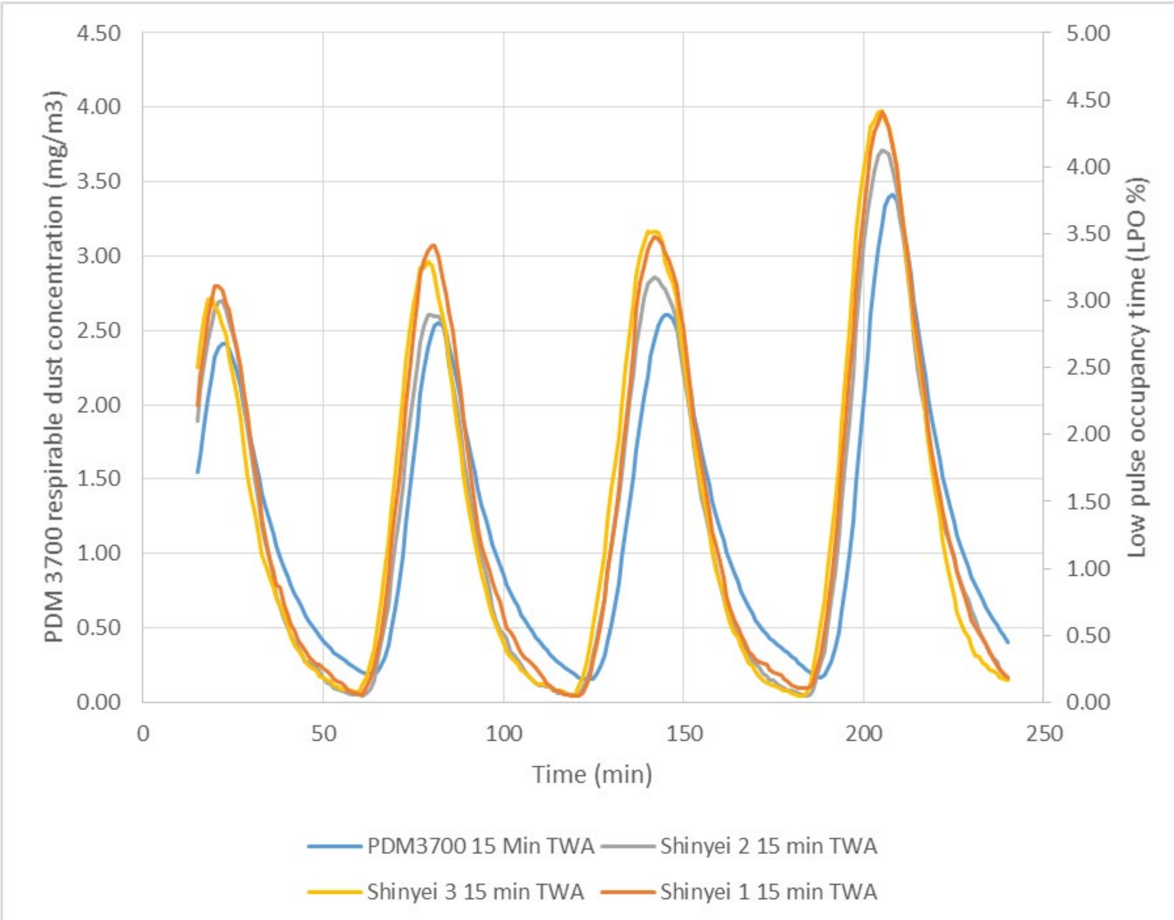

Figure 4.2. Comparison of PDM 3700 respirable dust concentrations (mg/m3) to Shinyei dust sensor output (low pulse occupancy time or LPO%).

Preliminary results showed that the sensors generally track reference instrument respirable dust concentrations very well, with some differences in variability within multiple sensors of the same type and across the different types of sensors. Given the general suitability of sensor performance, the final selection was based upon performance characteristics such as size and power requirements, simplicity and reliability of the sensor interface circuitry for connection with a microprocessor, and cost. A summary of operating parameters is presented in Table 4.1 which shows that based on an estimated cost per node, the Sharp and Shinyei sensors are comparable ($66-69/node), while the power requirements for the Shinyei are significantly higher (134 mA vs. 55 mA). Metrics associated with calibration, accuracy, and precision show little difference between the three sensors, and therefore cost, power, size, and connectivity formed the basis of selection.

A summary of preliminary calibration results for the sensors is presented in Figure 4.3. The output from each sensor is plotted against the respirable dust concentration measured by a reference instrument (PDR 1500). Each sensor has a different type of output: the Shinyei records the low pulse occupancy time (LPO%), the Sharp has an analog voltage that is proportional to dust concentration, and the laser sensor is programmed internally by the manufacturer to output estimates of concentration for the PM 2.5 size fraction in units of ug/m^3. In practice it has been found that efforts by the sensor manufacturers to provide factory calibrations for the devices has been unsuccessful, so empirical equations based on calibration using dust similar to what will be measured in the actual application is required.

Table 4.1. Comparison of sensor characteristics

Sensor / Attribute	Sharp (GP2Y1010AU0F)	Shinyei (PPD42NS)	Laser (Gravity PM2.5)
Current (mA)	55	134	122
Sensor Cost ($)[1]	15	12	47
Cost per node ($)[2]	69	66	101
Calibration R^2 [3]	0.90	0.87	0.94
1 min % Error [4]	-0.7 ± 54%	4.9 ± 59%	-4.0 ± 40%
240 min TWA % Error[5]	± 1%	± 1%	± 1%

[1] includes any required module / adapter / components

[2] includes Arduino Uno ($11), data logging board ($14), storage media ($10), wireless LoRa adapter ($19)

[3] calibration of sensors against corrected PDR 1500 respirable dust concentration

[4] 15 min TWA sensor respirable dust concentrations versus PDM 3700

[5] 4-Hr (240 min) TWA respirable dust concentrations versus PDM 3700 and gravimetric method (sampling pump, 10-mm Dorr-Oliver cyclone)

The plots in Figure 4.3a-c consist of the output from three of each type of sensor (two for Sharp due to a sensor malfunction) versus the reference instrument concentration. The results are linearly related to the reference instrument with the most precise relationship (highest R^2) resulting for the laser sensor (0.94) followed by the Sharp (0.90) and Shinyei (0.88) sensors. Using calibration equations resulting from regression of sensor output versus the reference instrument, each sensor yields an estimate of the actual respirable dust concentrations which are plotted in Figure 4.3d. The figure shows excellent agreement between calibrated sensor results and the reference measure of respirable dust concentration. Subsequent work focused on sensor calibrations for different test dusts in order to establish the most accurate empirical relationships between sensor response and respirable dust concentrations for the field application.

Calibrations were completed for three of each type of dust sensor considered (Sharp, Shinyei, and Laser), for three different size ranges of Arizona road dust, and for coal dust. Results for A1 Test Dust and the Sharp sensors are presented in Figure 4.4. The one-minute average voltage output from the sensor is plotted against the one-minute average respirable dust concentration measured by a reference instrument (PDR 1500). In the top plot the raw voltage output from the Sharp sensor is graphed versus the respirable dust concentration, while in the middle plot the Sharp sensor output is baseline corrected ("zeroed"), and in the bottom plot the Sharp data is baseline corrected and the calibration concentration range is limited to ≤ 3 mg/m^3.

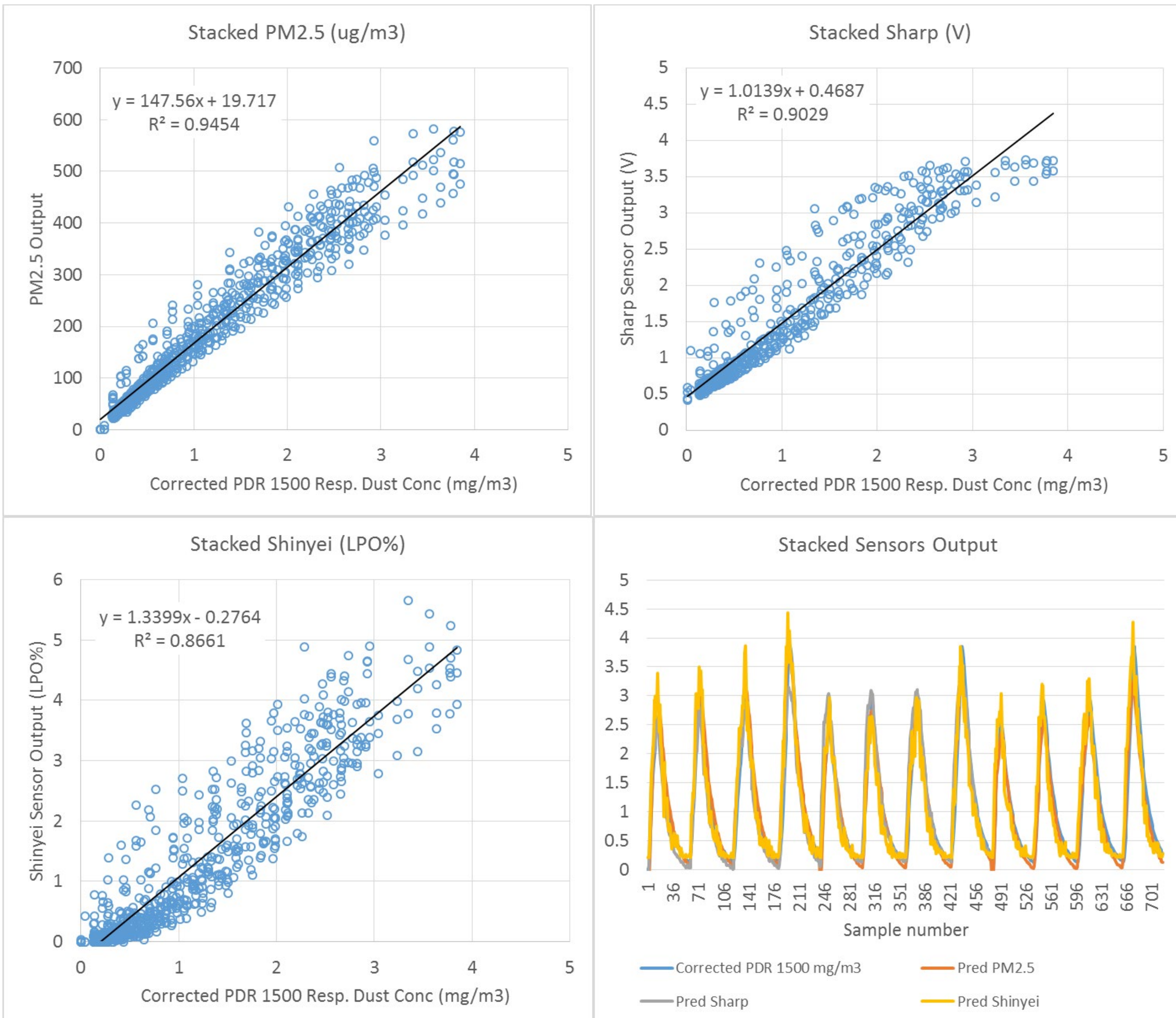

Figure 4.3. Respirable dust calibrations curves for PM2.5 (Laser), Sharp, and Shinyei sensors, and resulting predicted respirable dust concentration profiles.

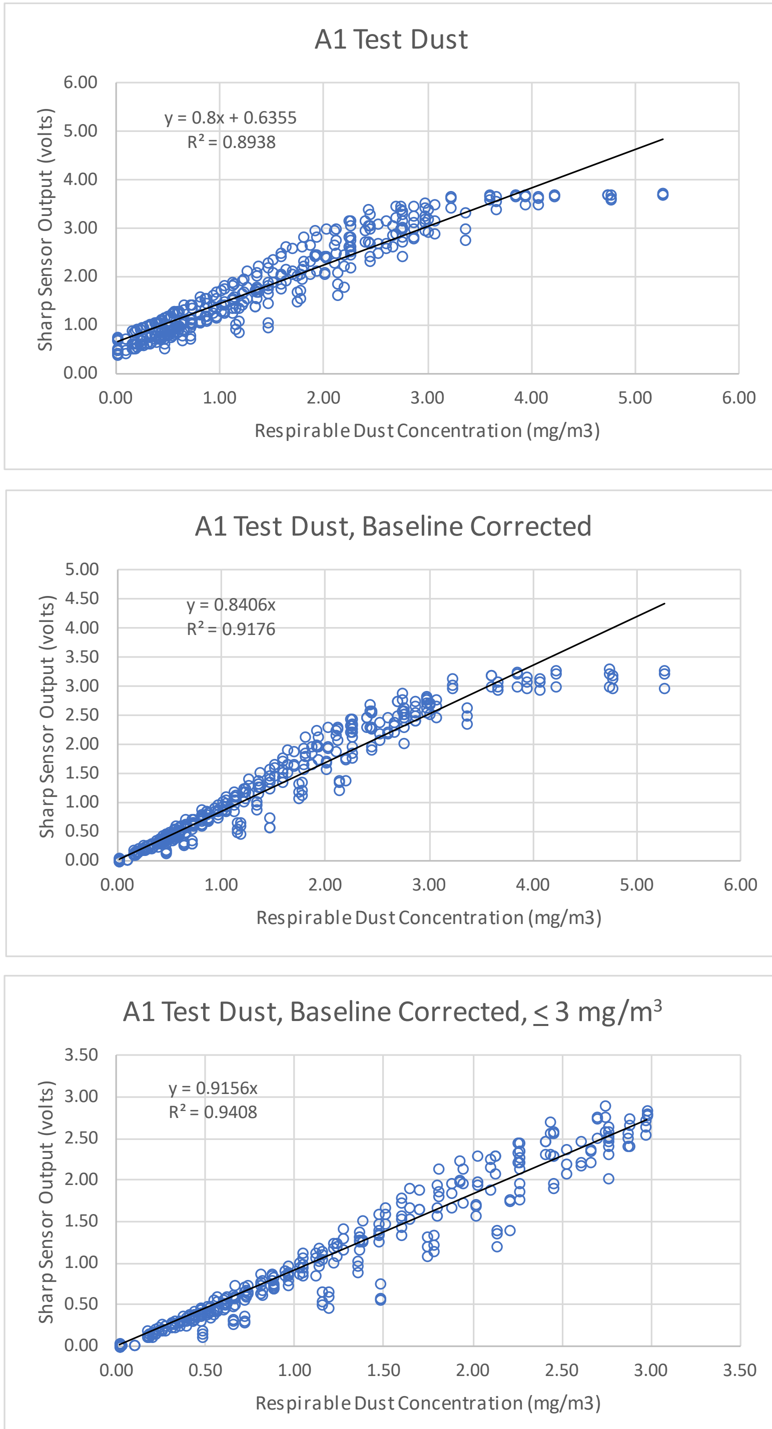

Figure 4.4. Respirable dust calibration results (A1 Test Dust) for Sharp sensor showing 1) uncorrected sensor output voltage versus concentration (top), 2) baseline corrected output voltage versus concentration (middle), and 3) baseline corrected output voltage versus a dust concentration range limited to $\leq$ 3 mg/m^3. All values are one-minute average results.

The regression equation for the upper plot in Figure 4.4 indicates a significant non-zero intercept which results from the voltage output that each Sharp sensor has even when no dust is present. This baseline voltage varies from sensor to sensor – for the three examined in this test the average baseline voltage was 0.54 volt (range = 0.49-0.71) with a standard deviation of 0.16 volt. Baseline correction, or zeroing the sensor, can minimize this source of variability and simplifies the resulting regression equation which can be forced through zero as shown in the middle plot. Finally, in the lower plot the concentration range over which the regression is applied is limited to ≤ 3 mg/m^3. As indicated previously, it can be difficult to precisely control dust generation during the experimental runs meaning that concentrations may at times significantly exceed the range of interest which was defined as approximately 0.15-3.0 mg/m^3. By filtering these points from the dataset, the respirable dust exposure limit of 1.5 mg/m^3 falls within the middle of the concentration range over which the regression is applied.

Calibrations similar to those shown in Figure 4.4 were completed for A1, A2, and A3 Arizona Road Dust, and coal dust (see Appendix). The resulting calibration curve slope for regression of the baseline corrected sensor data versus respirable dust concentrations (one-minute averages) is listed in Table 4.2 for each run. A number of variables affect the response of light scattering sensors including particle size and refraction, so it was expected that there could be differences between the resulting calibration results for the different sizes of test dust (A1, A2, A3) and the different types of dust (Arizona road dust versus coal dust). Referring to the results in Table 4.2 the differences in response for different size ranges of Arizona Road dust were relatively small (approximately 10%), while the difference in response between the road dust and coal dust was significantly larger (approximately 74%).

Table 4.2. Combined calibration summary for Sharp dust sensors (slope = 0.92) showing 15-min TWA respirable dust concentration compared to reference instrument measurement (pDR-1500).

Test Dust	Error Range	Ave. Error	SD	Slope[1]
ISO 12103-1, A1 Ultrafine	-26 – 19%	-4.5%	11%	0.92
ISO 12103-1, A2 Fine	-23 – 45%	2.1%	9.4%	1.01
ISO 12103-1, A3 Medium	-24 – 36%	7.6%	14%	0.95
Coal Dust	-52 – -25%	-38%	5.6%	0.58

[1] Regression result from individual dust calibration, baseline corrected, forced zero, conc. ≤ 3 mg/m^3

While it may be possible to use different calibration results for a wireless dust sensing network by applying specific individual calibration results to a particular sensing node based on some foreknowledge of the type and size of dust most likely to be present, a simpler first approach would likely involve pooling calibration data to estimate an overall average response factor or slope that would then be applied to all sensors in the network. Using this approach, a combined calibration dataset was created by pooling all results for the A1, A2, A3, and coal dust experimental runs. As shown in Figure 4.5, the resulting overall slope is approximately 0.92 volt/(mg/m^3).

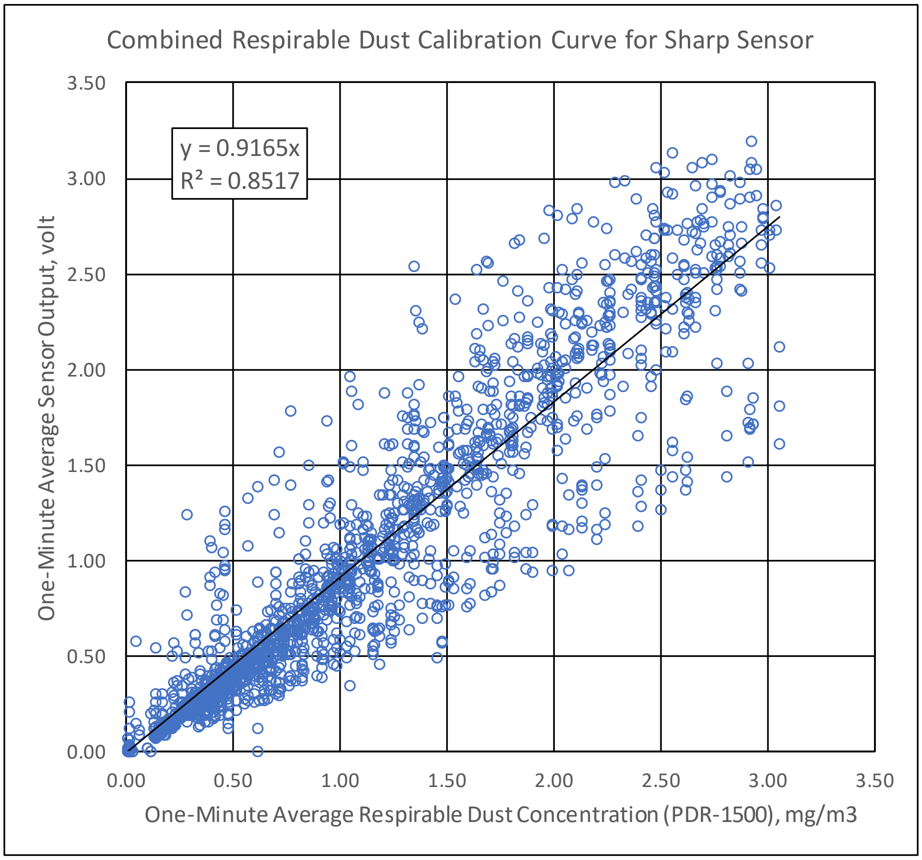

Figure 4.5. Pooled Sharp sensor calibration result for A1, A2, A3, and coal dust.

The overall slope value of 0.92 was used to estimate the 15-minute time weighted average respirable dust concentrations for the calibration data set, and these values were then compared with the “true” concentrations recorded by the PDM 3700 during the experimental runs. Baseline corrected one-minute average voltage output from the sensors was divided by the overall slope value of 0.92 to yield an estimate of one-minute average respirable dust concentration. These minute-by-minute estimates were then used to generate the predicted 15-min TWA respirable dust concentrations for comparison with the reference PDM 3700 instrument results. A summary of these comparisons is shown in Table 4.2. Results are good for Arizona road dust with average errors ranging from -4.5 to 7.6% for A1, A2, and A3 test dusts and individual measurement errors generally in the $\pm$ 25% range. The results for coal dust were not as good with an average error of -38% and errors ranging from -52 to -25%.

The negative bias for coal dust is a consequence of using the pooled calibration data and is consistent with the differences in the individual slope values shown in Table 4.2. Although the use of an overall calibration factor can result in less accurate results for coal dust, a monitoring protocol that employs appropriate alarm set-points could easily account for these levels of variability in sensor responses to different dusts, which are not unusual for field-based direct-reading instruments.

This portion of the project entailed the identification and selection of candidate dust sensors, and a supporting microprocessor platform, and included consideration of appropriate wireless transmission protocols. These components subsequently underwent laboratory performance evaluations and a series of calibration experiments using several different test dusts which established the quantitative relationship between sensor output and respirable dust concentrations. This work also led to the demonstration and implementation of a baseline correction protocol to simplify the quantitative relationship between sensor output voltage and dust concentrations. Completion of this work paves the way for subsequent field deployment and testing of prototype wireless dust sensing systems and comparison with reference measurements including the TSI enterprise respirable dust sensing node.

Research Objective 2: Characterize respirable dust exposures by occupation and operation at partnering mine location(s) using continuous personal dust monitors (CPDM), aerosol monitors, helmet-cam (video), and the EVADE software system.

Personal gravimetric monitoring for respirable dust and Helmet-Cam EVADE video monitoring was conducted on July 25-26, 2018, and June 14, 2019, at the Pax Loadout Facility (Table 4.3). Occupations sampled included sweeper operator, Bobcat operator/utility, loader operator, and dozer operator. In addition, area samples were collected on the loadout platform during rail car loading, and on both levels of the Sizer / Crusher. Helmet-Cam surveys were also conducted on July 25 and 26 for the scale house operator, utility worker, dozer operator, and loadout operator.

Table 4.3. Pax Loadout Sampling Results – Respirable Dust Concentrations

Date	Job	Sample Time	Concentration (mg/m^3)
7/25/18	Sweeper Operator	9:12-13:43	0.047
7/25/18	Bobcat Operator/Utility	9:37-13:45	0.23
7/25/18	Loader Operator	9:30-13:47	0.021
7/26/18	Loader Operator	8:51-14:20	0.034
7/26/18	Dozer Operator	8:45-14:20	0.012
7/26/18	Sweeper Operator	8:42-14:29	0.080
7/26/18	Area Sample – Loadout Platform	11:05-13:57	0.091
6/14/19	Utility Worker	9:27-13:38	0.16
6/14/19	Area Sample – Crusher Level 1	10:20-14:15	0.98
6/14/19	Area Sample – Crusher Level 2	10:06-14:10	0.12

*10-mm Dorr-Oliver Cyclone, 2 lpm, pre-weighed 37-mm PVC filter, 5-um pore size, gravimetric measurement

The respirable dust concentration for all worker were well below the 1.5 mg/m^3 exposure limit – this result is consistent with previous compliance sampling results for this location and these job titles. Results for the Crusher area samples were 0.98 and 0.12 mg/m^3 for Level 1 (ground) and Level 2 of the building, respectively. Dust concentrations at ground level were significantly higher most likely due to the fact that material is fed from the bottom of the crusher located on the second level to a conveyor on the lower level and there are openings that allow dust to escape.

The crusher was running continuously during the time period sampled as coal was being processed in preparation for the next train. Although the crusher building is not typically occupied for long periods by workers while in operation, it was identified as a potential source of exposure and was later used as a sampling location for the performance demonstration of the wireless dust sensors.

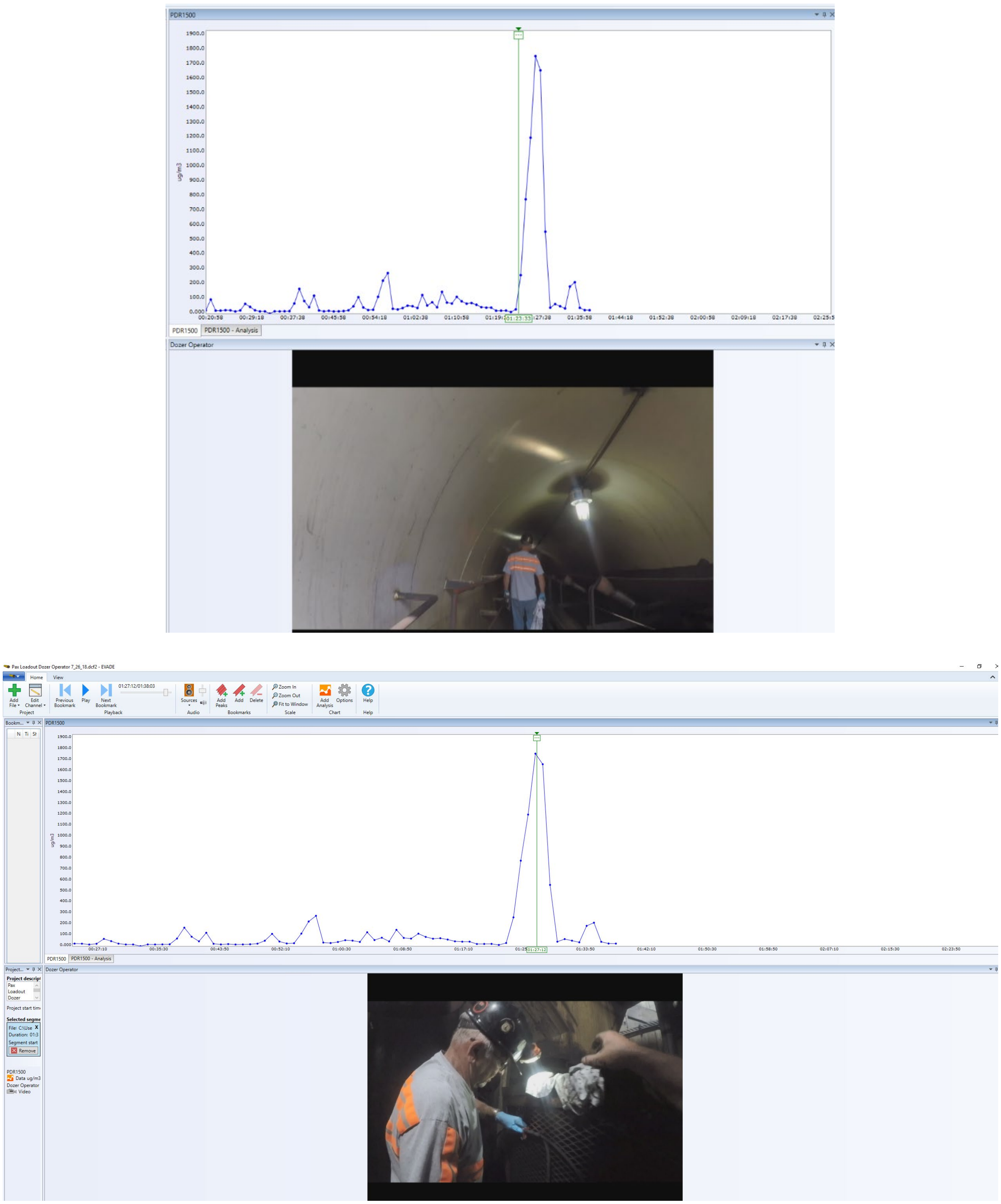

Figure 4.6. EVADE analysis for utility worker sample – truck dump belt tunnel – 6/14/19.

EVADE sample analysis proved to be very useful in identifying sources of exposure for the utility workers. While results for the equipment operators and fixed locations such as the dozer operator and scale operator showed relatively low and constant exposures to respirable dust, the utility worker position entails significant movement around the facility as workers lubricate and maintain conveyor belts at multiple locations. The EVADE software allows the recorded respirable dust exposure timeline to be reviewed very quickly and for the associated activities to be identified. Figure 4.6 shows an example of a significant spike in respirable dust exposure that occurred while the accompanying video indicates that this occurred as the utility worker entered the truck dump belt tunnel and proceeded to grease the conveyor belt. Although respirable dust sample results for utility workers were well below the MSHA PEL (Table 4.3), the average exposures for this position were higher than other jobs and the ability to pinpoint specific sources of exposure using EVADE would be very useful in controlling exposures even further.

Specific Aim 2 - Deploy and evaluate the performance of an integrated network of fixed- and mobile-wireless dust sensors capable of continuous real-time detection and reporting of respirable dust concentrations to a centralized location.

Research Objective 3: Design and deploy an integrated wireless respirable dust sensing network with centralized monitoring capability.

Research Objective 4: Evaluate the overall performance of the integrated wireless monitoring and response system for respirable dust.

There is extensive overlap in the Research Findings and Accomplishments for Research Objectives 3 and 4 so this content is combined in this report.

As described previously in the Research Approach section for Task 1.8, a wireless LoRa wide area network (LoRaWAN) was identified as the best wireless protocol for this project, and the subsequent selection of microprocessors and supporting hardware components was based on the availability of LoRa-compatible components. A preliminary laboratory demonstration of a single wireless dust sensing node was completed with results shown in Figure 4.7. The locally logged dust concentrations for the sensors and reference instruments are plotted in Figure 4.7a while the output from a single Sharp dust sensor was successfully transmitted wirelessly from within the dust chamber to a nearby LoRa gateway and then passed to a cloud-based data management system (ThingSpeak) using a Verizon mobile hotspot for transmission of data to the internet.

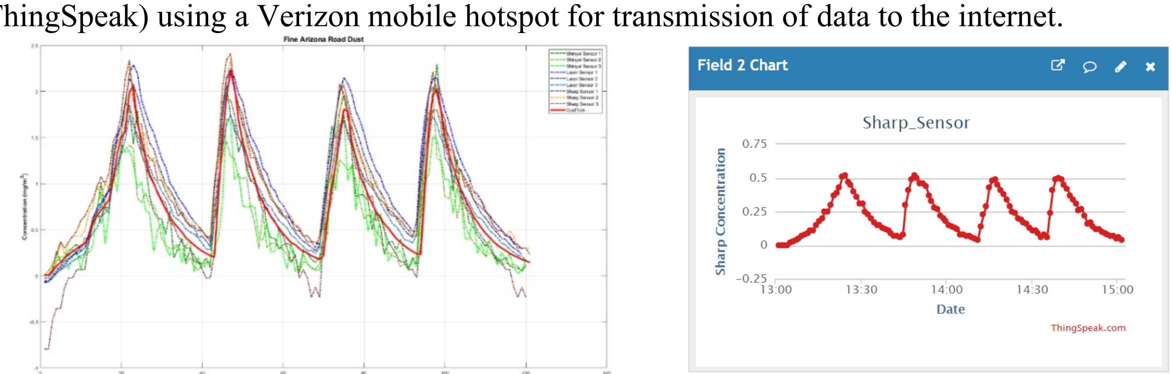

Figure 4.7. a) Locally recorded dust measurements versus b) wireless sensor data transmitted simultaneously to the cloud-based data management system for an A2 test dust experimental run.

After demonstrating wireless transmission of data in the laboratory, the first field demonstration of wireless dust measurement was conducted during a June 12-14, 2019, visit to the Pax Loadout facility. Details for this visit are described in the Research Approach section for Research Objective 3. Respirable dust sampling was conducted from approximately 10:15 AM to 2:15 PM at the Crusher Building Level 2 (Figure 3.9). Instrument measurements were monitored in real time using the Cayenne Mobile App for the prototype dust sensing nodes (Figure 4.8), and the Environet dashboard for the reference DustTrak DRX sensing node (Figure 4.9). Two of the prototype nodes (Uno3 and Uno4) successfully transmitted data from the Crusher Building to the gateway located in the Pax Loadout office at a distance of approximately 340 meters (Figure 3.10). The third prototype (Uno1) did not establish a connection at this range and was placed at another location (sampler crusher level of loadout) approximately 200 meters from the gateway where a connection was established. While LoRa devices have been demonstrated to achieve transmission distances of several kilometers, the current prototype devices and gateway have not been optimized in terms of the antennas used and placement of the gateway which are both critical for achieving the best range.

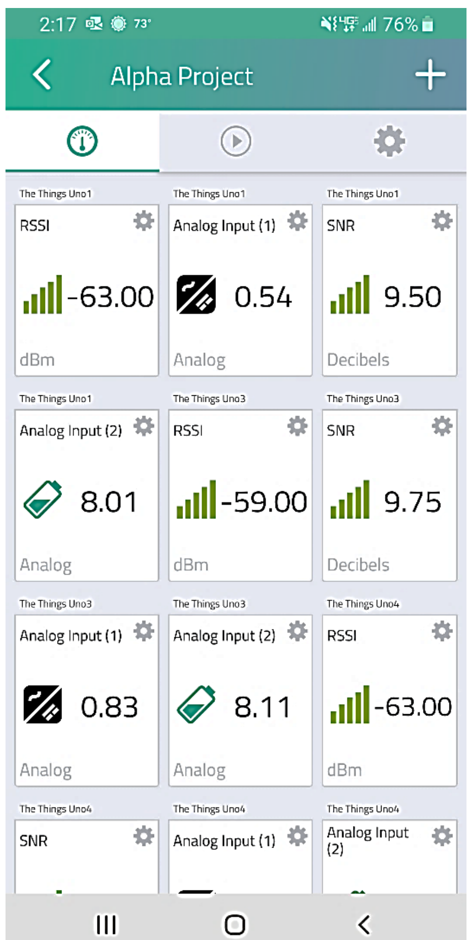

Figure 4.8. Smart phone screen capture showing dashboard display of output from three prototype dust sensing nodes. Display shows Received Signal Strength Indicator (RSSI), Signal to Noise Ratio (SNR), dust sensor voltage (Analog Input 1), and the battery voltage (Analog Input 2) for each dust sensing node (Uno1, Uno2, and Uno3), updated once per minute.

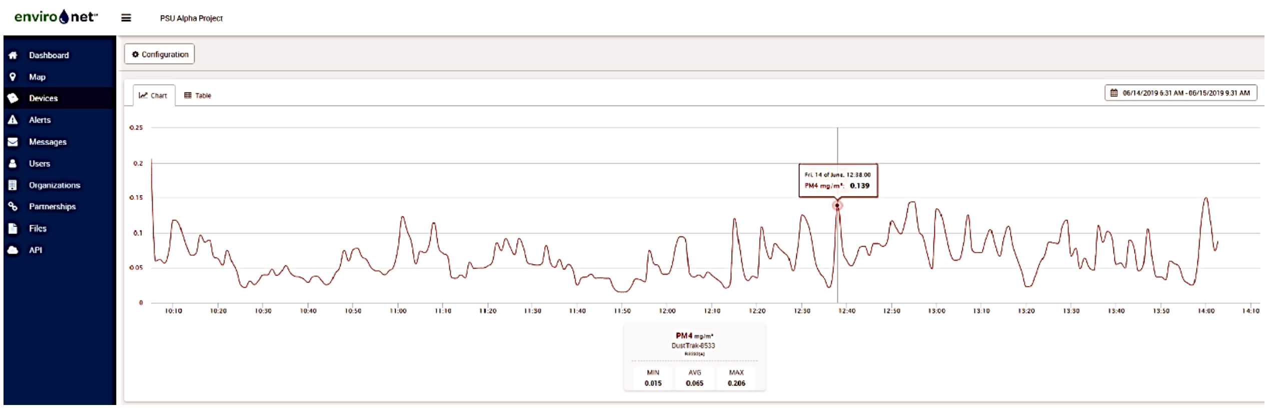

Figure 4.9. Environet cloud-based data management and display system showing dashboard and Dusttrak DRX measurements (each minute) for respirable dust (PM4) monitoring on June 14, 2019.

The prototype LoRa sensing nodes transmit data each minute but can experience packet loss depending on the strength of the signal and possible interference from other radio sources operating in the 915 MHz band. Over the course of this four-hour field demonstration, the Uno4 node successfully transmitted 83% of the packets which means that dust sensor output was received and displayed for 201 of the 249 minutes sampled. The Uno3 sensing node had a weaker signal despite being placed next to the Uno4 node and had a lower rate of transmission success with packet loss of approximately 50% (117 of 249 minutes sampled received). The third prototype sensing node (Uno1) achieved approximately 80% successful transmission at the sampler crusher level of the loadout which was 200 meters away from the gateway; however, since this location was not active at the time and there were no reference measurements taken, these results are not presented.

Prototype sensing nodes are programmed to send the average analog voltage from the Sharp dust sensor each minute. These numbers are then baseline-corrected and the pooled calibration result for Arizona Road Dust and coal (Figure 4.5) was used to convert the baseline-corrected voltage to a respirable dust concentration. Results for the reference dust sensing node (DustTrak DRX) also have to be calibrated/adjusted for a particular dust and this is done by calculating a correction factor using the results of the gravimetric respirable dust sample (Table 4.3 - Area Sample – Crusher Level 2, 0.12 mg/m^3). The correction factor (CF) is then calculated as the “true” average respirable dust concentration (0.12 mg/m^3) divided by the average (uncorrected) concentration measured by the DustTrak which was 0.065 mg/m^3: CF = (0.12 mg/m^3 / 0.065 mg/m^3) = 1.85. Therefore, each minute of logged data from the DustTrak is multiplied by the CF to yield the reference node respirable dust concentration. Finally, 15-min TWA average concentrations were calculated for the prototype and reference dust sensing nodes for comparison. The 15-min TWA is considered to be adequate for responding to changes in exposure conditions in practice and this average is significantly smoothed thereby aiding in comparisons and addressing the problem of missing data for the minutes when packet loss occurred for the prototype sensing nodes.

The results for the field demonstration of the prototype dust sensing nodes are presented in Figure 4.10a and 4.10b. Figure 4.10a shows the timeline for the respirable dust sampling and demonstrates excellent tracking of the reference dust sensing node results by the two prototype instruments. Results for the Uno3 node appear to be somewhat higher than the Uno4 and the

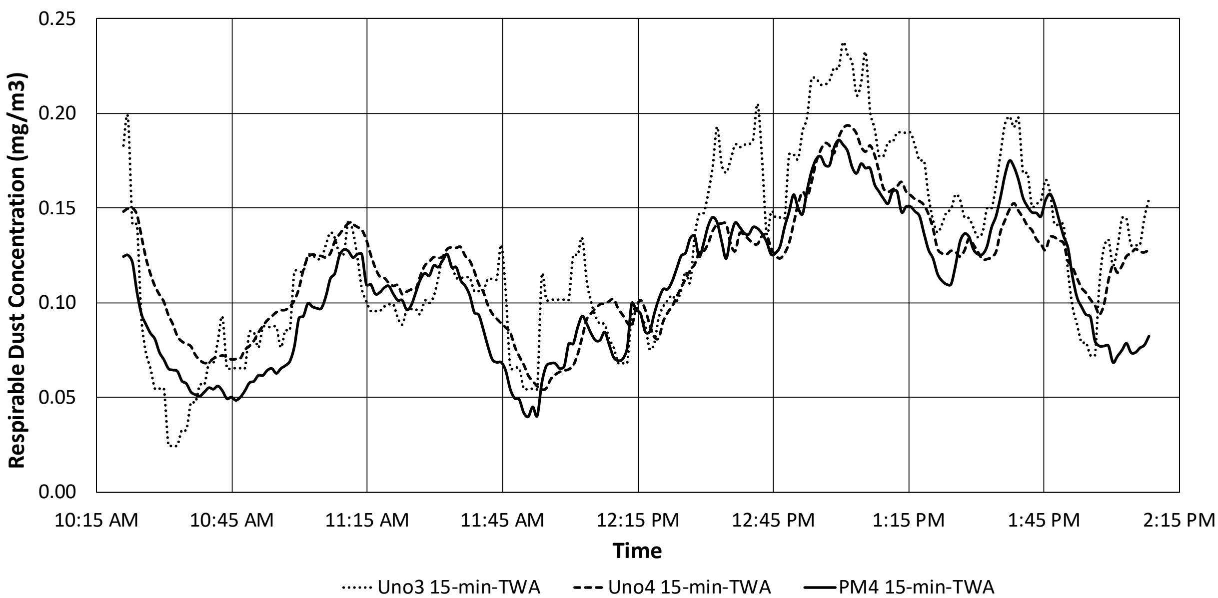

a)

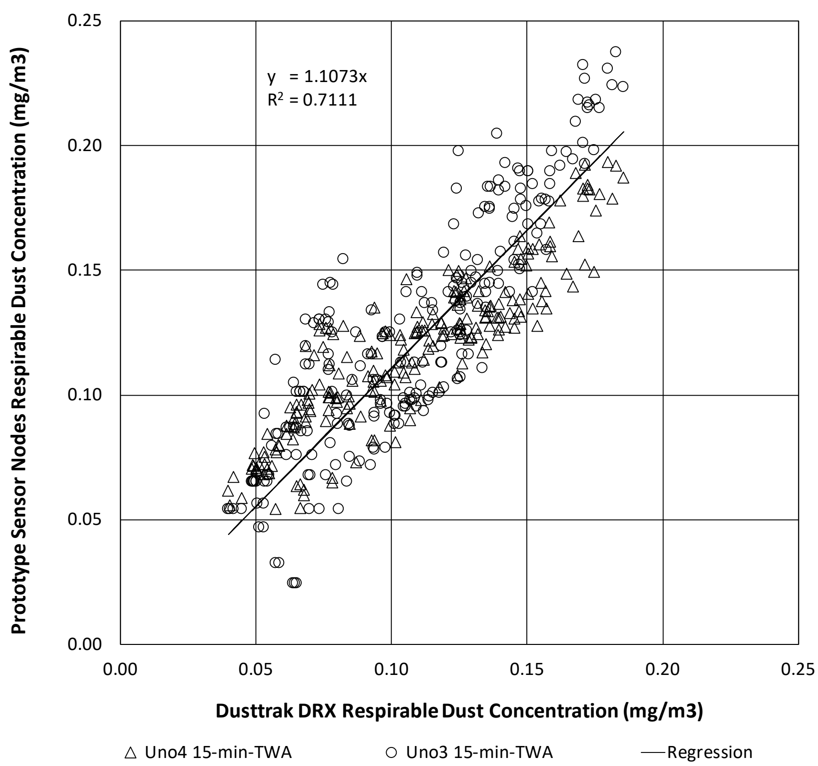

b)

Figure 4.10. Comparison of respirable dust concentrations measured by prototype wireless sensing nodes (Uno3, Uno4) and the reference dust sensing node (DustTrak DRX): a) sample timeline showing 15-min TWA respirable dust concentrations for each sampler and b) a plot of the prototype sensing node concentrations versus reference instrument results.

reference node, and are also noisier, most likely due to the higher packet loss of approximately 50%. Despite the packet loss, agreement between the prototypes and the reference sensing node was good with an average error of 15% relative to the reference node 15-min TWA concentrations. Figure 4.10b shows a scatterplot of prototype instrument 15-min TWA results versus the reference node results and further demonstrates the correlation between the measurements. The four-hour average respirable dust concentrations estimated by the prototype instruments were also in excellent agreement with the reference instrument with the Uno3 yielding a result of 0.14 mg/m^3, and the Uno4 a result of 0.11 mg/m^3, compared with the reference instrument result of 0.12 mg/m^3. It should also be noted that the respirable dust concentration range examined is on the low end of the range of interest which is approximately 0.5-2.0 times the OEL or approximately 0.8 – 3.0 mg/m^3 respirable dust.

Following the successful demonstration of wireless data transmission at Pax Loadout for the first three Prototype-1 units, the goal for the next field demonstration was to evaluate performance of the wireless dust sensing network on a larger scale with transmission over greater distances and for a larger number of sensing nodes. Toward that end, an additional 11 Prototype-1 units were fabricated bringing the total to 14 (Figure 4.11) and work also began on an improved second version of the dust sensing node (Prototype-2) to reduce power consumption, integrate the use of a rechargeable lithium-polymer battery, and develop weather resistant packaging. The improvement in power consumption and rechargeable battery were accomplished through incorporating a new microprocessor – the Adafruit Feather M0 RFM95 LoRa Radio - into the design of the node, and an appropriate weather resistant project enclosure was selected (Figure 4.11).

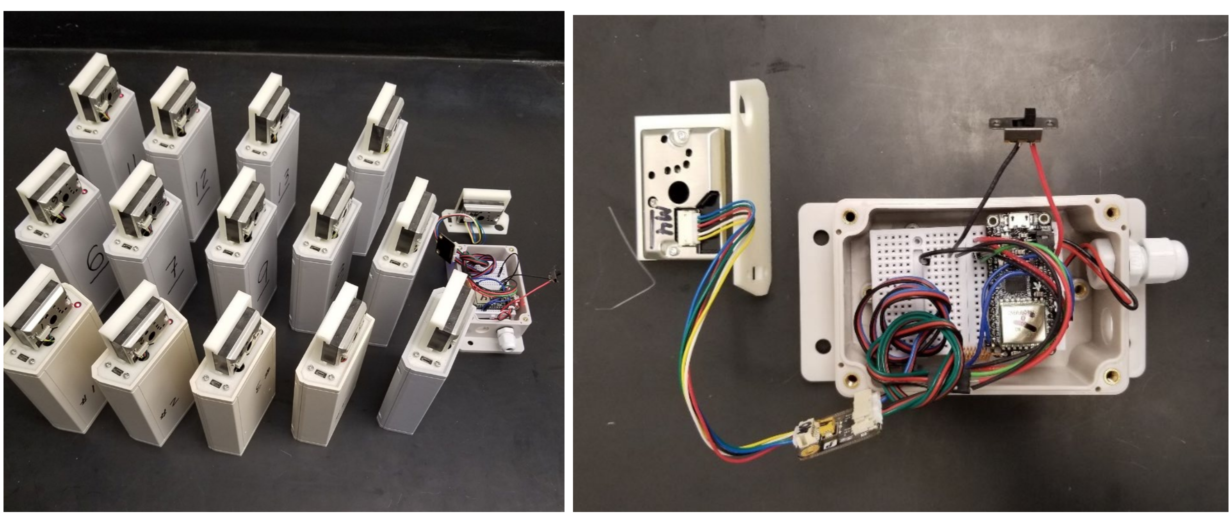

Figure 4.11. Fourteen Prototype-1 dust sensing nodes and a Prototype-2 dust sensing node based on the Adafruit Feather M0 RFM95 LoRa Radio (900MHz) microprocessor.

Prior to returning to the field the dust sensing nodes were calibrated for A2 Arizona Road dust. A total of 17 sensing nodes were placed in the dust chamber for calibration comprising 14-TTN Uno-based nodes (Prototype-1) and 3-Adafruit Feather m0-based sensing nodes (Prototype-2). Similar to previous calibration runs, respirable dust concentrations were varied over a range of approximately 0.3 – 3.0 mg/m^3, for a period of approximately 2 hours. One significant change for this experimental run was the use of wireless data transmission from all sensing nodes to the cloud-based data management server, rather than using individual local data-logging for each sensor. Data from the prototype sensing nodes was transmitted to a LoRa Gateway approximately once per minute.

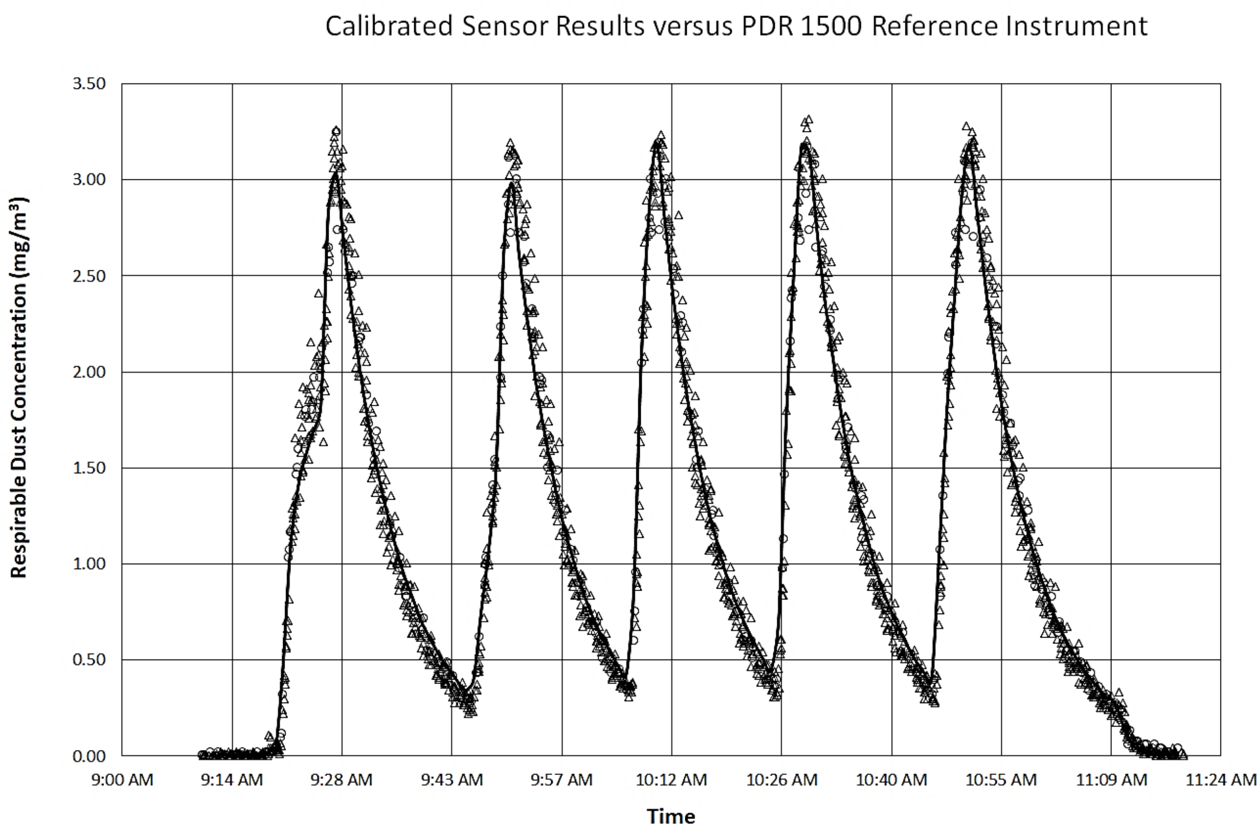

Figure 4.12. Combined ISO Fine (A2) respirable dust calibration results for 14-TTN Uno sensor nodes (uno1-uno14) (triangle symbols) and 3-Adafruit Feather M0 RFM95 LoRa Radio (900MHz) sensing nodes (m02-m04) (circle symbols) versus reference instrument results (Corrected PDR 1500 – solid line).

One-minute average sensor voltages for each node (n=17) were first transmitted from the dust chamber to the LoRa gateway which was located in a laboratory approximately 30 meters away. The gateway then transmitted the data packets to The Things Network (TTN) server by cellular connection. The TTN server passes the packets on to the Cayenne data service where results can be displayed and stored. At the completion of the run, the one-minute average sensor voltages for each node can be downloaded from the Cayenne site in the form of a comma delimited file (csv) for additional processing. Each sensor node's data was baseline corrected and stored in a master spreadsheet which contained a column of the one-minute average sensor voltages for each node and the corrected reference instrument respirable dust concentration results (Figure 4.13).

corrected PDR mg/m3	PDR 1500 Clock	Time	Time	uno1 bc Voltage	Time	uno2 bc Voltage	Time	uno3 bc Voltage
0.003	09:18:13	**9:18**	9:18:38	0.01	9:17:59	-0.01	9:18:24	0.00
0.013	09:19:13	**9:19**	9:19:41	0.04	9:19:07	0.00	9:19:27	0.09
0.017	09:20:13	**9:20**	9:20:44	0.06	9:20:05	0.02	9:20:30	0.03
0.433	09:21:13	**9:21**	9:21:47	0.64	9:21:08	0.20	9:21:33	0.64
1.067	09:22:13	**9:22**	9:22:50	1.23	9:22:11	1.06	9:22:36	1.50
1.391	09:23:13	**9:23**	9:23:53	1.40	9:23:15	1.22	9:23:39	1.74
1.560	09:24:13	**9:24**	9:24:56	1.67	9:24:17	1.61	9:24:42	1.95
1.690	09:25:13	**9:25**	9:25:59	1.74	9:25:20	1.59	9:25:45	2.18
1.817	09:26:13	**9:26**			9:26:23	1.48	9:26:48	2.41
2.826	09:27:13	**9:27**	9:27:02	2.26	9:27:26	2.62	9:27:50	2.89
3.038	09:28:13	**9:28**	9:28:05	2.95	9:28:32	2.80	9:28:53	2.86
2.686	09:29:13	**9:29**	9:29:08	2.61	9:29:32	2.27	9:29:56	2.53
2.348	09:30:13	**9:30**	9:30:10	2.27	9:30:34	1.83	9:30:59	2.27
2.050	09:31:13	**9:31**	9:31:13	1.90	9:31:37	1.64		
1.796	09:32:13	**9:32**			9:32:40	1.31	9:32:02	2.02
1.575	09:33:13	**9:33**	9:33:19	1.40	9:33:51	1.21	9:33:05	1.67
1.384	09:34:13	**9:34**	9:34:22	1.11	9:34:46	0.96	9:34:08	1.38
1.217	09:35:13	**9:35**	9:35:25	1.07			9:35:11	1.23
1.066	09:36:13	**9:36**	9:36:28	0.85	9:36:52	0.71	9:36:14	1.06
0.934	09:37:13	**9:37**	9:37:31	0.71	9:37:55	0.58	9:37:17	0.91
0.829	09:38:13	**9:38**			9:38:58	0.57	9:38:20	0.80
0.719	09:39:13	**9:39**					9:39:23	0.65

Figure 4.13. Master data worksheet for calibration results showing synchronization of reference instrument and sensing node results (showing only uno1 - uno3 columns).

Synchronization of the sensing node voltages with the reference instruments results is not a trivial matter as the time that individual sensing node results are transmitted is not precisely coordinated across devices, and there can also be the occasional packet loss meaning that a node may not have a reported result for every minute of the run. This is not expected to significantly affect the ability to make real time decisions as a 15-min TWA concentration should be adequate for that purpose and the loss of a small number of packets would not be expected to significantly alter that result.

The processed data for the calibration run are presented in Figure 4.14a-b for the two types of sensing nodes (TTN Uno and Adafruit Feather m0). Sensor responses are highly correlated and linear with respect to the reference instrument results. While variability around the regression line is apparent and there are some points located a significant distance away, these are generally associated with the times at which the concentration is changing rapidly and appear to reflect several factors including spatial and temporal variability within the dust chamber, as well as slight synchronization discrepancies across the sensing nodes. However, it is clear that on average this variability is moderated as reflected by the linear nature of the sensor response versus respirable dust concentrations and the relatively high r^2 values of 0.94 - 0.96.

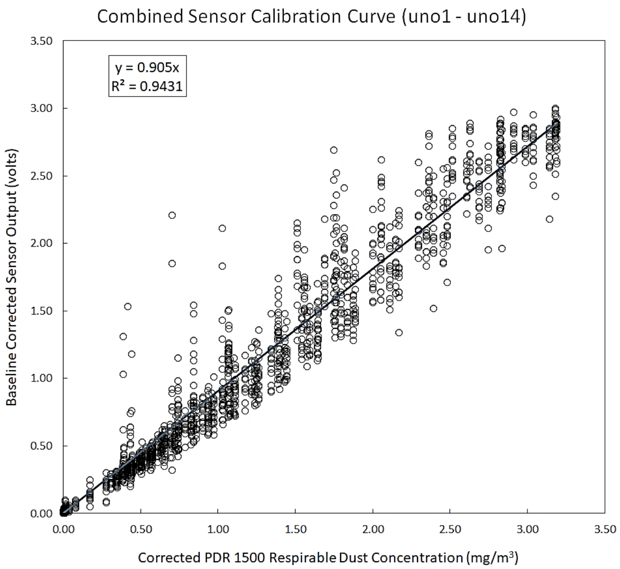

Figure 4.14. ISO Fine (A2) respirable dust calibration results for a) 14 TTN Uno sensor nodes (uno1-uno14) and b) three Adafruit Feather M0 RFM95 LoRa Radio (900MHz) sensing nodes (m02-m04), 10/4/19.

The slope of the regression line for the Uno-based sensor nodes was 0.905 volt / (mg/m^3) which compares favorably with the previously reported overall average result of 0.916 volt / (mg/m^3) for A1, A2, and A3 ARD and coal dust. The calibration curve for the Feather m0-based sensing nodes shows similar correlation between voltage and respirable dust concentration but has a different value for the slope of the regression line. This is to be expected since the Feather-m0 microprocessor is a based on 3.3V power / logic while the Uno is a 5V device. The Sharp dust sensor datasheet indicates that the sensor is designed to be operated with a 5V supply; however, since the Feather m0 runs at 3.3V and there was the potential for significant power savings using this device, the calibration run was conducted with the Sharp dust sensing module running at 3.3V. The device functioned normally at the lower voltage other than the different sensitivity as depicted in Figure 4.14b where the slope of the calibration curve is 0.53 volt / (mg/m^3), and therefore will be used in this configuration moving forward.

Results from the sensor calibrations were used to convert the recorded sensor node voltages for the Uno- and Feather m0-based devices to respirable dust concentrations which are presented in Figure 4.12 along with the reference instrument results (PDR 1500 - solid line). These results again demonstrate the excellent tracking of dust concentrations by the Sharp dust sensors for both the 5V and 3.3V microprocessors, and also the relatively low variability of the Sharp dust sensor response across devices – the approximately 2,000 data points represent the individual responses of 17 different sensing nodes from two different microprocessor sensing platforms and are in excellent agreement as shown in Figure 4.12.

In preparation for field testing on a larger scale, an outdoor LoRa gateway was purchased which offered many performance improvements including a weatherproof enclosure (IP-67), the capability for transmitting data to the internet by direct ethernet or cellular connection, and a higher gain antenna. Mine personnel identified the Pax North and South surface mines as potential locations for the wireless network testing and the ability of the LoRa gateway to transmit data via cellular modem was vital as access to direct wired ethernet connections was very limited at the surface mines. Further, locations that did have internet access (Field Offices) were not necessarily optimal for reception from dust sensing nodes.

Figure 4.15. Portable LoRa Gateway – South Substation.

Two potential gateway locations were examined at the Pax surface mines during the October 10-11, 2018, site visit. Locations were selected to be central to operations, elevated, and with cellular access. The LoRa Gateway (Figure 4.15) receives signals from any sensing nodes within range and passes the data to the internet via cellular service. The best performance for the wireless network is achieved when the gateway is placed such that there is line-of-sight between the gateway and nodes, which is often enhanced by an elevated placement of the gateway.

Results for the preliminary testing of the two gateway locations are summarized in Table 4.4. The first gateway location examined was identified as the South Substation and five dust sensing nodes placed at the South Field Office, Light Plant 1806, Light Plant 1802, the Repeater Station, and Little Eagle South successfully established connections with the gateway and passed data to the cloud-based data management server. Distances ranged from approximately 0.7-1.2 km. The second tested gateway location (Repeater South) was only able to establish a connection with two sensing nodes, although one of these was at a range of 2.3 km. Results emphasize the importance of an unobstructed line of sight between node and gateway, as well as range, in determining the success of each node in connecting to the gateway.

Table 4.4. Summary of LoRa gateway location results – nodes connecting and range

Gateway Location	South Field Office	North Field Office	LP1806	LP1802	Curve	34 Marker 25 Haul Road	Repeater Station	Little Eagle South
Substation / South (10/10/19)	OK (1.1 km)	?	OK (1.0 km)	OK (1.1 km)	?	?	OK (0.74 km)	OK (1.2 km)
Repeater / South (10/11/19)	OK (1.3 km)	OK (2.3 km)	Poor (1.3 km)	Poor (1.8 km)	Poor (0.78 km)	Poor (1.6 km)	NA	?

Following the successful field demonstration of data transmission over longer ranges at the Pax Surface Mines, work focused on the development and demonstration of solar power for the sensing nodes and LoRa gateway. This capability was required for planned longer deployments of the wireless dust sensing network for surface mines since the remote locations have very limited availability of power. The design of remote power systems for off-grid field studies requires several steps including a determination of individual power requirements, determination of battery requirements, determination of the size and orientation of the solar panel, selection of a charge controller, and field testing of the resulting design. This approach was applied to the development of remote power systems for the wireless dust sensing network using the Prototype-2 sensing node.

Power requirements for the sensing node were estimated to be approximately 75 mW based upon the specifications of the microprocessor and measurements of current during LoRa transmissions. This results in a power requirement of 1.8 watt-hour (Wh) per day assuming 24-hour operation of the network (0.075 W x 24 Hr = 1.8 Watt-Hour). The power requirement for the LoRa gateway was estimated in a similar fashion and the result was 168 Watt-Hour per day.

Sizing of a battery is based on several variables including the power requirements of the device, type of battery (e.g., lead-acid, lithium ion), the extent to which the battery can be discharged without damage, derating factors for inefficiency and temperature effects, and the desired number of days of operation without sun (days of autonomy). For three days of autonomy, 80% discharge, a derating factor of 1.2, and an operating voltage of 3.7V, the required capacity for a lithium-polymer type battery to power the dust sensing node was estimated to be approximately 2.2 amp-hours (Ah). Similar calculations for the LoRa gateway assuming three days of autonomy, 50% discharge (lead-acid battery), derating factor of 1.4, and an operating voltage of 12V resulted in a required battery capacity of 120 Ah.

Design of the photovoltaic panel including wattage and orientation is based on a number of factors including device power requirements and geographical location which determines the amount of solar energy typically available and the optimal tilt angle for the panel. Based on the field site location in WV, all solar panels should face due South, and the optimal tilt angle for maximizing solar energy in the winter is approximately 61 degrees. Using the energy requirements of the dust sensing node (1.8 Wh), peak sun hours (PSH) of 3.45 hours, and a derating factor of 1.5 it was estimated that the photovoltaic wattage required was approximately 0.8 watts. Similar calculations for the LoRa gateway yielded a result of 74 watts for the solar panel.

The results of these design calculations were used in the selection of components, and subsequent assembly, and preliminary testing of remote power systems in preparation for the planned long-term field testing of the wireless dust sensing network. More complete versions of these calculations are provided in an Appendix.

In preparation for the deployment of dust sensing nodes to remote locations, an appropriate photovoltaic panel, rechargeable battery, and charge management module (Figure 4.16) were identified and incorporated into a prototype sensing node. The panel selected is a flexible, waterproof, monocrystalline design with up to 21% conversion efficiency, 5V operating voltage, and 5W power capacity. The panel measures approximately 29 x 15 x 0.135 cm and has a working temperature range of -20 to 60 °C. The high efficiency solar management module is designed for a 5V solar panel and employs a MPPT (Maximum Power Point Tracking) function to maximize efficiency while providing up to 900mA charging current to a 3.7V Li battery. The battery selected is of lithium-ion polymer construction (LiPo) with output ranging from 4.2V when completely charged to 3.7V, and a capacity of 2000mAh.

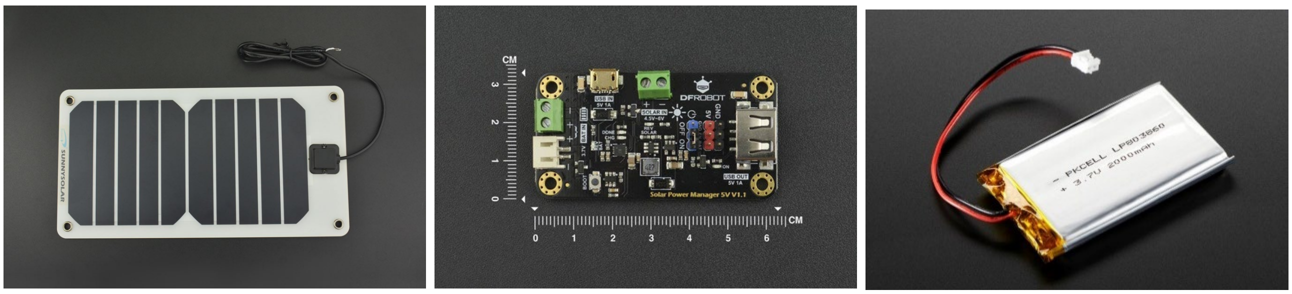

Figure 4.16. Components for photovoltaic battery charging consisting of a) solar panel (DFROBOT), b) solar power manager module, and c) rechargeable lithium-ion battery.

The resulting solar powered prototype dust sensing node was mounted on a 6-foot T-post using brackets shaped to provide appropriate support for the solar panel and sensor enclosure (Figure 4.17). For preliminary testing, the solar panel was installed facing the equator at an angle approximately equal to the latitude of the location which was 40.8 degrees.

The solar powered dust sensing node was deployed locally for the purpose of evaluating performance and determining whether the selected panel, battery, and charge manager module function properly and are sized adequately to maintain continuous operation. Weather during this time frame was mostly sunny with occasional rain and one instance of heavier cloud cover and a downpour. The programming of the dust sensing node includes provisions for reading and transmitting battery voltage each minute and a plot of these data is shown in Figure 4.18. There are approximately eight days / cycles shown in the figure, with battery voltage generally increasing during daylight hours, until the battery is fully charged at approximately 4.2V, and at which time the charge manager cycles off and the battery charge begins to be depleted as the instrument continues to draw power. During daylight, once the battery charge decreases to approximately 4.1V the charge manager begins recharging the battery again. This daytime cycling of the charge manager function explains the series of voltage peaks seen during daylight hours for each cycle in Figure 4.18. The longer/larger battery voltage decay that is seen occurs between sunset and sunrise each day with the voltage generally decreasing from a peak of approximately 4.2V to a minimum of 4.0V.

Figure 4.17. Solar powered wireless dust sensing node consisting of the solar panel and prototype instrument package mounted with support brackets on a 6-foot T-post driven into the ground.

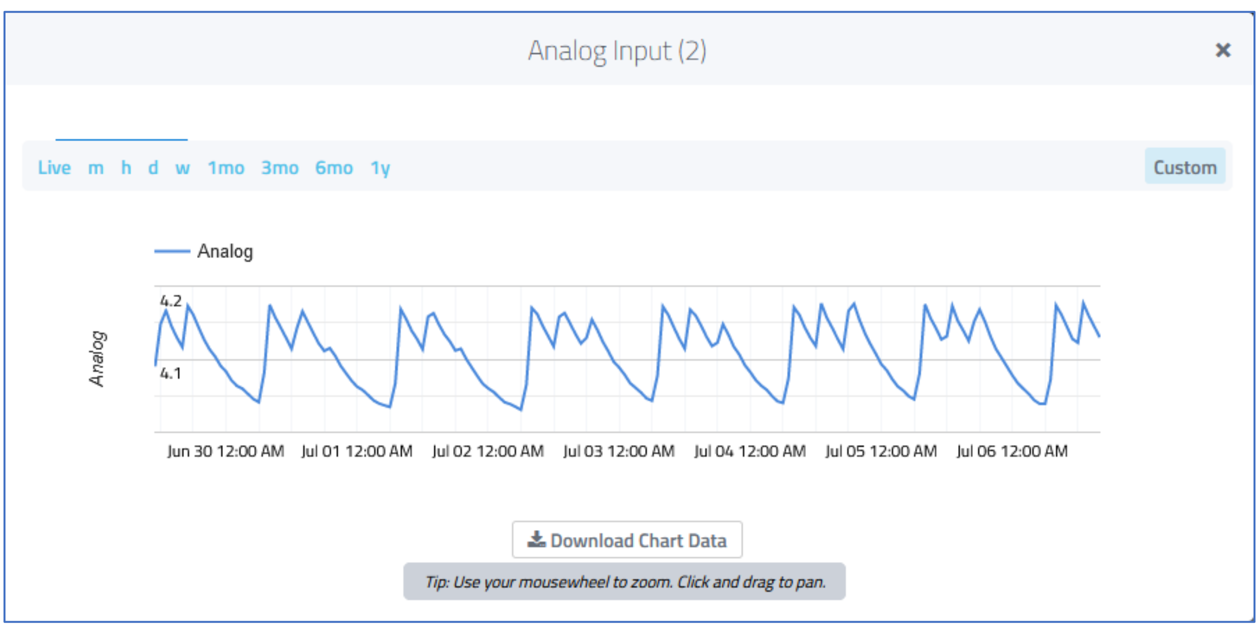

Figure 4.18. Battery voltage for wireless solar powered dust sensing node over approximately one-week period.

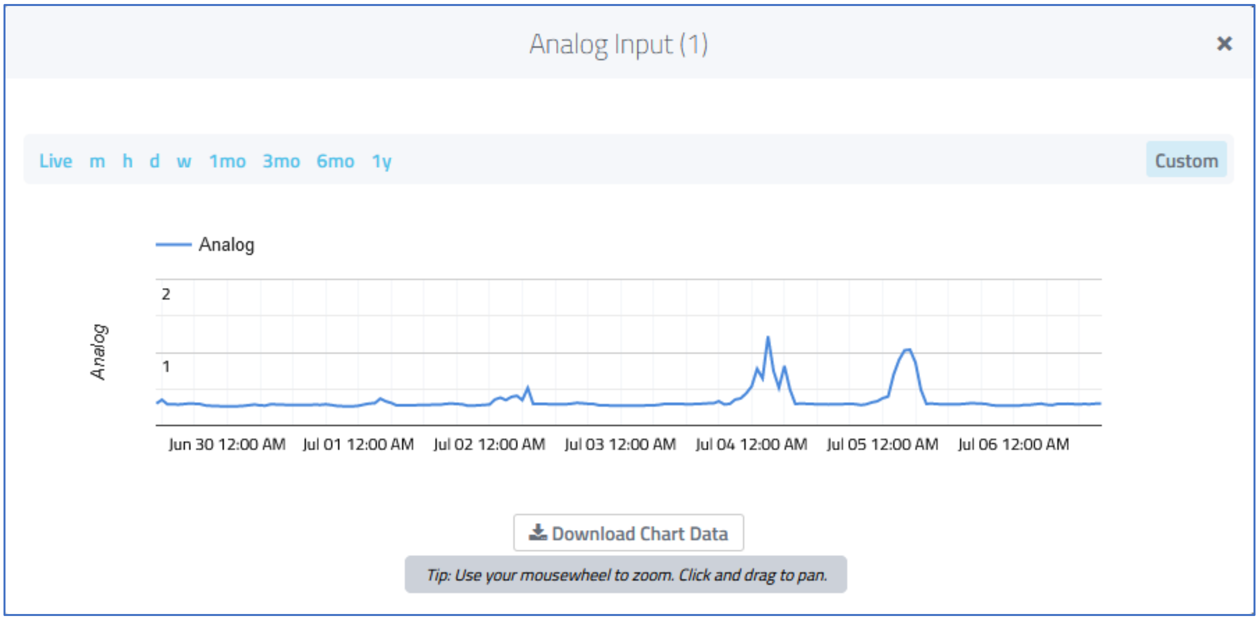

Figure 4.19. Dust sensor voltage for wireless solar powered node over one-week period.

The corresponding dust sensor output for the solar powered sensing node is shown in Figure 4.19 for the eight-day period. The baseline voltage for this particular sensor is approximately 0.28V and there is little deviation from this value during daylight hours. This is due to the fact that there were no significant dust-producing operations at this location and ambient dust levels are relatively low. However, there were several elevations in sensor output voltage that occurred during daytime precipitation events and overnight when conditions promoted the formation of fog and/or condensation within the dust sensor. In these instances, it was found that a can of compressed air could be used to carefully blow out the sensing region of the dust sensor, thereby restoring the baseline output, but in several cases the sensor returned to the original baseline output once the unit was exposed to direct sun and without any intervention.

A photovoltaic (solar) power management system was also developed and tested for the LoRa gateways based on a 12V, 100Ah deep cycle AGM SLA lead-acid battery, and a 100W, 12V monocrystalline solar panel. These components along with a pulse width modulation (PWM) solar charge controller were assembled in a Pelican-style weatherproof case and then used to power the gateway (Figure 4.20).

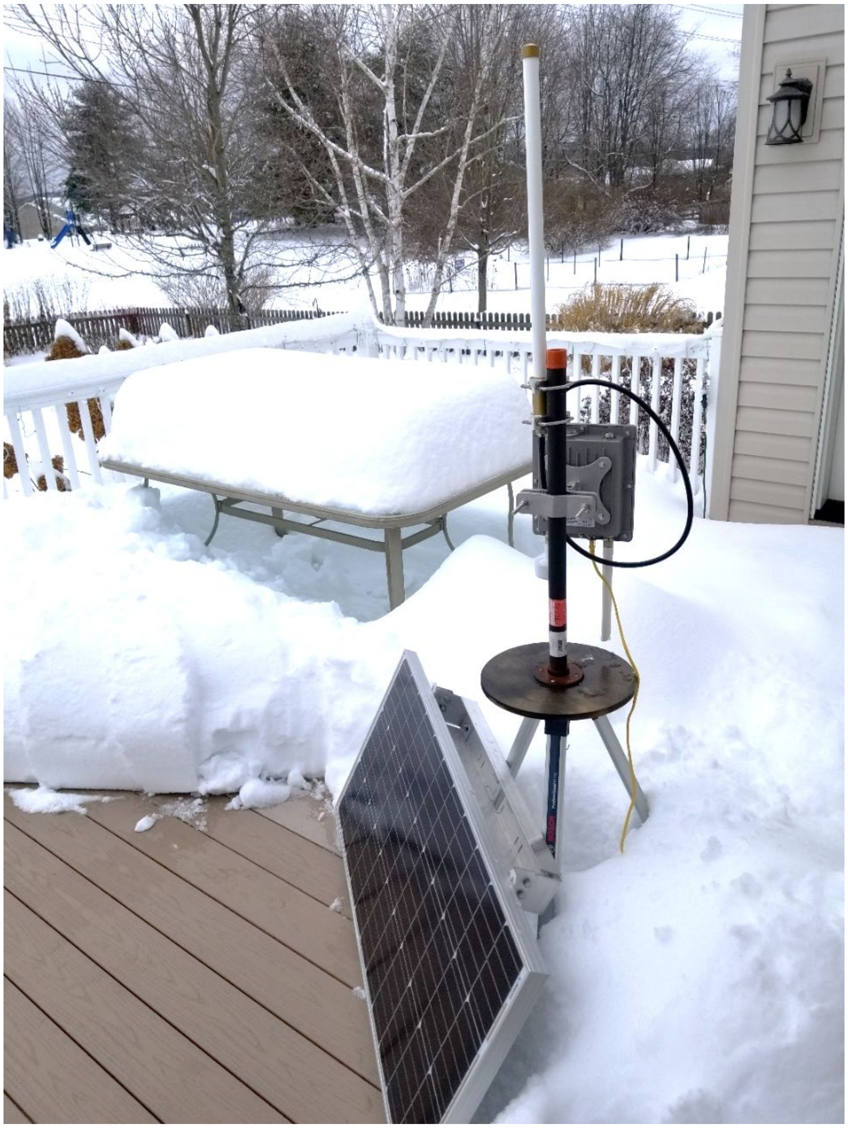

Figure 4.20. LoRa gateway with solar panel (deep discharge SLA battery and solar charge manager housed in pelican-type case which is beneath snow).

In final preparation for the planned large-scale deployment and testing of the dust sensing network, additional dust sensing nodes were fabricated along with modifications and improvements to the hardware including the design and implementation of a photovoltaic battery charging system, and provision for mounting of the sensing nodes in remote field locations using an improved weather-resistant project box. Thirteen of the original prototype sensing nodes are shown in Figure 4.21a along with 13 of the second-generation prototype sensing nodes. An enlarged view of the second-generation prototype is shown in Figure 4.21b with the enclosure top, dust sensor, and holder removed. In addition to the Feather m0 microprocessor, the project box (Fig 4.21b) contains a Maximum Power Point Tracking (MPPT) solar battery charge manager module and an attached lead (red and black wire and plug) used for connecting the node to a photovoltaic (solar) panel.

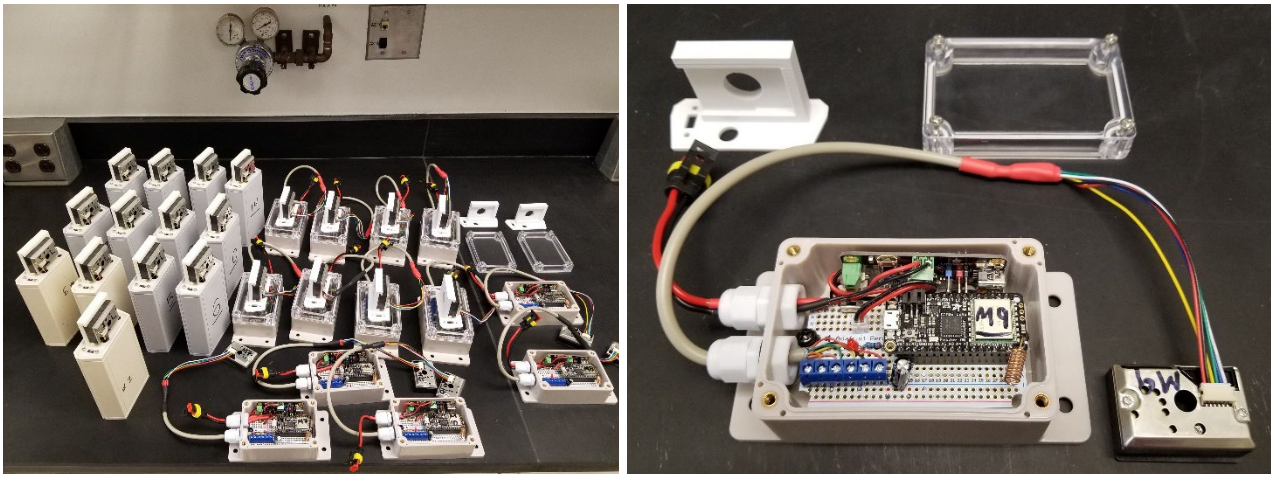

a) b)

Figure 4.21. Prototype dust sensing nodes including a) thirteen of the original Prototype-1 nodes based on The Things Network Uno (TTN Uno) and thirteen of the second-generation prototypes (Prototype-2) with the Feather m0 RFM95, and b) an enlarged view of the second-generation sensing node with weather resistant enclosure.

Prior to returning to field work in May 2021, a laboratory calibration of the dust sensors was conducted on April 30, 2021. Five each of the Uno (Prototype-1) and m0 (Prototype-2) sensing nodes were placed in the dust chamber and calibrated against the PDR 1500 reference direct reading instrument using ISO A2 Arizona Road Dust over a range of approximately 0.3-3 mg/m^3 respirable dust. Results are presented in Figure 4.22. Overall results were in excellent agreement with previous calibration runs with a slope of 0.92 volt/mg/m^3 (previous result of 0.90 volt/mg/m^3) for the Uno nodes and 0.52 volt/mg/m^3 (previous result of 0.53 volt/mg/m^3) for the m0 sensing nodes. Current results were within 5% of previous calibration results demonstrating the reproducibility of sensor node performance.

During a May 19-21, 2021, site visit to the Pax Loadout facility, six each of the Prototype-1 and Prototype-2 sensing nodes were deployed to evaluate wireless dust sensing network performance including data transmission using a new gateway located on top of the loadout (Figure 4.23), and to compare dust sensor measured concentrations to reference direct-reading instruments (PDM 3700, DustTrak DRX, and PDR 1500) and gravimetric sample results for respirable dust. Reference direct-reading instruments were placed at three locations expected to have the highest respirable dust concentrations based on previous site visits: 1) Crusher / Sizer, 2) Clean Coal Stacker Belt, and 3) Truck Dump Belt. One each of the Prototype-1 (Uno) and Prototype-2 (m0) nodes and a gravimetric sample were also placed at each location. An additional three sampling locations were selected to span the area of the loadout facility to evaluate data transmission.

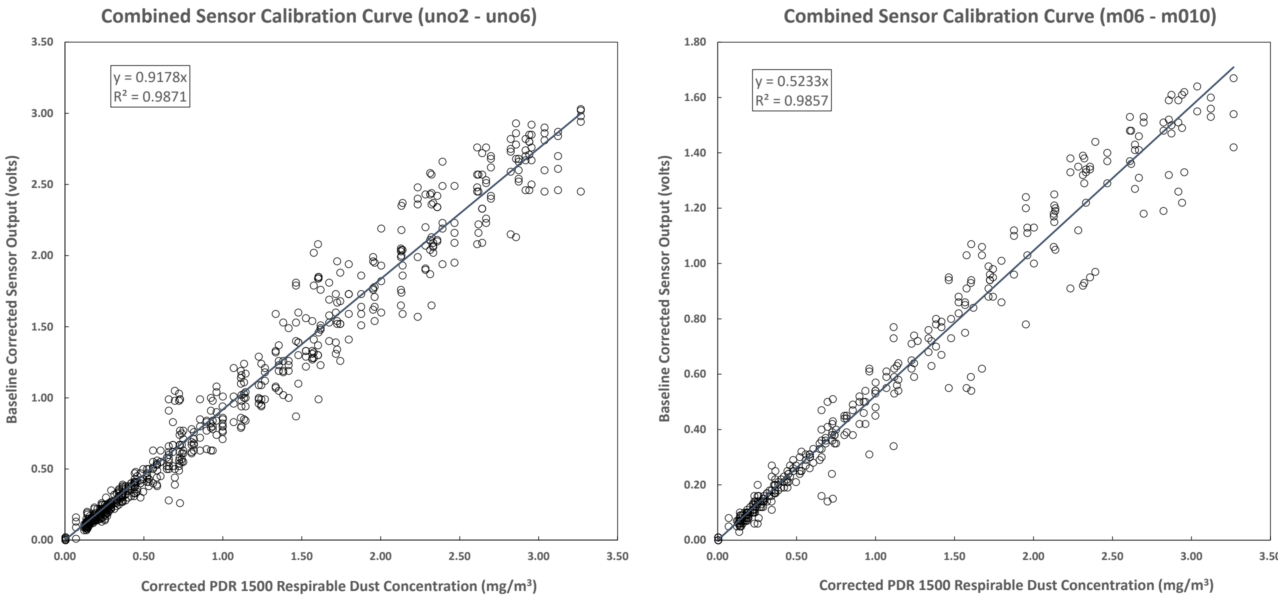

Figure 4.22. Laboratory respirable dust (ISO A2 ARD) calibration results for Uno and m0 sensor nodes – PRD1500 reference direct reading instrument versus five each of Uno and m0 sensors – 4/30/21.

Figure 4.23. Pax gateway position a) on top of loadout structure, and b) DustTrak DRX, Uno and m0 nodes, and gravimetric sampler at Crusher / Sizer – Pax Loadout 5/10/21.

Respirable dust sample results are summarized in Table 4.5 with sample locations shown in Figure 4.24. Agreement between the dust sensing nodes and gravimetric sample results was relatively good for the three locations with the highest dust concentrations with an overall error of 20% (sd = 8%) and errors ranging from -0.4 - 40%. Sensor node performance was poor for the three locations with the lowest respirable dust concentrations; however, the nodes are calibrated for occupational exposure assessment in the range of the 1.5 mg/m^3 respirable dust exposure limit and are not intended to be used for quantification of concentrations more than an order of magnitude lower than the PEL. Agreement between the dust sensing nodes and reference direct reading instruments was very good as shown in Figure 4.25 with the sensors tracking reference instrument results closely.

Results in Table 4.5 also demonstrate excellent data transmission for the m0 sensing nodes with packet loss less than 1.5% for all locations and transmission distances up to 600 m. The Uno nodes did not perform as well with packet loss ranging from 4.5-15%, likely due to the difference in the antennae used for the nodes – the Uno boards use a copper antenna that is integrated onto the microprocessor board while the m0 nodes uses a separately mounted coiled-spring antenna which seems to result in better range.

Table 4.5. Respirable dust sample results (mg/m^3) – Pax Loadout – May 20, 2021

Location	Sample Time	Gravimetric [1]	m0 Sensor (error) [2]	Uno Sensor (error) [2]	Distance to GW	m0 (v2) PL[3]	Uno (v1) PL[3]
Sizer / crusher	10:00-14:20	0.264	0.340 (29%)	0.284 (8.0%)	270 m	< 1.0%	15%
Clean coal stacker belt	10:32-14:30	0.119	0.158 (33%)	0.119 (-0.40%)	190 m	1.5%	4.5%
Truck dump belt	10:58-14:28	0.180	0.202 (12%)	0.253 (40%)	300 m	1.5%	13%
Auger	11:10-14:56	0.039	0.078 (100%)	0.061 (56%)	270 m	0%	11%
Pax main entrance	11:20-15:19	0.044	0.085 (93%)	0.054 (23%)	200 m	0%	8.5%
Sediment ponds	11:35-14:45	0.032	0.12 (280%)	0.092 (190%)	600 m	0%	10%

[1] 2.0 L/min, 10-mm Dorr-Oliver Cyclone, pre-weighed 37-mm PVC filter, 5-um pore size
[2] Percent error relative to gravimetric result
[3] Packet loss

Figure 4.24. Pax locations for air samples, sensor nodes, and LoRaWAN gateway – 5/20/21.

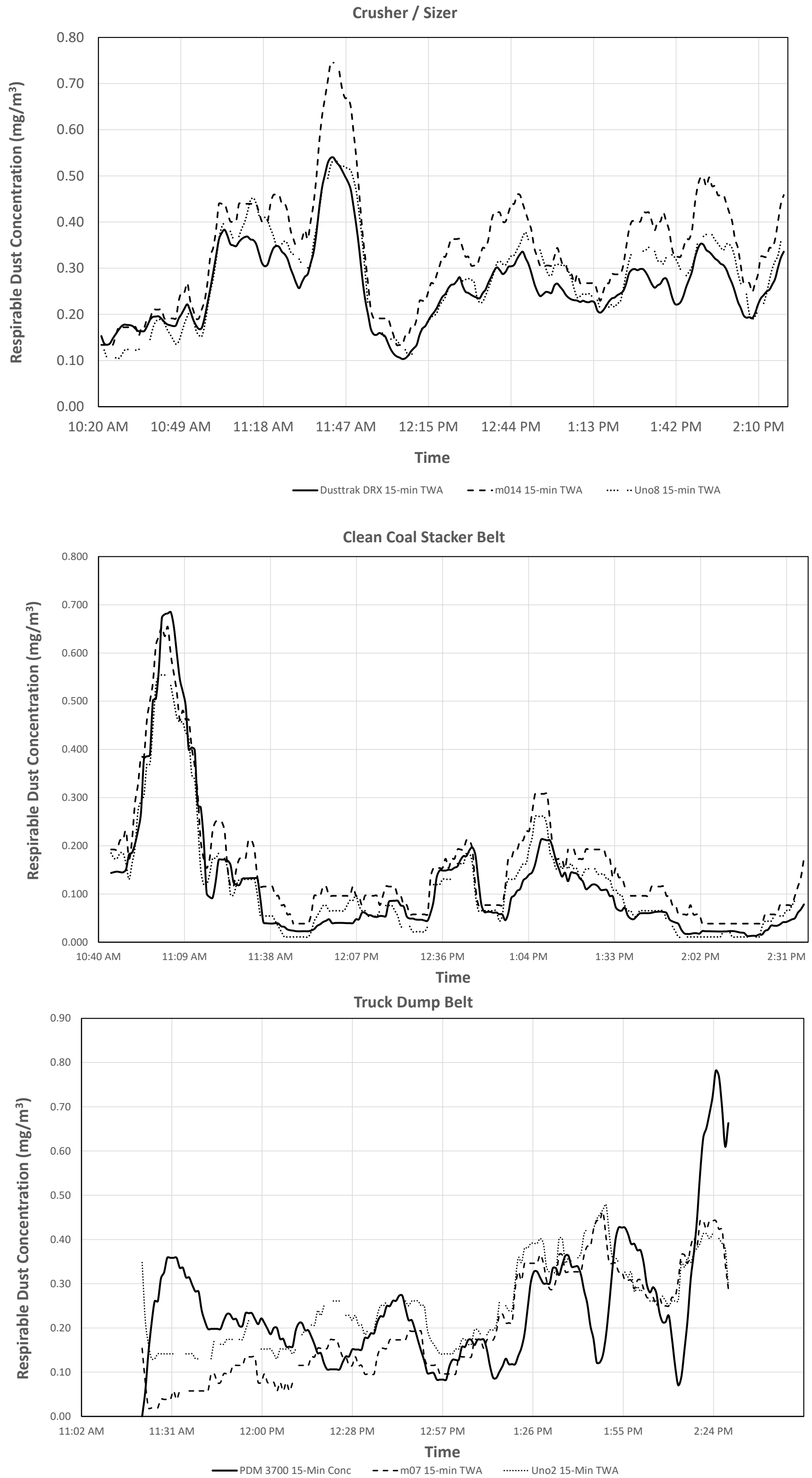

Figure 4.25. Reference direct reading instrument respirable dust concentrations versus dust sensing nodes for the Crusher/Sizer, Clean Coal Stacker Belt, and Truck Dump Belt locations.

Following the successful field testing at Pax Loadout, the complete wireless dust sensing network including 13 solar-powered dust sensing nodes and a solar powered gateway was deployed at the Workman Creek North (WCN) surface mine from June 10 – July 15, 2021. Sensor nodes were placed in portable sampling stations that were fabricated by WCN personnel to secure respirable dust monitoring equipment (Figure 3.14). The gateway placement is shown in Figure 3.15 and while not permanently installed, the system functioned continuously for approximately one month.

Figure 4.26 shows the cloud-based dashboard for monitoring solar panel and gateway battery voltages and it can be seen that the battery voltage never fell below 13.4V which is approximately fully charged for the type of lithium battery employed.

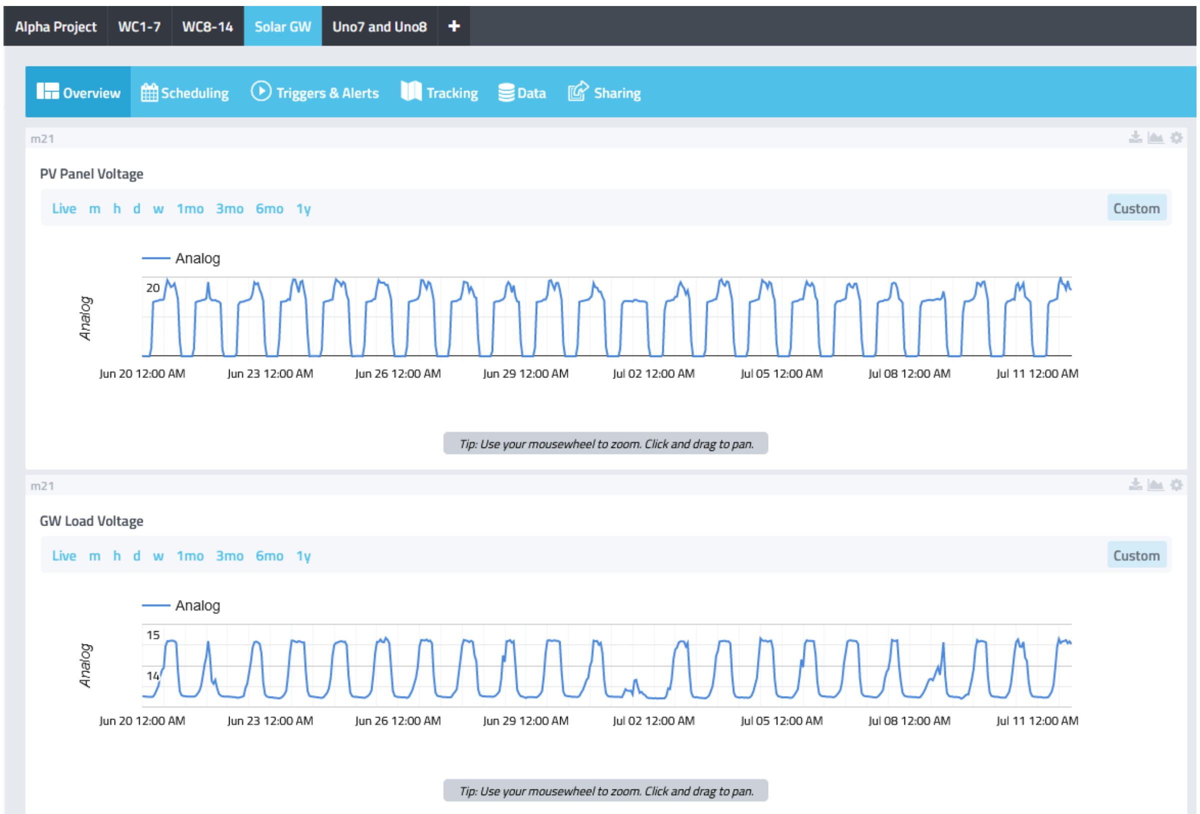

Figure 4.26. WCN LoRa gateway with solar power showing a) shot occurring in background and water truck in foreground, and b) monitored solar panel and battery voltage while deployed for the period of June 11 – July 11, 2021.

Figure 4.27. Workman Creek North sensor node and gateway locations – 6/11/21.

Table 4.6. Workman Creek North Sensor Node Locations – 6/11/21

Location	Node	Description	GPS	Elev.	SNR[1]	Distance (miles)	Packet Loss[2]
#1	m05	Offsite Employee House (14)	37.91575, -81.34669	1508	-13 – (-12)	1.5 (2.4 km)	100%
#2	m012	Pax Guard House Pax Haul Road Guard House (13)	37.89617, -81.33996	1633	-15 – (-7.5)	2.1 (3.4 km)	100%
#3	m011/m013	Warehouse Workman Creek Warehouse (12)	37.89094, -81.35694	1650	-13.8-1.0	1.6 (2.6 km)	99% / 66%
#4	m09	CP WCN Field Office (3)	37.89605, -81.37033	2368	5.0-13	0.99 (1.6 km)	3%
#5	m06	Valley Fill Access McDowell 1 (1)	37.89992, -81.37250	2199	1.8-9.5	0.71 (1.1 km)	5%
#6	m07	Valley Fill Pond WCN Pond (2)	37.90005, -81.37772	2159	-14-10	0.73 (1.2 km)	10%
#7	m014	3-Pole Structure Power Line Structure (10)	37.89330, -81.38464	2884	-11.8-10.5	1.3 (2.1 km)	6%
#8	-	Collins Fork High Point (11)	37.8963, -81.3767	2674	-	-	
#9	m018	Top Fill of Dozer Box Cut (LP1705) Unnamed (9)	37.89517, -81.38086	2810	-9.8-6.0	1.1 (1.8 km)	6%
#10	m016	Island Dozer Box 1 -2 (8)	37.90047, -81.38392	2737	-3.2-11.2	0.86 (1.4 km)	3%
#11	m017	Right Side Hoe Box Cut Eagle Point (7)	37.90289, -81.38755	2568	-13-(-4.5)	0.89 (1.4 km)	99%
#12	m015	Top of Hill Channel 40 Boyd's Knob (6)	37.90608, -81.38303	2745	5.5-13	0.57 (0.92 km)	3%
#13	m010	Old Island – Coal Stockpile Dump (5)	37.91017, -81.37405	2691	8.2-14	-	4%
#14	m08	Valley Fill – Bottom of 33 Road McDowell 2 (4)	37.90400, -81.37550	2256	-2.8-7.2	0.43 (0.69 km)	10%

[1]With Solar GW at #13 (37.91017, -81.37405), GW location moved on Tuesday 6/15/21 to 37.91154, -81.37057
[2] Measured on 6/10/21 from approximately 10AM to 10PM
https://boulter.com/gps/distance/

The WCN nodes and gateway location are shown in Figure 4.27 and a summary of the locations as well as the distance to the gateway and packet loss is presented in Table 4.6. Results showed good transmission (packet loss <10%) for 9 of the 13 locations, with no reception for three of the locations furthest away (2.4-3.4 km) from the gateway. These results indicated that at least one additional gateway would be required to provide coverage of the 14 sampling locations listed in Table 4.6, which were identified by WCN personnel as locations of interest for respirable dust monitoring. While it has been documented that LoRa devices are capable of transmitting over distances greater than 10 km, optimal transmission requires line-of-sight and any obstruction by wooded areas or ground structure / topography will reduce the working range of LoRa devices. This is demonstrated by the poor transmission from the node at Eagle Point (Location #11) that is likely due to the structure of Boyd's Knob (Location #12) which has an elevation that is approximately 200 feet higher than Eagle point and therefore blocks line-of-sight between Eagle Point and the gateway location at the coal stockpile (Location #13 in Table 4.6).

Following an approximately one-month long deployment at the WCN Surface Mine (6/11/21-7/15/21), sensing nodes were collected and returned to the laboratory for post-calibration and analysis. At the time of retrieval, 9 of the 13 nodes deployed were still functioning normally, although several had experienced some amount of baseline shift over the course of deployment. Outputs from three of the sensor nodes had gone irreversibly to full-scale after significant baseline shift, and one node had lost power due to a solar panel failure. Two of the full-scale sensors contained insects while the third was caked with mud and appeared to have been immersed in water – mine personnel indicated that the portable sample stands had to be moved in some cases and that it is possible that some sensing nodes had come into contact with the ground during that process.

Using the Cayenne dashboard created for WCN surface mine it was possible to monitor and review sensor node output. Figure 4.28 shows data for three of the nodes for the one-month deployment and examples of sensor drift, irreversible full-scale response, and response to weather are apparent. Figure 4.28a shows the m09 sensor node output and a steady upward drift in the baseline occurs starting at a value of approximately 0.32 volt in early June and increasing to 0.97 volt by the end of the deployment in July. A significant baseline drift has implications for quantifying sensor responses and would need to be accounted for through periodic "zeroing" of the instrument. This is a common characteristic of many direct-reading field instruments and re-zeroing is specifically noted as a requirement for optical dust sensors including the TSI reference instrument used for this study.

Another complication for dust measurements is created by interference from fog and condensation within the dust sensors. The WCN surface mine location frequently experiences fog and low cloud cover after precipitation, overnight, and in the mornings. Fog droplets can be detected by the optical sensors and condensation within the body of the sensors can result in full-scale response. This can be observed in the first days of the response plots in Figure 4.28 as each of the sensors shows large responses during a time when rain and fog occurred. In most cases, the sensors have been relatively resilient and will return to a normal baseline after fog clears and condensation dries. However, if significant exposure to dust occurs while the sensors are wet, it is likely that a film can be deposited on the sensor optics and if these events are repeated, the accumulation of dirt could be expected to cause an upward baseline drift as seen for several nodes.

a)

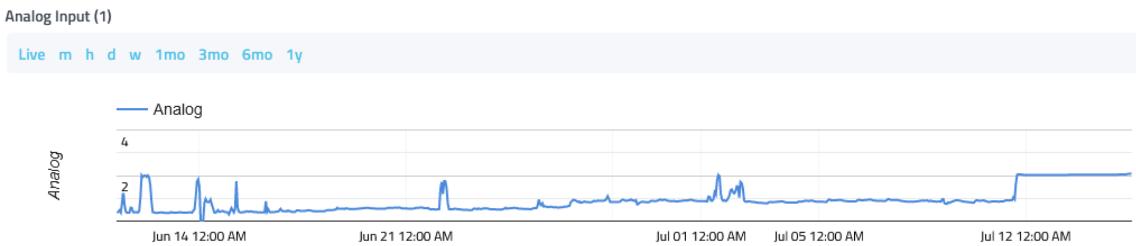

b)

Figure 4.28. Cayenne dashboard display of sensor readings for a) m09, and b) m010 locations.

The problem of insect infiltration is also apparent in Figure 4.28b for the m010 sensor node. The output shows an upward baseline drift as seen for m09 until July 12 when the m010 response goes irreversibly to full-scale (~ 2.0 volt). When this sensor was retrieved on July 15 it was noted that a spider had nested within the sensing region. This problem could likely be addressed with a modified sensor housing and inlet screens on the sensor openings.

A comparison of calibration results from before and after the June 11-July 15 WCN deployment is presented in Figure 4.29 for three of the Prototype-2 sensors (m06, m07, and m09). This direct comparison could not be made for the sensors that had irreversible full-scale output (m08, m010, m016) or for sensors that were not among the five sensors (m06, m07, m08, m09, m010) in the April 30, 2021, calibration set shown in Figure 4.22.

The m06 and m07 sensors show pre- and post-calibration responses that are within 10%; however, the m09 sensor shows a significant decrease in the calibration slope from 0.56 V/mg/m^3 to 0.46 V/mg/m^3. This change in sensitivity is due to the non-linear response seen for dust concentrations above 2 mg/m^3 (Figure 4.29) which appears to be related to the baseline shift noted above for m09 in Figure 4.28. Each sensor has a finite dynamic output voltage range that is defined by the voltage used to power the microprocessor and sensor. The maximum output response for Prototype-1 devices (5V logic) is approximately 3.8V while the maximum output for Prototype-2 units is 2.0V due to the lower 3.3V logic of the microprocessor and lower sensor power supply. This means that when the baseline response significantly increases, the dynamic range for the sensor decreases as it can't go any higher than 2.0V. The loss of dynamic output range with increasing baseline response is not something that could be adjusted by re-zeroing and would eventually require cleaning or replacement of the sensor.

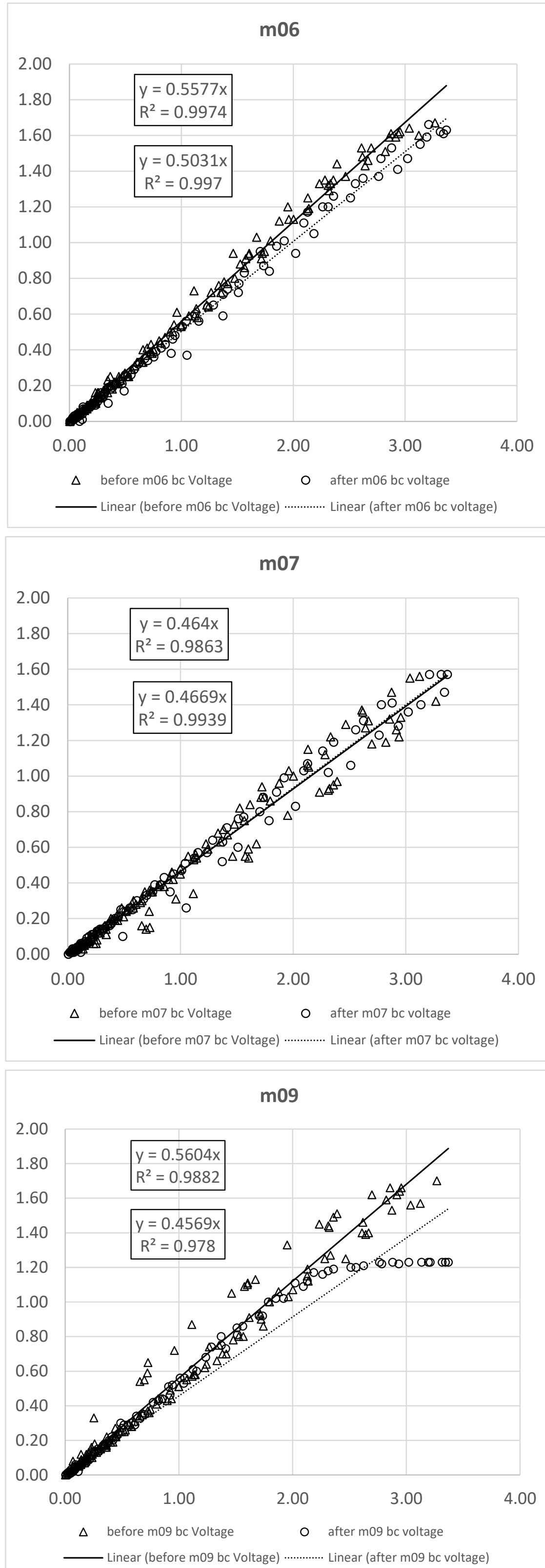

Figure 4.29. Comparison of A2 Arizona Road Dust calibration results from before (4/30/21) and after (8/27/21) one-month deployment at WCN surface mine from June 11 – July 15, 2021 (y-axis Volt, x-axis respirable dust mg/m^3).

The final field deployment of the integrated wireless respirable dust sensing network took place from September 29 – December 9, 2021, at the WCN surface mine. Goals for this deployment included evaluation of the effectiveness of a 120-mesh stainless steel inlet screen in mitigating insect infiltration, interference from fog and precipitation, and baseline drift. As described in the Research Approach section for Task 3.5, stainless-steel screens (120-mesh) were installed over the sensor inlets on seven of the dust sensors while the remaining seven sensors remained open to the air. The screened and unscreened sensors were calibrated in the laboratory prior to deployment and nodes were then placed at seven sampling stations, pairing one screened sensing node with one unscreened sensing node at each location (Figure 3.17) and performance was compared.

Combined pre-deployment calibration results for the 7-screened and 7-unscreened sensors are shown in Figure 4.30. Although the slope of the fitted calibration curve (0.50 V/mg/m^3) is within 10% of previous Prototype-2 calibration results (Figure 4.14 - 0.53 V/mg/m^3; Figure 4.22 – 0.52 V/mg/m^3), there is significantly more scatter of the data. An examination of the separate calibration curves for screened and unscreened sensors show that the screened sensors largely account for the additional scattering (Figure 4.31). This is likely due to changes in the dynamic response of the screened sensors as the 120-mesh would dampen the movement of air through the sensing zone. This effect was not seen in preliminary test results with different mesh sizes so it may be that responses are very sensitive to the orientation of the nodes in the dust chamber when calibration runs are performed. This suggests that field performance could also be significantly affected depending on the direction and magnitude of ambient air currents.

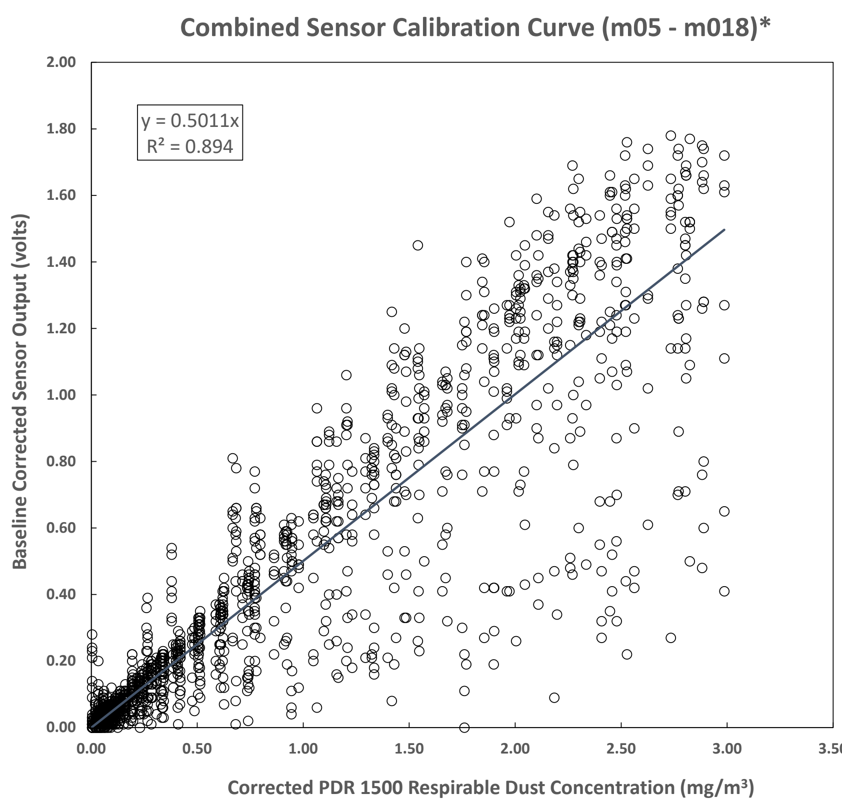

Figure 4.30. Combined pre-deployment calibration results for 7-screened (120-mesh) and 7-unscreened Prototype-2 nodes (9/26/21, A2 Arizona Road Dust).

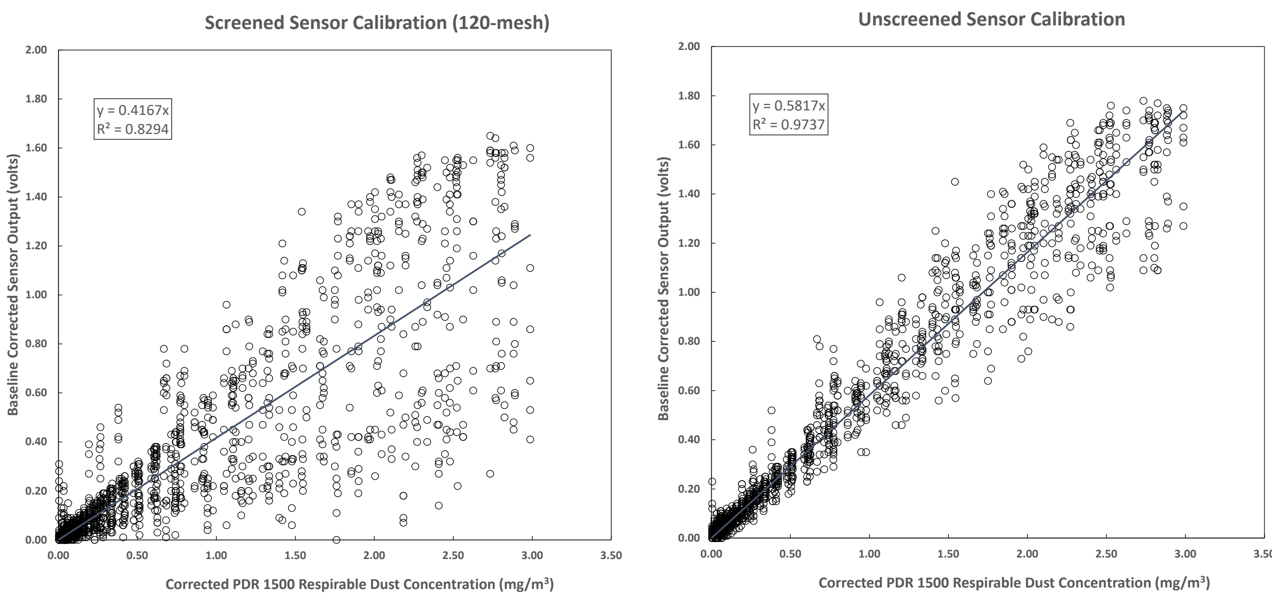

Figure 4.31. Pre-deployment calibration results for 7-screened (120-mesh) and 7-unscreened Prototype-2 nodes (9/26/21, A2 Arizona Road Dust).

A summary of the locations and transmission distances to the gateway and packet loss is presented in Table 4.7. Results showed good reception (packet loss <20%) for all seven locations. These results reflect the use of a permanent LoRa gateway installed at the WCN Field Office, and a second solar powered gateway located at the Power Line Structure ("three-pole structure") shown in Figure 4.27. As mentioned previously, reception and range are maximized when line-of-sight exists between the sensor nodes and gateways. Given the mountainous terrain at the WCN surface mine and the prevalence of wooded topography the optimal placement of gateways is largely trial-and-error based on visualizing sight lines. However, a software program used by amateur radio hobbyists to model radio propagation (Radio Mobile Web Edition) was found to be helpful in predicting sensor node coverage for different gateway placements (Figure 4.32).

The Cayenne dashboard (Figure 4.33) was used to monitor dust sensor responses and battery status for all fourteen nodes over the course of the deployment. In addition to displaying the sensor outputs by day, week, or month, the Cayenne service also enables users to set triggers and alerts for each individual sensor. Automated actions that can be triggered include sending of texts, emails, or passing of data to another server or website through the use of HTTP or MQTT protocols. This feature could be used to notify mine personnel in the event of elevated dust levels or low battery levels for individual sensors. The performance of this feature was verified by turning on a trigger to detect when battery voltage dropped below 3.7V and the system did successfully send an email when the condition occurred. The Cayenne dashboard also enables stored data to be retrieved in a spreadsheet format; however, this function is limited for the free service to one month storage and there were several problems experienced over the course of the project with missing or lost data. The subscription service may be more reliable and offers longer term storage and access.

Table 4.7. Workman Creek North Sensor Node Locations (9/30/21)

Location	Node	Description	GPS	Elev. (ft)	SNR[1,2]	Distance[1] (km)	Packet Loss[2]
1	m05, m06	CP - WCN Field Office	37.89605, -81.37033	2368	11 - 12.8	88 m	1-5%
2	m07, m08	Little Italy	37.913861, -81.369444	2671	-5.8 – (-4.2)	2.1	13-19%
3	m09, m010	Old Island – Coal Stockpile	37.91017, -81.37405	2589	2.5 – 9.2	1.6	2-3%
4	m011, m012	LP1705	37.895028, -81.379167	2782	-3.8	0.82	18-19%
5	m013, m014	Coal Handling Facility (CHF)	37.883389, -81.378139	2221	4.5 - 6.5	1.5	1-5%
6	m015, m016	Valley Fill Access Road	37.89992, -81.37250	2199	-9 – 9 [3]	0.56	2-7%
7	m017, m018	Valley Fill – Bottom of 33 Road	37.90400, -81.37550	2256	6 – 12.5	1.1	2-4%

[1] With fixed gateway at WCN Field Office (GW3 installed 9/29/21 AM; 37.895378, -81.369793)

[2] Solar gateway (GW2) installed at 3-pole structure on 9/30/21, lost connection approximately 9-11 PM 10/2/21 37.89315, -81.38492; connection restored at approximately 3:45 PM Tuesday 10/5/21.

[3] Highly variable SNR at times starting around 10/5/21

https://boulter.com/gps/distance/; Elevation Finder (freemaptools.com)

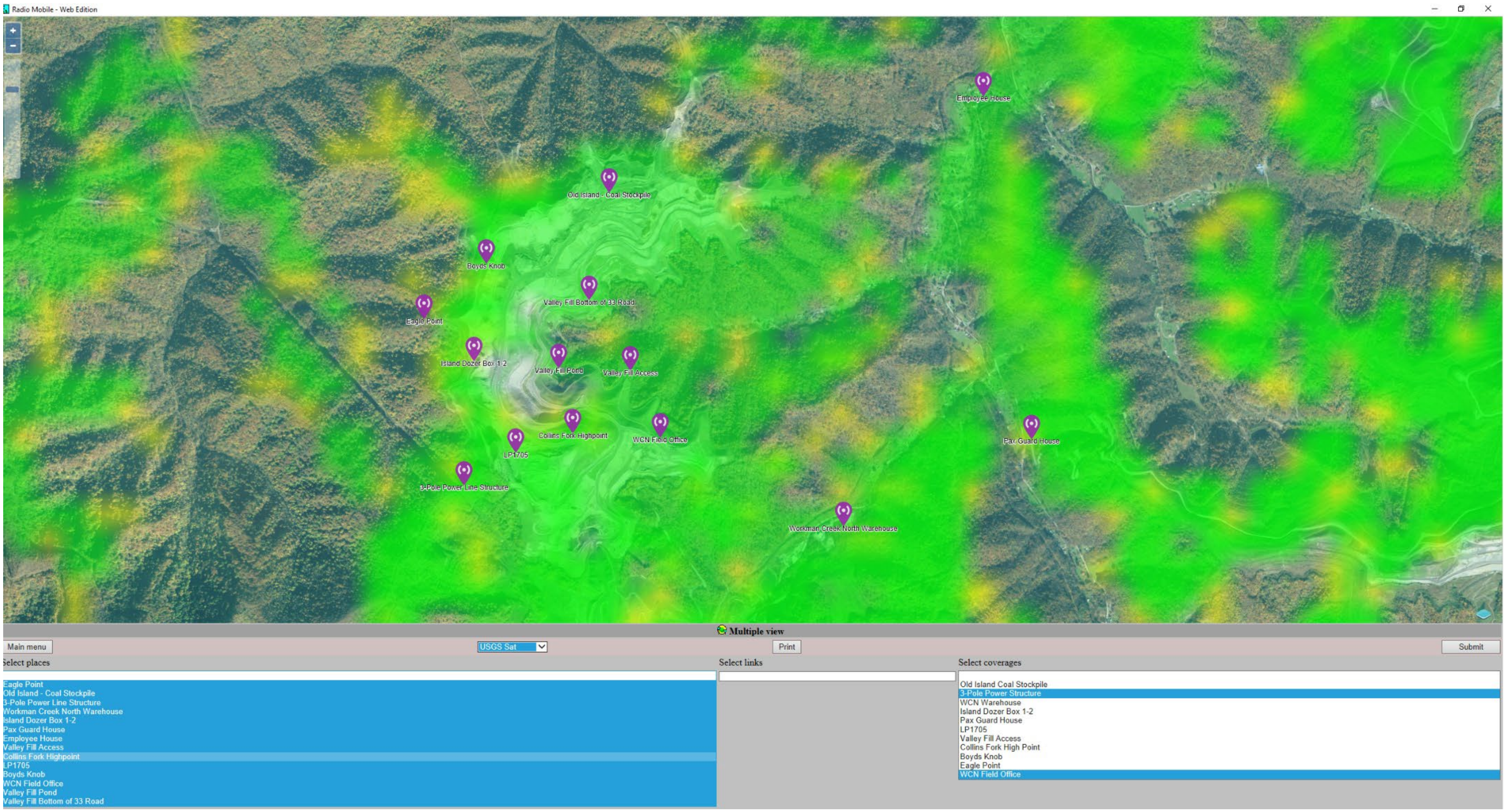

Figure 4.32. Predicted wireless LoRa network coverage with gateways placed at the WCN Field Office and the 3-Pole Power Line Structure - Radio Mobile Web Edition.

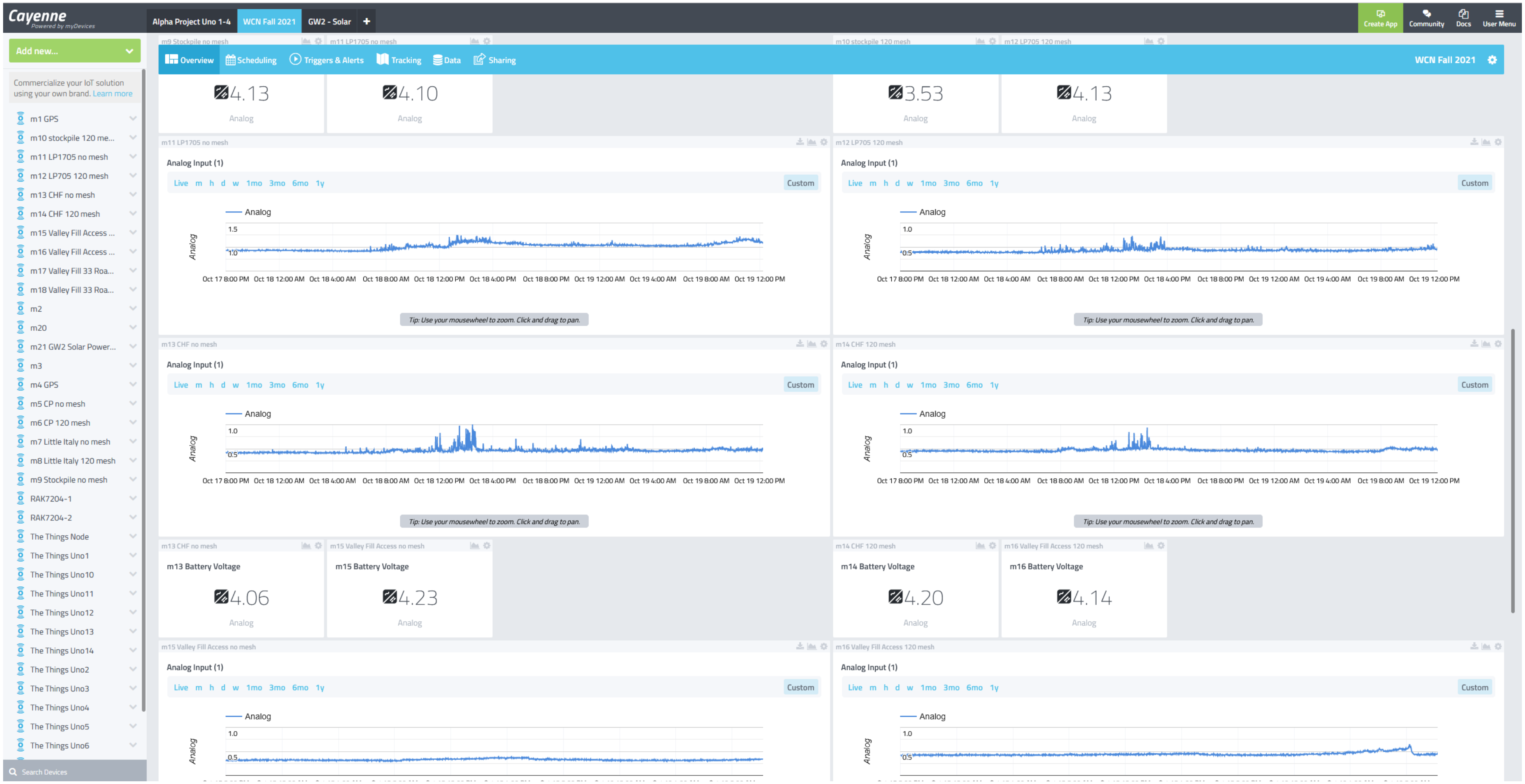

Figure 4.33. Cayenne dashboard display of sensor node output and battery voltage (10/19/21).

A secondary method of storing data was developed in response to the problems experienced with Cayenne, which involved the use of features available through The Things Network (TTN) application server. The application server provides the ability to create integrations that allow data that flows though the LoRa server to be passed on to third party services such as Cayenne. TTN also allows users to create their own integrations including "webhooks" which are a way for the server to provide other applications with real-time information through the use of the HTTP push API. Using Google Apps Script, and the associated Base url, it is possible to setup a webhook in the TTN application server that sends live data to be stored in the spreadsheet. An example script used to send sensor data to a Google sheets spreadsheet is included in an Appendix.

The 24-hour view in the Cayenne dashboard displays sensor data updated each minute which is shown for the Coal Handling Facility (CHF) sample location in Figure 4.34. Plots are included for the 120-mesh-screened (m014) and the unscreened node (m013). A comparison of the two nodes shows good agreement with similar exposure profiles over the 24-hour period, although the m014 profile does appear to be slightly attenuated or dampened compared to the unscreened sensor. This is likely due to the difference in dynamic response resulting from the presence of the 120-mesh screen which could also be consistent with behavior noted during the calibration run. Similar plots are available for all seven of the paired sensor locations with results generally showing performance comparable to these examples for the CHF location.

As stated previously, goals for this field demonstration included evaluation of whether the addition of the 120-mesh screen mitigated performance problems noted in earlier evaluations including 1) interference from fog, precipitation, and condensation, 2) baseline drift, and 3) insect infiltration. The openings in 120-mesh screen are approximately 125 um and this would not be expected to stop the entrance of fog or mist droplets which can be 20 um and smaller; however, it was desired to determine whether there would be any beneficial effect on response characteristics as a result of reduced movement of air and at least some potential reduction in the number of larger aerosol particles entering the sensor. Weather conditions and sensor responses were monitored continuously, and the first heavy rain occurred on approximately October 8, 2021. The subsequent comparison of sensor responses for the screened and unscreened sensor nodes did not show significant differences in susceptibility to interference from moisture.

An example response profile is shown in Figure 4.35 for the m07 and m08 sensor nodes at the "Little Italy" location using the dashboard's weekly timeline which shows one measurement per hour. Both response profiles approach full-scale response and a review of the minute-by-minute data shows that both sensors were at full scale for much of the 24-hour period on October 8-9, 2021. While there may be a slight difference in the duration for which sensor output remained at full-scale (the 120-mesh sensor response appears to be attenuated slightly lower compared with the unscreened sensor response), in practice neither sensor provided useful data during this event. It could be argued that it is unlikely that there would be significant respirable dust levels present during heavy precipitation; however, it is not unusual for drilling and blasting to occur following precipitation and significant airborne dust may result from these processes.

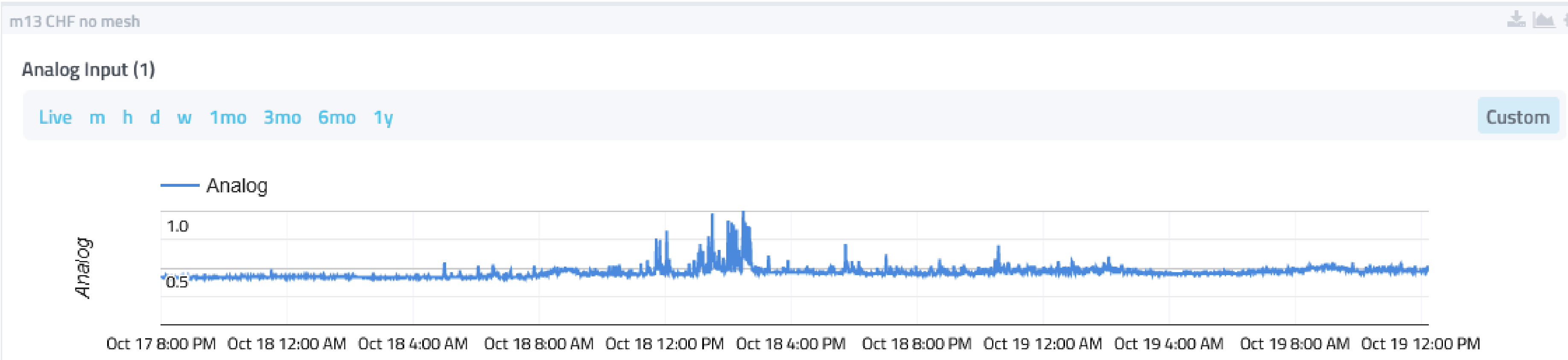

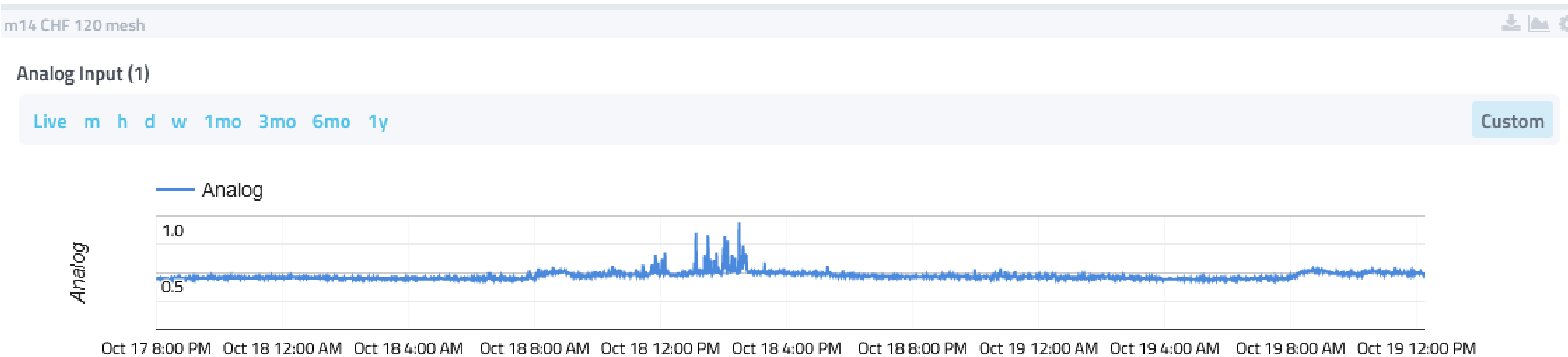

Figure. 4.34. Cayenne dashboard display of dust levels at coal handling facility (CHF) location for screened (lower) and unscreened (upper) sensors (10/19/21).

Figure. 4.35. Cayenne dashboard display of sensor response to heavy rain at "Little Italy" location for 120-mesh-screened m08 (lower) and unscreened m07 (upper) sensors (10/9/21).

Insect infiltration had been a problem in previous field evaluations and the response changes associated with a foreign body blocking the optical path of the sensor is typically a relatively sudden full-scale response that isn't accompanied by fog, precipitation, or mining activity. Approximately one month into the September 29, 2021, field deployment, two sensors had already exhibited abrupt transition to full-scale response (m09, m017), while two other sensors had lost power (m010, m013), and a third (m011) was showing frequent step changes in baseline that could be consistent with insects. Based on these factors the decision was made to return to WCN surface mine to repair or replace sensors as needed, and also to add a coarse 40-mesh screen over the inlets of all of the unscreened sensors. It was apparent that the 120-mesh screen did little to reduce the effect of rain and fog on sensor response and it was desired to observe the extent to which a coarse mesh would prevent insect infiltration while presenting less resistance to the movement of air through the sensing zone. For these reasons a return to the WCN surface mine took place on October 27, 2021.

One day before returning to WCN a review of the status of all fourteen sensing nodes revealed the following: nine of the fourteen sensors appeared to be functioning normally while five showed some type of malfunction: two sensors showed irreversible full-scale response, two sensors had lost power, and one sensor displayed frequent step changes in baseline. Upon return to the site all locations and sensors were inspected and each of the previously unscreened sensors was equipped with 40-mesh inlet screens (Figure 3.17b). It was discovered that the two sensors with full-scale response (m09, m017) contained nesting spiders and the two sensors that had lost power had malfunctioning solar panel cables or components. No explanation could be found for the sensor with the shifting baseline response. At the conclusion of the visit all nodes were functioning again after the following actions: replacing the m011 and m017 sensors, replacing the solar panels for m010 and m013, and cleaning out m09. In addition, previously unscreened sensors m05, m07, m09, m011, m013, m015, and m017 were equipped with 40-mesh inlet screens.

The final field deployment was completed on December 9, 2021, when all sensors were retrieved and returned to the laboratory for post-calibration and analysis. At the time of retrieval, 11 of the 14 sensor nodes were functioning, while one sensor had an irreversible full-scale response (m09), and two had lost power with one showing a severed solar panel cable (m018) and the second (m011) appearing to have the solar panel cable crushed in the sampling stand access door. In total, 8 of the 14 sensors originally placed on September 29, 2021, were still functioning without repair or replacement at the end of the field evaluation on December 9, 2021, after a duration of 71 days deployed: m05, m06, m07, m08, m012, m014, m015, m016.

The combined results for the post-deployment calibration (40-mesh and 120-mesh) are presented in Figure 4.35. The slope of the combined calibration curve decreased from a pre-calibration result of 0.50 V/mg/m^3 to the post-calibration value of 0.44 V/mg/m^3. In addition, several sensors show signs of a reduced dynamic response due to baseline shift as indicated by the horizontal lines of data for concentrations above1.5 mg/m^3. Referring to the individual calibration plots for the 120-mesh and 40-mesh sensors separately (figure 4.36) it can be seen that the most severe non-dynamic response appears to lie among the 40-mesh sensors and a review of calibration data for the individual sensors shows that m07 and m013 account for two of the prominent horizontal lines of data while m010 displays a similar pattern in the 120-mesh calibration plot. A review of sensor baselines from the September 26, 2021, pre-deployment calibration shows that the m07, m010, and m013 sensors had baselines of 0.30, 0.39, and 0.32V, respectively at that time, versus values of 1.31, 1.24, and 0.95V for the post-deployment calibration. Given that the maximum output for the Prototype-2 sensors is approximately 2.0V, it can be seen that very little “headroom” remains for dynamic response for these three sensors. For example, with the m07 baseline of 1.31V in December, a sensitivity of 0.47V/mg/m^3, and maximum output of 2.0V, non-dynamic response would begin at approximately (2.0V– 1.3V) / (0.47 V/mg/m^3) = 1.5 mg/m^3 which is consistent with what is shown in Figures 4.35 and 4.36. For this application which focuses on occupational exposure evaluation with a permissible exposure limit of 1.5 mg/m^3, a loss of dynamic range near or below the PEL would be a significant problem and monitoring of the baseline shift would be a requirement to ensure that adequate dynamic range is available for all sensors to maximize measurement accuracy near the PEL.

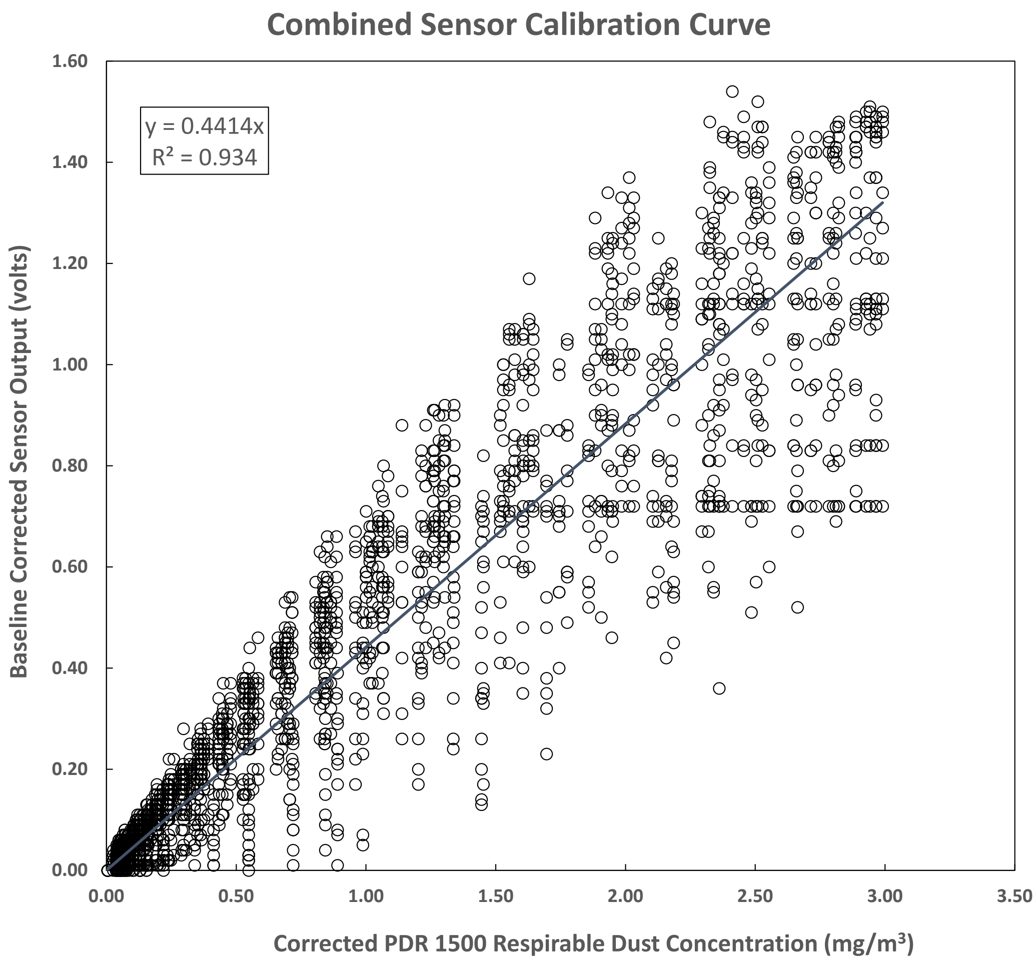

Figure 4.35. Combined post-deployment calibration results for seven 120-mesh-screened and seven 40-mesh-screened Prototype-2 nodes (12/11/21, A2 Arizona Road Dust).

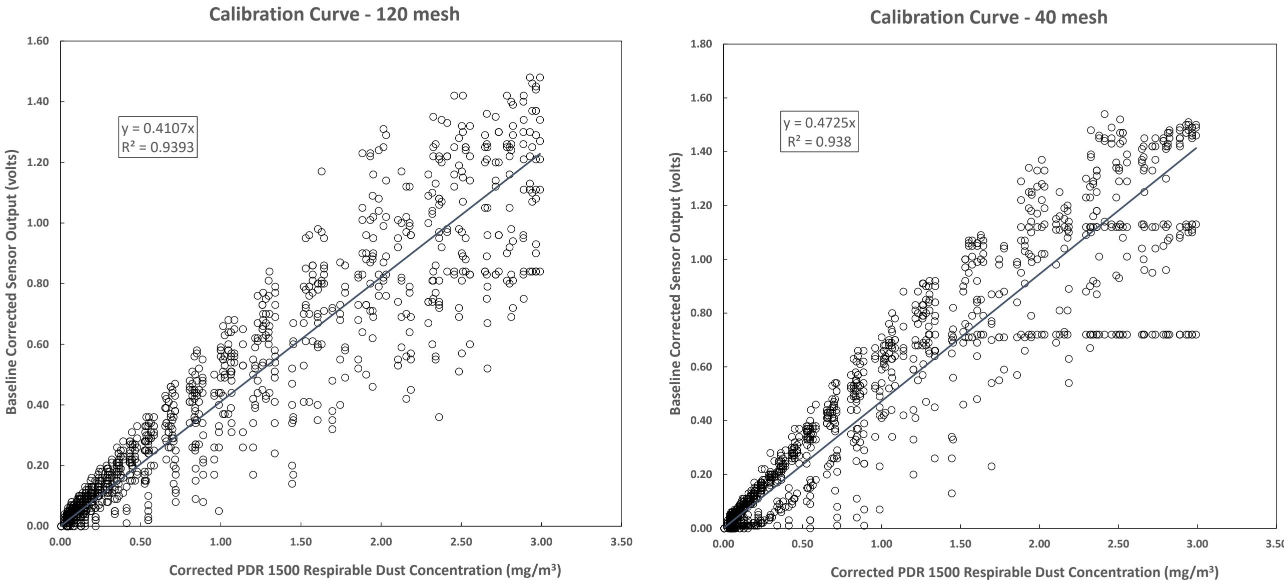

Figure 4.36. Post-deployment calibration results for seven 120-mesh-screened and seven 40-mesh-screened Prototype-2 nodes (12/11/21, A2 Arizona Road Dust).

A summary of baseline behavior for the different inlet screen configurations is presented in Table 4.8. These data show baseline response in volts measured at the time of the pre- and post-deployment calibrations for sensors that were continuously deployed in the field from 9/29/21 to 12/9/21. Results show that in all cases, baselines increased with time, most likely due to the deposition of dust or a film on the sensor optics including lenses, the LED lamp, and the photodetector element. Since dust levels may vary by location, the baselines are examined using paired sensors at shared locations – four pairs of sensors were deployed continuously for the entire field evaluation and found to be still functioning at the final calibration, so the analysis focuses on these eight sensors.

Baseline shift in the table is defined as the difference between the 12/11/21 and 9/26/21 baselines in volts divided by the length of time deployed which was 71 days. The baseline shift represents the average rate at which an individual sensor's baseline increased over the course of the field deployment in units of volt/day. The last column in the table presents the ratio of the unscreened/40-mesh screened sensor's baseline shift to the 120-mesh screened sensor's baseline shift for each of the paired sensors / locations. Results of this analysis show that on average the unscreened / 40-mesh screened sensors showed baseline increases at a rate of approximately nine times that of the 120-mesh screened devices. This suggests that the 120-mesh inlet screen does mitigate baseline drift relative to unscreened sensors or those using a coarse 40-mesh filter (the approximate opening size for 40-mesh screen is 400 um, while the size for 120-mesh is 125 um). While the use of the 120-mesh inlet screens appears to reduce the sensitivity of the sensors and increase calibration variability, this may be an acceptable tradeoff for what would potentially appear to be a much longer time to replacement in the field for sensors.

Table 4.8. Baseline shifts for sensor pairs deployed September 29-December 9, 2021

Sensor[1]	9/26/21 Baseline (volt)	12/11/21 Baseline (volt)	Baseline Shift (volt / day)	Ratio[3]
m05	0.26	0.54	0.0039	**14**
m06	0.46	0.65	0.00027	
m07	0.30	1.30	0.014	**4.7**
m08	0.20	0.41	0.0030	
m013	0.32	0.95	0.0089	**6.8**
m014	0.47	0.56	0.0013	
m015	0.32	0.43	0.0015	**11**
m016	0.45	0.46	0.00014	
			AVE (SD) =	**9.1 (4.2)**

[1] Even-numbered sensors had 120-mesh inlet screens while odd-numbered sensors were unscreened from 9/29-10/27/21 and then had 40-mesh inlet screens from 10/27-12/9/21.

[2] Based on 71-day duration of field deployment: (12/11 baseline - 2/26 baseline) / 71 days

[3] (Baseline shift for unscreened–40-mesh sensors) / (Baseline shift for 120-mesh sensors)

Overall quantitative performance of the dust sensors was assessed using the results of field deployments conducted at the Pax Loadout in June 2019, and May 2021, and using the results of post-deployment calibration studies following the June 9-July 15, 2021, and September 29-December 9, 2021, field evaluations at WCN Surface Mine. A summary of these results is presented in Table 4.9. During the first field demonstration of Prototype-1 dust sensing nodes at Pax Loadout, measurements recorded for two of the nodes placed at the crusher facility were on average within 22% (SD=19%) of the reference TSI DustTrak sensing node measurements of 15-min-TWA respirable dust concentration based on the mean absolute percentage error (MAPE). This result was considered to be acceptable given that the dust concentrations produced by this process were relatively low during sampling, ranging from 0.04-0.18 mg/m^3. Respirable dust concentrations were again relatively low (0.02-0.78 mg/m^3) on the follow-up visit to the Pax Loadout in May 2021. In this case, the results for the dust sensing nodes for the 4-hr-TWA exposure were relatively good with a mean absolute percentage error (MAPE) of 34% (SD=6%) for the three Prototype-2 sensor nodes compared with paired reference instruments (PDR-1500, PDM-3700, DustTrak).

Post-deployment calibration studies were used to evaluate the quantitative performance of dust sensing nodes following the 35-day and 71-day field evaluations conducted at the WCN Surface Mine. For these analyses the results of pre-deployment calibrations were used to estimate respirable dust concentrations in the dust chamber during a post-deployment calibration / experimental run. Following the first deployment, a pre-deployment calibration result for the Prototype-2 sensors (Figure 4.22, calibration slope = 0.52 V/mg/m^3) was used to quantify sensor responses for the post-deployment experimental run. Sensor-predicted respirable dust concentrations were then compared with the reference PDR-1500 results and the MAPE calculated for recorded minute concentrations. Table 4.9 shows that the mean absolute error for sensors after the first deployment was14% with a standard deviation of 11%, indicating that the majority of measurements made with these devices after having been deployed outdoors at the mine site for approximately one-month are expected to be within 25% of the reference measurement (14 $\pm$ 11%).

Using a similar approach for the 71-day field evaluation, the pre-deployment calibration results for screened (120-mesh) and unscreened sensors (Figure 4.31) were used to quantify sensor responses in a post-deployment calibration / experimental run. The pre-deployment calibration slopes for the 120-mesh screened and unscreened sensors were 0.42V/mg/m^3 and 0.58V/mg/m^3, respectively. Using these values, the mean absolute error was 23% (SD = 16) and 22% (SD=17), respectively, for the 120-mesh and unscreened sensors (note that the unscreened sensors were equipped with 40-mesh inlet screens on October 27, 2021, for the remaining portion of the deployment and continuing through the post-deployment experimental run).

The larger errors seen for the sensors following the 71-day deployment likely reflect a number of factors including baseline shift and the loss of dynamic response for several of the sensors – data for these devices was included in the analysis to realistically reflect expected performance changes over the course of a deployment in the estimates of measurement error. Another source of error for the sensors that were originally unscreened and then subsequently equipped with 40-mesh inlet screens, is the use of the original calibration slope which was based on the unscreened devices. Although the larger openings of the 40-mesh screen don't appear to reduce sensitivity as much as the 120-mesh screens, it is possible that some decrease in sensitivity occurs and this would not be reflected in the calibration slope that was used to quantify sensor responses in the post-deployment run.

NIOSH requirements for direct-reading instruments generally require 95% confidence that measurements are within +/- 25% of the true value (within a specified concentration range). Although the accuracy metrics shown in Table 4.9 for the Prototype-1 and Prototype-2 sensing nodes would not meet requirements for required compliance or regulatory monitoring, there is still significant value in the information provided by these devices, particularly in the consideration of exposure control strategies, evaluating their effectiveness, and in detecting and responding to transient changes in operations and exposures. This capability is further supported by the comparison of costs for turnkey or enterprise respirable dust monitoring systems versus the integrated wireless network developed for this project presented in the next section (Table 4.10).

Table 4.9. Summary of wireless dust sensing network performance for field studies and post-deployment calibrations studies.

Date / Event	Description	Respirable Dust Concentration Range (mg/m^3)	Mean Absolute Percentage Error (SD)
June 14, 2019 Pax Loadout Field Demonstration	Three Prototype-1 nodes deployed with reference node (TSI DustTrak) and gravimetric samples, real-time data transmitted wirelessly (LoRa) to cloud-based display and storage.	0.04 – 0.18 mg/m^3 15-min-TWA	22% (19)
May 20, 2021 Pax Loadout Field Demonstration	Six each of Prototype-1 and Prototype-2 nodes deployed in pairs with reference instruments (TSI DustTrak, PDR-1500, PDM-3700, and gravimetric samples), real-time data transmitted wirelessly (LoRa) to cloud-based display and storage.	0.02 – 0.78 mg/m^3 4-Hr-TWA	34% (5.6)
June 10 - July 15, 2021 WCN Surface Mine Field Demonstration	Thirteen Prototype-2 nodes deployed for approximately one month, pre-deployment calibration results used to calculate dust concentrations recorded during post-deployment calibration run. Accuracy calculated relative to reference PDR-1500 instrument.	0.75 – 3.0 mg/m^3 Minute concentrations	14% (11)
September 29-December 9, 2021 WCN Surface Mine Field Demonstration	Fourteen Prototype-2 nodes deployed for 71 days, pre-deployment calibration results used to calculate dust concentrations recorded during post-deployment calibration run. Accuracy calculated relative to reference PDR-1500 instrument. Screened sensor inlets using 120-mesh (7-nodes) and 40-mesh (7-nodes).	0.75 – 3.0 mg/m^3 Minute concentrations	22% (17) 40-mesh 23% (16) 120-mesh

Table 4.10. Estimated costs for integrated wireless dust sensing networks

Enterprise Respirable Dust Sensing System	**Cost ($)**	**Prototype-1**	**Cost ($)**	**Prototype-2**	**Cost ($)**
TSI Dusttrak DRX	10,950	Sharp dust sensor and interface module	16	Sharp dust sensor	12
TSI Environmental Enclosure	1,765	TTN UNO	62	Adafruit Feather M0	40
TSI Internal Battery System	615	Project Enclosure Box	9	Weatherproof Enclosure	10
TSI Wiring Harness	70	Sensor mount	9	Sensor mount	9
Netronix Thiamis GSM/GPS Modem	1,250	9V Battery / USB Pack	10	5V Solar Panel	18
Environet Annual Service Plan	1,470			Solar Power Manager	8
				Lithium-Ion Battery - 3.7v 2000mAh	13
Cost per node without LoRa GW	**16,120**		**106**		**110**
		TTN LoRa Indoor Gateway	350 / 14	TTN LoRa Outdoor Gateway	640/14
Cost per node with LoRa GW [1]	**16,120**[2]		**131**		**155**
TOTAL COST [3] **(14 Node Network)**	**$225,680**		**$1,834**		**$2,170**

[1]Prototype systems require at least one LoRa Gateway (GW) to function. Cost per node with LoRa GW calculation assumes a 14-node network and divides the cost of one LoRa gateway across the network nodes.

[2]TSI System does not require a LoRa gateway as each node would include its own cellular GPS modem.

[3]Total cost estimate does not reflect quantity discounts that could likely be obtained

A summary of estimated costs for the Reference Respirable Dust Monitoring System (TSI DustTrak and accessories), and the Integrated Wireless Dust Sensing Network developed for this project is presented in Table 4.10. For the purpose of this analysis, it is assumed that a 14-node network is required and that the LoRa-based networks require at least one LoRa Gateway. With a total price of approximately $2,000 for a 14-node network, the prototype systems are 1/100th the cost of the turnkey system. Estimates show that there is little difference between the prototype systems developed – costs are very similar for most components, and this would likely still be the case for the next prototype. The most expensive components are typically the microprocessor and potentially the dust sensor if a laser-based sensor with an integrated fan were to be selected. In any case, the difference in total cost between turnkey and low-cost LoRa based systems is striking, and for applications that require geospatially distributed real-time estimates of dust concentrations and for which regulatory compliance monitoring levels of accuracy are not necessary, the low-cost systems offer many advantages.

5.0 Publication Record and Dissemination Efforts

This section contains a listing of refereed publications, manuscripts published and in progress, research reports, presentations, and a brief summary of plans related to the ongoing dissemination of project findings and technologies.

REFEREED PUBLICATIONS

1. Mohammad Ghamari, Cinna Soltanpur, Pablo Rangel, William A Groves, Vladislav Kecojevic, "Laboratory and Field Evaluation of Three Low-Cost Particulate Matter Sensors", IET Wireless Sensor Systems, accepted for publication December 7, 2021.

MANUSCRIPTS IN PROGRESS

1. Ghamari, A., Groves, W., and V. Kecojevic. "Evaluation of Inexpensive Dust Sensors for Measuring Respirable Dust in Surface Mines", in preparation for submission to Mining, Metallurgy & Exploration (Journal of SME).

RESEARCH REPORTS TO SPONSORS

1. Groves, W.A. AFC417-39 - A Holistic Approach to Reducing Coal Worker's Pneumoconiosis (CWP), 1/1/21 – 6/30/21, 23 pages.
2. Groves, W.A. AFC417-39 - A Holistic Approach to Reducing Coal Worker's Pneumoconiosis (CWP), 7/1/20 – 12/31/20, 18 pages.
3. Groves, W.A. AFC417-39 - A Holistic Approach to Reducing Coal Worker's Pneumoconiosis (CWP), 1/1/20 – 6/30/20, 17 pages.
4. Groves, W.A. AFC417-39 - A Holistic Approach to Reducing Coal Worker's Pneumoconiosis (CWP) 7/1/19 – 12/31/19, 15 pages.
5. Groves, W.A. AFC417-39 - A Holistic Approach to Reducing Coal Worker's Pneumoconiosis (CWP) 12/1/19 – 6/30/19, 14 pages.
6. Groves, W.A. AFC417-39 - A Holistic Approach to Reducing Coal Worker's Pneumoconiosis (CWP) 7/1/18 – 12/31/18, 20 pages.
7. Groves, W.A. AFC417-39 - A Holistic Approach to Reducing Coal Worker's Pneumoconiosis (CWP) 1/1/18 – 6/30/18, 14 pages.

PRESENTATIONS AT TECHNICAL AND PROFESSIONAL MEETINGS

1. W. Groves, V. Kecojevic, "Field Demonstration of an Integrated Wireless Respirable Dust Sensing Network Based on Low-Cost Optical Sensors", accepted for presentation at 2022 SME Annual Conference and EXPO, Salt Lake City, UT, March 2, 2022.
2. W. Groves, A. Ghamari, V. Kecojevic, "Integrated Wireless Dust Sensing Network for Measuring Respirable Dust in Surface Mines – Remote Power Using Photovoltaic Devices", SME 2021 Conference (virtual), March 1-5, 2021.
3. W. Groves, A. Ghamari, V. Kecojevic, "Wireless Measurement of Respirable Dust using Inexpensive Sensors in Surface Mines", 1st International Symposium on Mine Dust and Aerosol Research (virtual), November 15-16, 2021.

4. W. Groves, A. Ghamari, V. Kecojevic, "Evaluation of Inexpensive Dust Sensors for Measuring Respirable Dust in Surface Mines", American Industrial Hygiene Conference and Exposition (AIHCE), Minneapolis, MN, May 21, 2019.
5. W. Groves, A. Ghamari, V. Kecojevic, "Calibration of Inexpensive Dust Sensors for Measuring Respirable Dust in Surface Mines", SME 2020 Conference, Phoenix, Arizona, February 25, 2020.

INVITED PRESENTATIONS

1. W. Groves, A. Ghamari, V. Kecojevic, "Evaluation of Inexpensive Dust Sensors for Measuring Respirable Dust in Surface Mines – Field Demonstration", American Conference of Governmental Industrial Hygienists (ACGIH) Invited Webinar Presentation, August 6, 2020.
2. W. Groves, A. Ghamari, V. Kecojevic, "Evaluation of Inexpensive Dust Sensors for Measuring Respirable Dust in Surface Mines –Laboratory Calibration", Central Pennsylvania Safety Association Professional Development Conference, Nittany Lion Inn, University Park, PA, April 10, 2019.

KICKOFF MEETINGS

Kickoff meetings were held at Republic Energy Mine, Eskdale, WV, at 9:00 AM Wednesday 5/30/18, and on June 1, 2018 (the President of Republic Energy had a scheduling conflict and missed the first meeting). Those attending included the following: Jimmie Wood, President, Republic Energy, David McGraw, Engineer, Republic Energy, Wayne Persinger, Safety Director, Republic Energy, Doug Barker, Republic Energy, Steve Giles, On-Site Safety Representative, Republic Energy, William Groves, Penn State, Mohammad Ghamari, Penn State, Vladislav Kecojevic, West Virginia University

DISSEMINATION PLAN

Our partners at Alpha Metallurgical Resources have expressed an interest in continuing to develop and field-test the integrated wireless respirable dust sensing network and have installed a permanent LoRa Gateway at the Workman Creek North Surface Mine. This installation will facilitate ongoing deployment of improved prototype dust sensing nodes for exposure monitoring. While continuing to be focused on occupational exposure assessment and control, this site is particularly interested in the ability to continuously monitor and document fugitive dust emissions and potential drift resulting from operations. This type of monitoring represents a significant challenge based on the relatively low levels of dust that would be of interest, but discussions are already underway with regard to modifications and alternative sensing platforms that might be appropriate. We have also discussed the possibility of moving the cloud-based data storage and management capabilities from the free open-source services used for this project to private network-based services secured by Alpha Metallurgical Resources facilities and personnel. While no formal plan or schedule is currently in place, it is expected that the collaboration will continue in the upcoming season when conditions in the field improve.

6.0 Conclusions and Impact Assessment

A primary contribution of this work is the development and demonstration of a low-cost integrated wireless dust sensing platform. The network employs a relatively new wireless protocol (LoRa) designed specifically for low power, long range, low bandwidth transmission of data. While the use of LoRa in the United States is still in the early stages of development, rapid growth of the technology has occurred in Europe and Asia where the use of connected devices (Internet of Things or IoT) is widespread in communities and throughout industry. Examples of applications for "smart" LoRa-based sensing include the following (https://www.semtech.com/lora/lora-applications):

- Agriculture – measurement of environmental conditions to maximize yield, minimize expenses, reduce environmental impact, track livestock, reduce water consumption
- Cities – geolocation, asset tracking, improved efficiency in monitoring services such as lighting, parking, waste removal
- Environmental monitoring – temperature, humidity, numerous chemical sensors, particulate matter, pH, liquid level, suspended solids
- Utilities – remote centralized data collection and metering and monitoring
- Smart Mines – remote monitoring of conveyors, detection of belt tears, belt idler bearing temperatures, scheduling of preventative maintenance, increased operating efficiency

While the focus of this project was specifically on the use of a LoRa network for monitoring respirable dust exposure, the platform that was developed is extremely flexible and could be used with many commercially available LoRa-compatible sensors which includes hundreds of different devices from a variety of suppliers. Some devices are based on proprietary protocols and subscription based-services; however, the LoRa protocol is open-source and there are many suppliers of open-source sensing devices that can easily be added to an existing LoRa wide area network (LoRa WAN). The installation of a fixed LoRa gateway at the WCN Field Office, opens the door to many possibilities for remote monitoring including continued use of the system to monitor respirable dust exposures, but also for other applications related to environmental health and safety as well as productivity and operational efficiency. This gateway installation and the associated options for cloud-based data monitoring with optional triggering and alarm notifications, provides an opportunity for the WCN surface mine to explore the use of these technologies at a low-cost and with little risk.

The primary contribution of this work to the science of respirable dust monitoring is applied in nature and focuses on the development, calibration, and field evaluation of a network of inexpensive wireless optical dust sensors. An innovative aspect of the project is the use of LoRaWAN as the framework for the wireless network. The use of LoRa in the U.S. is still relatively new, and there has been little work published that describes specific application to occupational exposure monitoring and control. Likewise, there has not been detailed descriptions of specific hardware combinations for wireless sensing using LoRaWAN, nor for the design and implementation of remote power systems for long-term field deployment for these applications. In addition, the characterization of sensor and network performance over extended field deployments in harsh conditions represents a significant contribution to the understanding of these technologies and their potential use in occupational health and safety applications.

While results indicate that inexpensive wireless respirable dust sensing networks are not likely to satisfy regulatory or compliance monitoring requirements for accuracy, there is still significant value to the information that can be provided and its potential impact on mining operations. The ability to remotely monitor respirable dust levels even semi-quantitatively at a large number of strategic locations across a surface mine enables a response to detected elevations in respirable dust concentrations including actions such as the dispatch of water trucks to reduce dust on haulage roads, use of water sprays at digging and loading benches and for dumping at the crushing facility, the repair or adjustment of existing control (e.g. ventilation) systems, or the investigation of previously unidentified sources or variables of exposure. The ability to measure exposure to respirable dust in real-time allows for an immediate and proactive control response to what can often be very transient exposure scenarios, and for which traditional sampling and analysis approaches are ineffective. Knowledge gained through the use of the integrated monitoring and response system can also be used by other researchers to develop more effective dust control technologies that target true sources of high dust concentrations. Successful development and deployment of these systems as well as the use of the resulting monitoring results in the development of improved interventions and ongoing training of workers in surface mines is expected to contribute toward reduction in the occurrence of CWP within this population.

7.0 Recommendations for Future Work

Based on the findings of this study and the results presented in this report, the following recommendations for future work are presented:

1. Examine in greater detail the effect of different size mesh inlet screens on the performance characteristics of inexpensive diffusion-based (passive) optical dust sensors.

2. Consider redesigned dust sensor packaging that better protects devices from exposure to the environment, precipitation, pests, and stray light.

    a. Evaluate the use of low power micro-fans for improving air movement through the sensing zone

    b. Examine options for drying air streams and heated sensor inlets

    c. Evaluate methods for ruggedizing inexpensive optical dust sensors to achieve longer service life in the field

    d. Include temperature and humidity sensing in dust sensing node packaging

3. Evaluate new versions of inexpensive dust sensors as available including recently released smaller versions of the Plantower brand of optical / laser dust sensors.

4. Develop dust sensing nodes with GPS tracking specifically designed for installation and continuous operation in mobile equipment including haul trucks, surface drill rigs, dozers, graders, and excavators.

5. Examine the use of wireless dust sensing networks for ambient environmental monitoring, e.g., fugitive dust emissions, fence line monitoring

6. Explore the use of LoRa Gateways that have integrated/embedded versions of the Gateway Server, LoRaWAN Network Server, Join Server, Applications Server, and Console. This could eliminate the need for cloud-based subscription versions of these services.

8.0 References

Alvarado M, Gonzalez F, Fletcher A, Doshi A. Towards the Development of a Low Cost Airborne Sensing System to Monitor Dust Particles after Blasting at Open-Pit Mine Sites. Sensors 2015, 15, 19667-19687.

Blackley DJ, Halldin CN, Laney AS. Resurgence of a debilitating and entirely preventable respiratory disease among working coal miners. Am J Respir Crit Care Med. 2014 Sep 15;190(6):708-9.

Cecala AB, Reed WR, Joy GJ, Westmoreland SC, O'Brien AD. Helmet-Cam: tool for assessing miners' respirable dust exposure. Min Eng. 2013 Sep;65(9):78-84.

Cecala AB, O'Brien AD. Here Comes the Helmet-Cam. Rock Products, 2014, October 26-30.

Centers for Disease Control and Prevention. Pneumoconiosis and Advanced Occupational Lung Disease Among Surface Coal Miners — 16 States, 2010–2011. MMWR 2012; 61:23:431-434.

Colinet JF, Rider JP, Listak JM, Organiscak JA, Wolfe AL. Best Practices for Dust Control in Coal Mining. National Institute for Occupational Safety and Health, Office of Mine Safety and Health Research. Information Circular 9517, January 2010, DHHS (NIOSH) Publication No. 2010–110.

Federal Register. Lowering Miners' Exposure to Respirable Coal Mine Dust, Including Continuous Personal Dust Monitors. A Rule by the Mine Safety and Health Administration on 05/01/2014. 79 FR 24813.

Haas EJ, Cecala AB, Hoebbel CL. Using Dust Assessment Technology to Leverage Mine Site Manager-Worker Communication and Health Behavior: A Longitudinal Case Study. J Progress Res Soc Sci. 2016 Jan 6;3(1):154-167.

Halldin CN, Reed WR, Joy GJ, Colinet JF, Rider JP, Petsonk EL, Abraham JL, Wolfe AL, Storey E, Laney AS. Debilitating lung disease among surface coal miners with no underground mining tenure. J Occup Environ Med. 2015 Jan;57(1):62-7.

Jovanovic UZ, Jovanovic ID, Petrusic AZ, Petrusic ZM, Mancic DD, Low-cost wireless dust monitoring system. Telecommunication in Modern Satellite, Cable and Broadcasting Services (TELSIKS), 2013 11th International Conference, vol.02, pp.635-638, 16-19 Oct. 2013.

Kosmoski CL. Assessing the Safety Culture of Underground Coal Mining: Results and Recommendations,
2014 SME Annual Meeting, February 23 - 26, Salt Lake City, Utah, Preprint 14-029. NIOSHTIC2 Number: 20045053, Englewood, CO: Society for Mining, Metallurgy, and Exploration, Inc., 2014 Feb; 1-14.

Lashgari A, Kecojevic V., Comparative analysis of dust emission of digging and loading equipment in surface coal mining, International Journal of Mining, Reclamation and Environment, (2016), 30:3, 181-196.

Lashgari A, Kecojevic V., Assessment of environmental impact of digging and loading equipment in surface coal mining, 2013 Transactions of the Society for Mining, Metallurgy and Exploration, (2013), Vol. 334, pp. 465-471.

LoRa Alliance, https://lora-alliance.org/about-lorawan/

Marple VA, Liu BY, Rubow KL. A dust generator for laboratory use. Am. Ind. Hyg. Assoc. J. (1978), 39:26-32.

Marple VA, Rubow KL. An aerosol chamber for instrument evaluation and calibration. Am. Ind. Hyg. Assoc. J. (1983), 44:361-367.

Minerals Council of Australia, Safety Culture Survey Report, Australian Minerals Industry, July 1999.

MSHA, Questions and Answers MSHA's Final Rule to Lower Miners' Exposure to Respirable Coal Mine Dust, 2014.

Organiscak JA, Page SJ. Field assessment of control techniques and long-term dust variability for surface coal mine rock drills and bulldozers, International Journal of Surface Mining, Reclamation and Environment, 1999, 13:4, 165-172.

Organiscak JA, Reed WR. Characteristics of fugitive dust generated from unpaved mine haulage roads. International Journal of Surface Mining, Reclamation, & Environment, 2004, Vol. 18, No. 4, pp. 236–252.

Organiscak JA, Controlling Respirable Silica Dust at Surface Mines, Chapter 5 in Best Practices for Dust Control in Metal/Nonmetal Mining, By Jay F. Colinet, Andrew B. Cecala, Gregory J. Chekan, John A. Organiscak, and Anita L. Wolfe, Information Circular 9521, DHHS (NIOSH), 2010.

Organiscak JA, Silica Dust Controls for Surface Mines, https://www.cdc.gov/niosh/mining/UserFiles/workshops/silicaMNM2010/5-Organiscak-DustControSurface.pdf, 2010.

Reed WR, Organiscak JA. Evaluation of dust exposure to truck drivers following the lead haul truck. 2005 SME Annual Meeting, February 28 - March 2, Salt Lake City, Utah, preprint 05-10. Littleton, CO, Society for Mining, Metallurgy, and Exploration, Inc., 2005 Feb; 1-9.

Reed WR, Organiscak JA. Haul Road Dust Control Fugitive dust characteristics from surface mine haul roads and methods of control. Coal Age, 2007, 112, pp. 34–37.

Reed WR, Kwitowski AJ, Helfrich WJ Cecala AB, Joy GJ. Guidelines for performing a helmet-CAM respirable dust survey and conducting subsequent analysis with the Enhanced Video Analysis of Dust Exposures (EVADE) software. National Institute for Occupational Safety and Health, DHHS (NIOSH) Publication No. 2014-133, (RI 9696), 2014 Jul; 1-78, a.

Reed WR. Silica Dust Controls for Surface Mines, Presentation for Best Practices for Controlling Respirable Dust in Coal Mines, October 28, 2014, b.

9.0 Appendices

APPENDIX A -Sharp Sensor Calibration Results for A1, A2, A3 ARD and Coal Dust

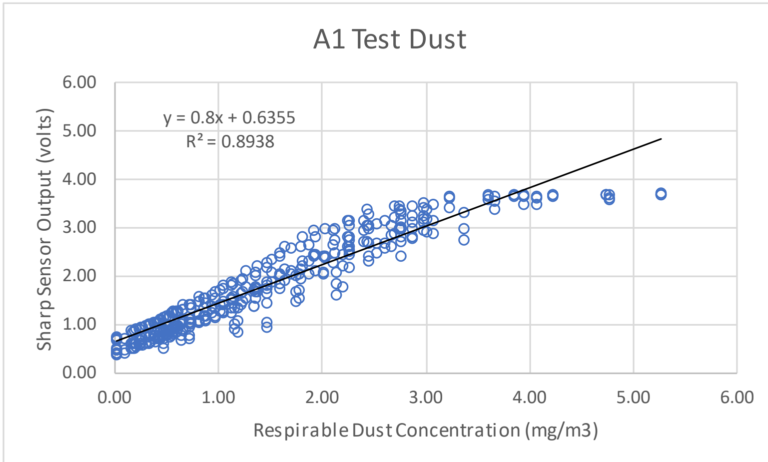

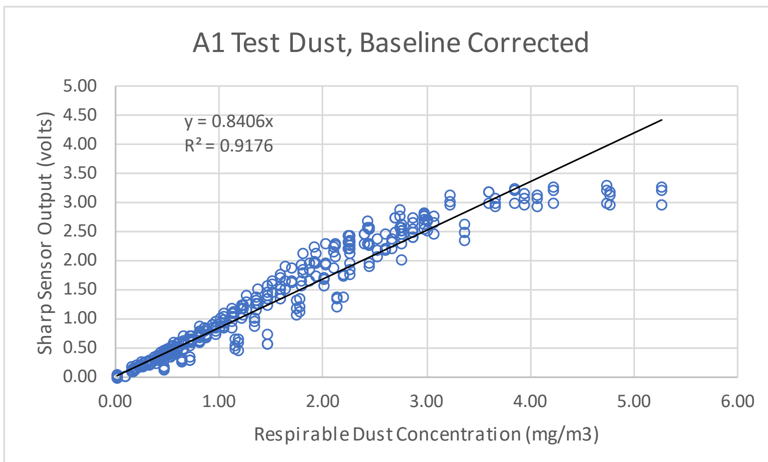

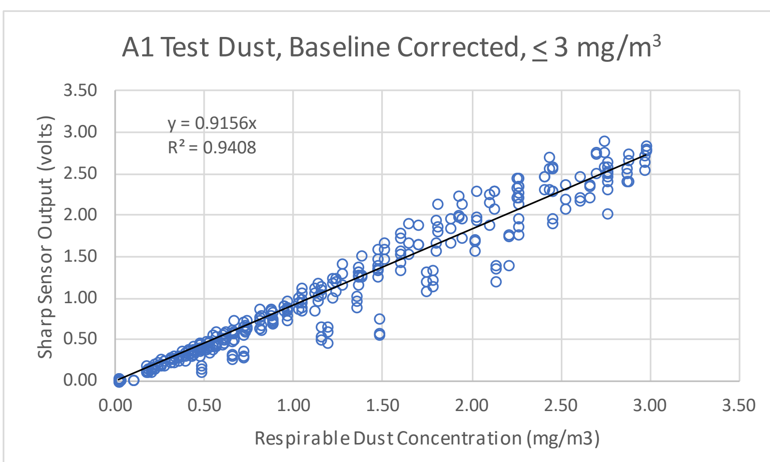

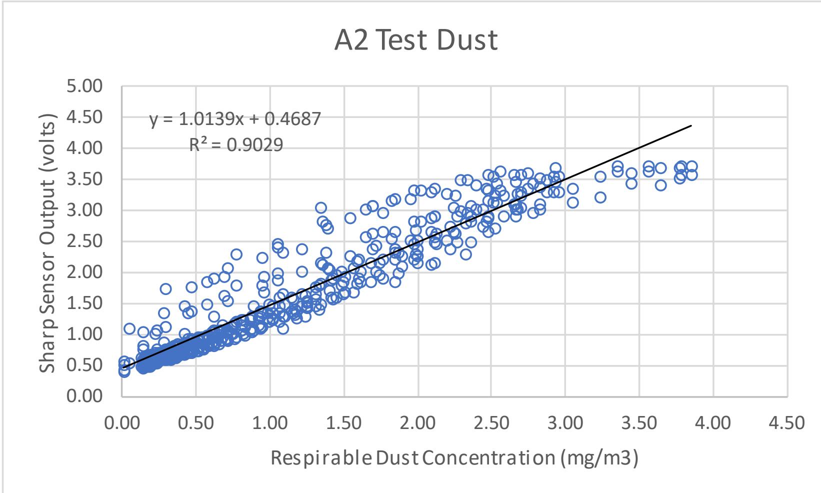
A2 Test Dust
y = 1.0139x + 0.4687
R² = 0.9029
Sharp Sensor Output (volts)
Respirable Dust Concentration (mg/m3)
5.00
4.50
4.00
3.50
3.00
2.50
2.00
1.50
1.00
0.50
0.00
0.00 0.50 1.00 1.50 2.00 2.50 3.00 3.50 4.00 4.50

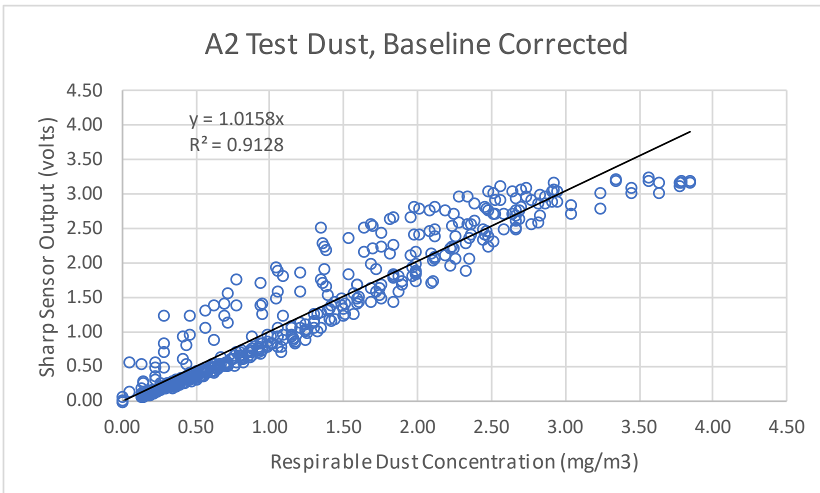
A2 Test Dust, Baseline Corrected
y = 1.0158x
R² = 0.9128
Sharp Sensor Output (volts)
Respirable Dust Concentration (mg/m3)
4.50
4.00
3.50
3.00
2.50
2.00
1.50
1.00
0.50
0.00
0.00 0.50 1.00 1.50 2.00 2.50 3.00 3.50 4.00 4.50

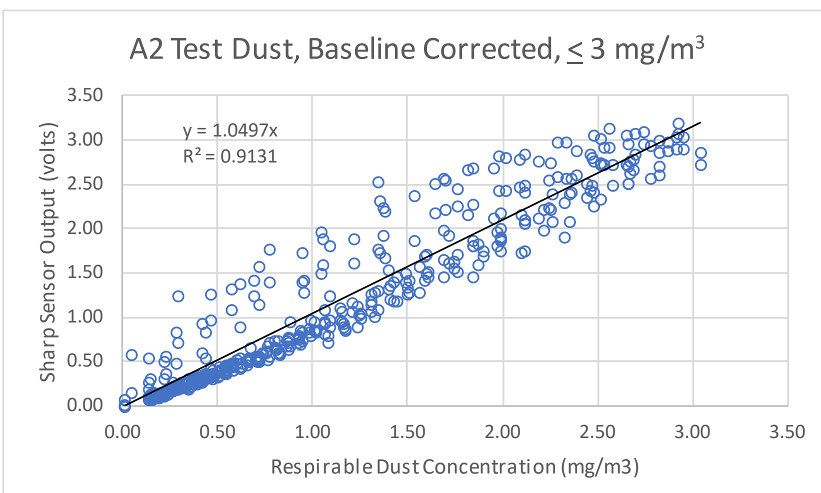
A2 Test Dust, Baseline Corrected, ≤ 3 mg/m³
y = 1.0497x
R² = 0.9131
Sharp Sensor Output (volts)
Respirable Dust Concentration (mg/m3)
3.50
3.00
2.50
2.00
1.50
1.00
0.50
0.00
0.00 0.50 1.00 1.50 2.00 2.50 3.00 3.50

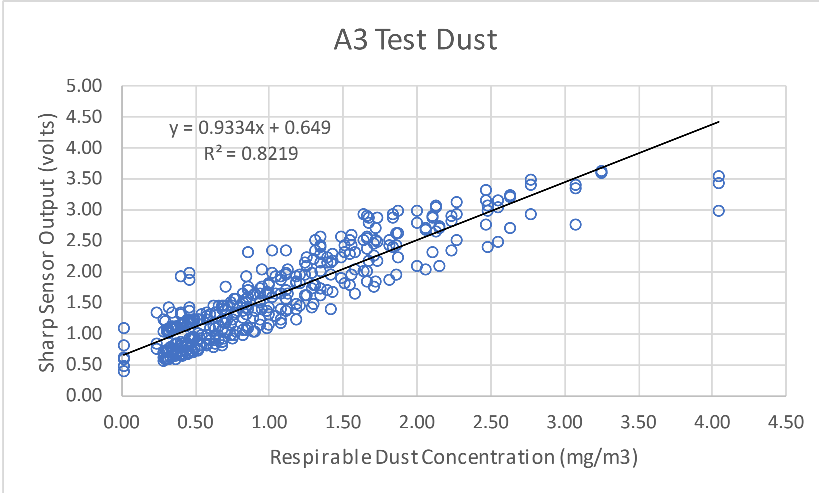
A3 Test Dust
y = 0.9334x + 0.649
R² = 0.8219
Sharp Sensor Output (volts)
Respirable Dust Concentration (mg/m3)
5.00
4.50
4.00
3.50
3.00
2.50
2.00
1.50
1.00
0.50
0.00
0.00
0.50
1.00
1.50
2.00
2.50
3.00
3.50
4.00
4.50

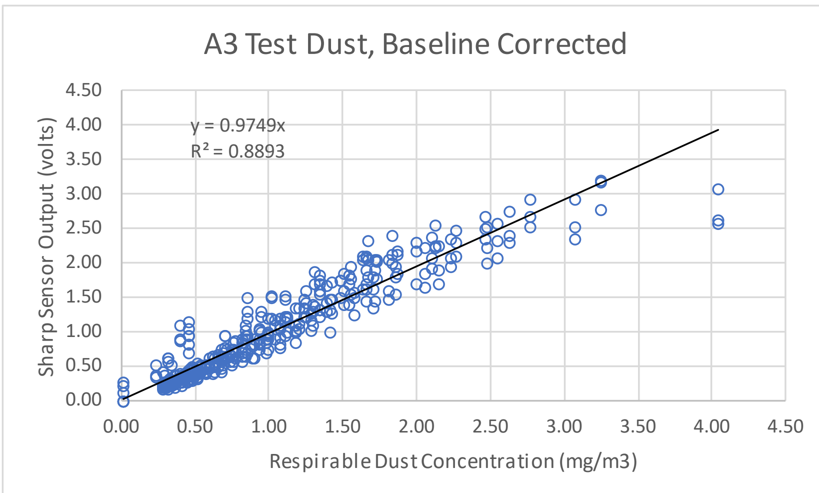
A3 Test Dust, Baseline Corrected
y = 0.9749x
R² = 0.8893
Sharp Sensor Output (volts)
Respirable Dust Concentration (mg/m3)
4.50
4.00
3.50
3.00
2.50
2.00
1.50
1.00
0.50
0.00
0.00
0.50
1.00
1.50
2.00
2.50
3.00
3.50
4.00
4.50

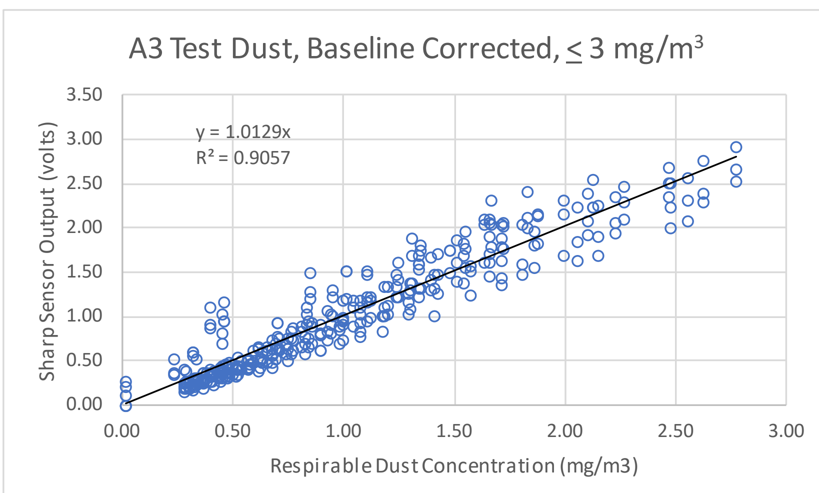
A3 Test Dust, Baseline Corrected, ≤ 3 mg/m³
y = 1.0129x
R² = 0.9057
Sharp Sensor Output (volts)
Respirable Dust Concentration (mg/m3)
3.50
3.00
2.50
2.00
1.50
1.00
0.50
0.00
0.00
0.50
1.00
1.50
2.00
2.50
3.00

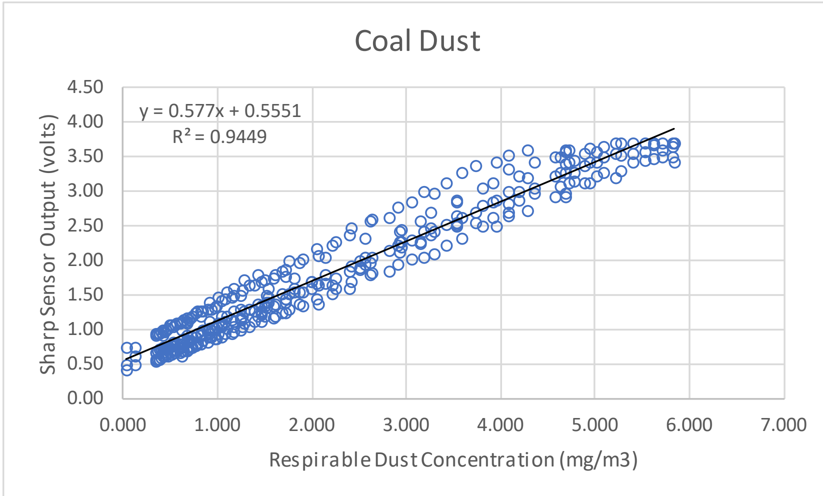
Coal Dust
y = 0.577x + 0.5551
R² = 0.9449
Sharp Sensor Output (volts)
4.50
4.00
3.50
3.00
2.50
2.00
1.50
1.00
0.50
0.00
0.000
1.000
2.000
3.000
4.000
5.000
6.000
7.000
Respirable Dust Concentration (mg/m3)

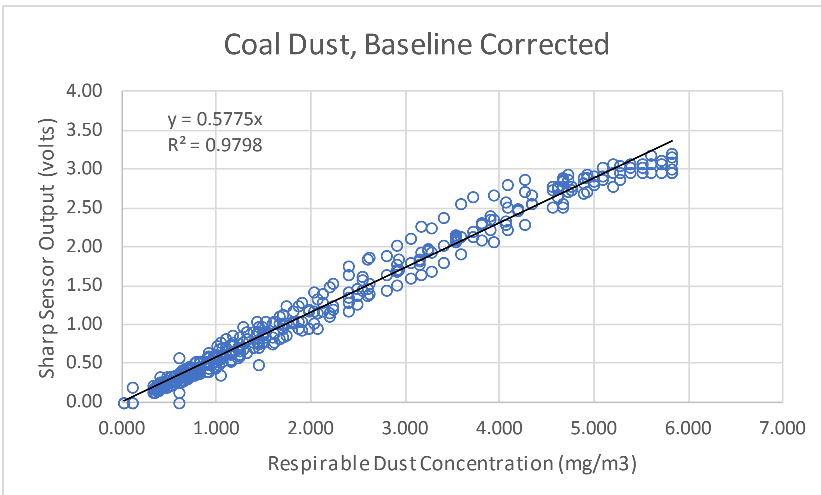
Coal Dust, Baseline Corrected
y = 0.5775x
R² = 0.9798
Sharp Sensor Output (volts)
4.00
3.50
3.00
2.50
2.00
1.50
1.00
0.50
0.00
0.000
1.000
2.000
3.000
4.000
5.000
6.000
7.000
Respirable Dust Concentration (mg/m3)

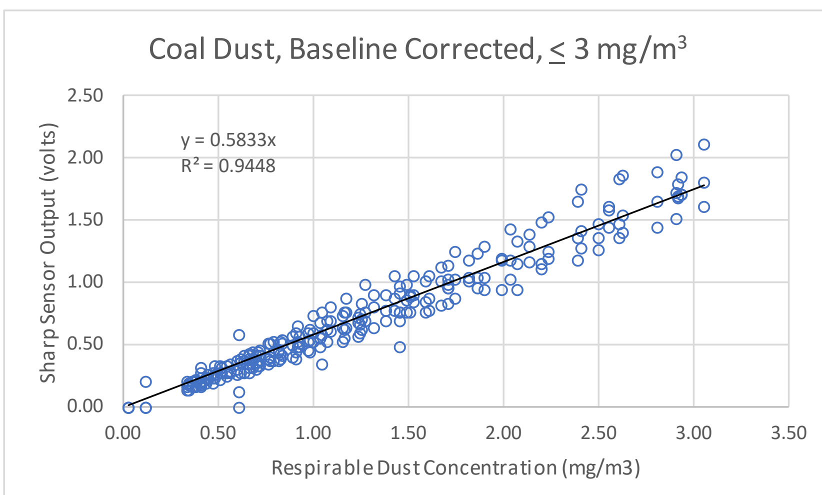
Coal Dust, Baseline Corrected, ≤ 3 mg/m³
y = 0.5833x
R² = 0.9448
Sharp Sensor Output (volts)
2.50
2.00
1.50
1.00
0.50
0.00
0.00
0.50
1.00
1.50
2.00
2.50
3.00
3.50
Respirable Dust Concentration (mg/m3)

APPENDIX B – Remote Power Design

Remote Power Design - References

- Stand-Alone PV Systems (Chapter 7), *Photovoltaic Systems Engineering*, 3rd Edition, Messenger, Roger A., Abtahi, Amir; CRC Press, 2010. ISBN-10: 1439802920
- Sizing Solar Power for Off-Grid Field Studies, Eosense Environmental Gas Monitoring, http://eosense.com/wp-content/uploads/2019/11/Sizing-Solar-Power-for-Off-grid-Field-Studies.pdf
- *Off Grid Solar: A Handbook for Photovoltaics with Lead-Acid or Lithium-Ion Batteries*, 2nd Edition, Joseph P O'Connor, Old Sequoia Publishing, 2019. ISBN-10: 0578546191

Remote Power Design

1. Determine power requirements
2. Determine battery requirements
3. Determine size and orientation of PV array
4. Select charge controller
5. Deploy and test system

Power Requirements – Sensor Nodes

Adafruit Feather m0 LoRa

- ATSAMD21G18, 3.3V logic
- Quiescent current ~ 15 mA
- Transmitting ~ 135 mA (50 ms)
- Approximately 75 mW total
- 0.075 W x 24 hr = 1.8 watt-hour (Wh)

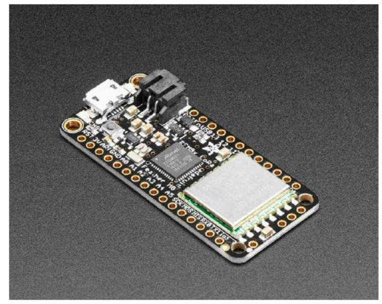

Power Requirements - Gateway

TTN Outdoor Gateway

- LoRa, GPS, and 3G/4G antennas
- 802.3af/at PoE (55VDC)
- Current drawn from 12V battery ~ 0.6A
- Approximately 7 W
- 7 W x 24 hr = 168 watt-hour (Wh)

CMA SME MINEXCHANGE 2021 SME Annual Conference & EXPO CMA 123rd NATIONAL WESTERN MINING CONFERENCE

Battery Requirements – Sensor Nodes

Adafruit Feather m0 LoRa

Ave Energy per Day: 1.8 Wh

Multiply by 3 Days of Autonomy: 3 x 1.8 Wh = 5.4 Wh

Max 80% Discharge: 5.4 Wh x 1.25 = 6.8 Wh

Temperature/inefficiency derating: 1.2 x 6.8 Wh = 8.2 Wh

Divide by 3.7V: 8.2 Wh / 3.7V = 2.2 Ah

34 grams 2.4 x 1.4 x 0.3 in.

Battery Requirements – Gateway

TTN Outdoor Gateway

Ave Energy per Day: 168 Wh

Multiply by 3 Days of Autonomy: 3 x 168 Wh = 500 Wh

Max 50% Discharge: 500 Wh x 2 = 1000 Wh = 1 kWh

Temperature/inefficiency derating: 1.4 x 1000 Wh = 1400 Wh

Divide by 12V: 1400 Wh / 12V = 120 Ah

60 pounds 13 x 9.45 x 6.77 in.

SME MINEXCHANGE 2021 SME Annual Conference & EXPO
CMA 123rd NATIONAL WESTERN MINING CONFERENCE

Photovoltaic Array Design

- Solar insolation and Peak Sun Hours (PSH) used to size solar panel(s)
- Design for worst case solar irradiance for the location (Winter PSH)
- Array tilt for fixed panels also based on winter / worst case scenario
- Winter PSH can be estimated using NREL PVWatts Calculator

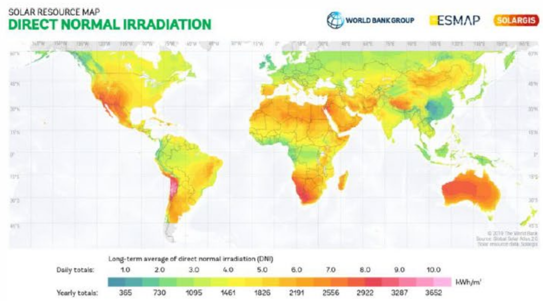

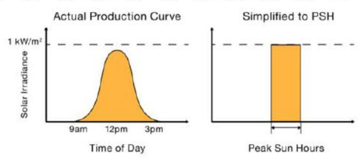

Photovoltaic Array Design

- Optimal array tilt based on worst case conditions
- Angle set to get maximum benefit at solar noon on the winter solstice

$$A = L - \left(23.45 \times \sin\left[\left(\frac{T}{365.25}\right) \times 360\right]\right)$$

where L is the latitude of the installation,

T is the number of days from spring equinox, and

A is the ideal panel angle for that day

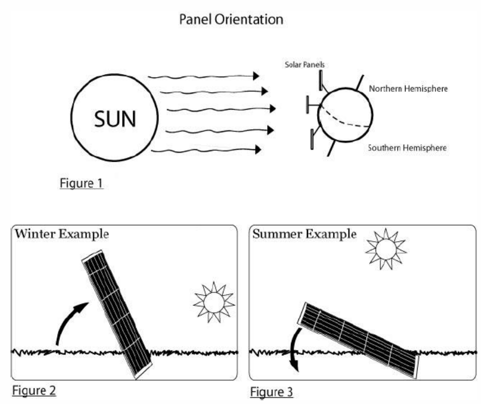

https://store.sundancesolar.com/panel-tilt-angle-1/

Photovoltaic Array Design

- Winter PSH for selected tilt angle estimated using PVWatts Calculator
- Minimum solar production estimated using Winter PSH and daily energy requirement (derated) for equipment

$$PV\ Watts\ Required = \frac{Daily\ energy\ (Wh)}{Winter\ PSH\ (h)}$$

- A DC derating factor can adjust for inefficiencies from the PV array to the battery (0.66 used)

Month	61 Degree Tilt Solar Radiation (kWh/m2/day)	38 Degree Tilt Solar Radiation (kWh/m2/day)
January	3.68	3.48
February	4.15	4.11
March	4.41	4.69
April	4.53	5.23
May	4.38	5.35
June	4.35	5.49
July	4.38	5.44
August	4.85	5.71
September	5.07	5.52
October	4.99	5.01
November	4.58	4.32
December	3.45	3.19
Annual	4.40	4.80

MINEXCHANGE 2021 SME Annual Conference & EXPO

PV Array Design– Sensor Nodes

Adafruit Feather m0 LoRa

Ave Energy per Day: 1.8 Wh

Derated Energy per Day: 1.8 Wh / 0.66 = 2.7 Wh

PV Watts Required: 2.7 Wh / 3.45 h = **0.8 Watts**

- Semi Flexible Monocrystalline Panel (5W 5V 1A)
- Efficiency 21%
- Waterproof design
- Lightweight - 87 grams
- 11.41 x 5.9 x 0.05 in

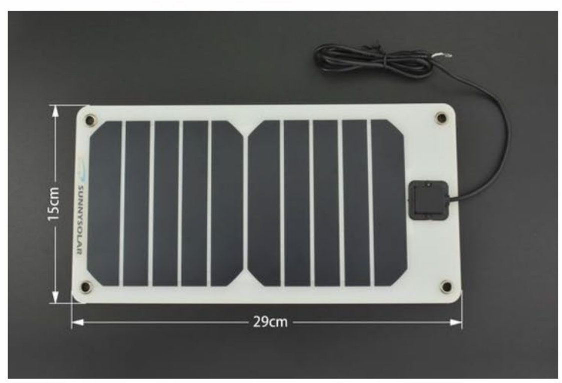

MINEXCHANGE 2021 SME Annual Conference & EXPO

PV Array Design - Gateway

TTN Outdoor Gateway

Ave Energy per Day: 168 Wh

Derated Energy per Day: 168 Wh / 0.66 = 254 Wh

PV Watts Required: 254 Wh / 3.45 h = **74 Watts**

https://www.renogy.com/100-watt-12-volt-monocrystalline-solar-panel-compact-design/

- 100W 12 V Monocrystalline
- Efficiency 21%
- Optimum Operating Voltage: 17.9V
- Optimum Operating Current: 5.72A
- 42.2 x 19.5 x 1.4 in
- 14 lbs

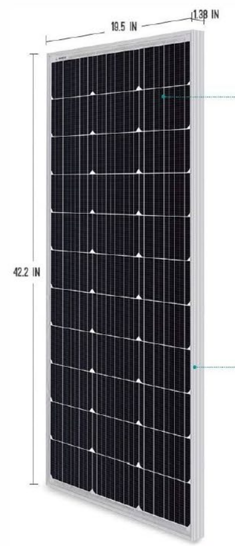

Solar Charge Controllers

Charge Controllers used to:

- Regulate voltage, prevent overcharging/discharge
- Prevent reverse voltage (from battery to solar panel)
- May provide additional fuse or circuit breaker and reverse connection/polarity protection

Two common types of charge controllers:

- Pulse Width Modulation (PWM)
- Maximum Power Point Tracking (MPPT)

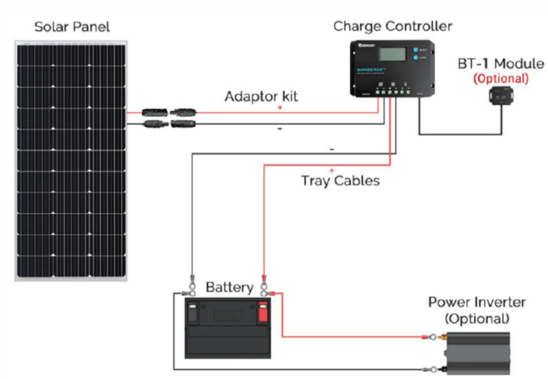

Solar Charge Controllers

LoRa Gateway - PWM

- Max PV Input: 130W / 12V
- Rated Charge Current: 10A
- Working Temperature: -25 to 45°C

Renogy Wanderer 10A PWM Charge Controller

Sensor Node - MPPT

- Max PV Input: 10W / 6V
- Rated Charge Current: 0.9 A
- Working Temperature: -40 to 85°C

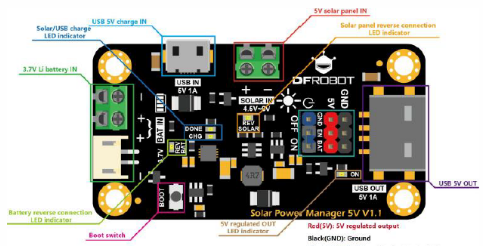

DFR0559 5V Solar Power Manager

APPENDIX C–Arduino Code for Prototype-1 Dust Sensing Node

```
//*********************************************************************

#include <TheThingsNetwork.h>
#include <CayenneLPP.h>

// Set your AppEUI and AppKey
const char *appEui = "APPEUI Goes Here";
const char *appKey = "AppKey Goes Here";

#define loraSerial Serial1
#define debugSerial Serial

// Replace REPLACE_ME with TTN_FP_EU868 or TTN_FP_US915
#define freqPlan TTN_FP_US915

TheThingsNetwork ttn(loraSerial, debugSerial, freqPlan);
CayenneLPP lpp(51);

//*********************************************************************

/*
 Standalone Sketch to use with a Arduino UNO and a
 Sharp Optical Dust Sensor GP2Y1010AU0F
*/
int measurePin = 0; //Connect dust sensor to Arduino A0 pin
int ledPower = 2;   //Connect 3 led driver pins of dust sensor to Arduino D2
int battPin = 2;   //measuring battery voltage from voltage divider at arduino A2 pin

int samplingTime = 280;
int deltaTime = 40;
```

```
int sleepTime = 9680;

float voMeasured = 0;
float sum_voMeasured = 0;
float min_ave_voMeasured = 0;
float calcVoltage = 0;
float dustDensity = 0;
float battvoMeasured=0;
float Battery=0;

void setup(){
//*******************************************
  loraSerial.begin(57600);
  debugSerial.begin(9600);

  // Wait a maximum of 10s for Serial Monitor
  while (!debugSerial && millis() < 10000)
    ;

  debugSerial.println("-- STATUS");
  ttn.showStatus();

  debugSerial.println("-- JOIN");
  ttn.join(appEui, appKey);

//*******************************************

  //Serial.begin(9600); //from Dust1
  pinMode(ledPower,OUTPUT);
}

void loop(){
```

```
sum_voMeasured = 0;
min_ave_voMeasured = 0;

for (int i = 1; i <= 60; i++) { //loop to measure voltage once per second and calculate average for 1 min

  digitalWrite(ledPower,LOW); // power on the LED
  delayMicroseconds(samplingTime);

  voMeasured = analogRead(measurePin); // read the dust value

  delayMicroseconds(deltaTime);
  digitalWrite(ledPower,HIGH); // turn the LED off
  delayMicroseconds(sleepTime);

  // 0 - 5.0V mapped to 0 - 1023 integer values
  // recover voltage
  calcVoltage = voMeasured * (5.0 / 1024.0);
  sum_voMeasured = sum_voMeasured + calcVoltage;
  min_ave_voMeasured = sum_voMeasured / i;

  // linear eqaution taken from http://www.howmuchsnow.com/arduino/airquality/
  // Chris Nafis (c) 2012
  dustDensity = 0.17 * calcVoltage - 0.1;

  Serial.print("Raw Signal Value (0-1023): ");
  Serial.print(voMeasured);

  Serial.print(" - Voltage: ");
  Serial.print(calcVoltage);

  Serial.print(" - Dust Density: ");
  Serial.println(dustDensity); // unit: mg/m3
```

```
    Serial.println(sum_voMeasured);
    Serial.println(min_ave_voMeasured);
    Serial.println(i);

    delay(1000);
  }
  debugSerial.println("-- LOOP");

  battvoMeasured = analogRead(battPin); // read the battery voltage from divider (330k / 220k)
  Serial.println(battvoMeasured);
  Battery = battvoMeasured * (5.0 / 1024.0);
  Serial.println(Battery);
  Battery = Battery * 2.506 ; // (330 + 219)/219 ==> voltage divider

  Serial.println(battvoMeasured);
  Serial.println(Battery);

  lpp.reset();
  lpp.addAnalogInput(1,min_ave_voMeasured);
  lpp.addAnalogInput(2,Battery);
  //lpp.addTemperature(1, 22.5);
  //lpp.addBarometricPressure(2, 1073.21);
  //lpp.addGPS(3, 52.37365, 4.88650, 2);

  // Send it off
  ttn.sendBytes(lpp.getBuffer(), lpp.getSize());

  //delay(10000);

}
```

APPENDIX D - Arduino Code for Prototype-1 Dust Sensing Node – 15 min TWA version

```
//**************************************************************************

#include <TheThingsNetwork.h>
#include <CayenneLPP.h>

// Set your AppEUI and AppKey
const char *appEui = "APPEUI Goes Here";
const char *appKey = "AppKey Goes Here";

#define loraSerial Serial1
#define debugSerial Serial

// Replace REPLACE_ME with TTN_FP_EU868 or TTN_FP_US915
#define freqPlan TTN_FP_US915

TheThingsNetwork ttn(loraSerial, debugSerial, freqPlan);
CayenneLPP lpp(51);

//**************************************************************************

/*
 Standalone Sketch to use with a Arduino UNO and a
 Sharp Optical Dust Sensor GP2Y1010AU0F
*/
int measurePin = 0; //Connect dust sensor to Arduino A0 pin
int ledPower = 2;   //Connect 3 led driver pins of dust sensor to Arduino D2
int battPin = 2;   //measuring battery voltage from voltage divider at arduino A2 pin

int samplingTime = 280;
int deltaTime = 40;
```

```
int sleepTime = 9680;

int minute_counter =1;

float voMeasured = 0;
float sum_voMeasured = 0;
float min_ave_voMeasured = 0;
float calcVoltage = 0;
float battvoMeasured=0;
float Battery=0;

//*********************************************************Moving Average
// Define the number of samples to keep track of. The higher the number, the
// more the readings will be smoothed, but the slower the output will respond to
// the input. Using a constant rather than a normal variable lets us use this
// value to determine the size of the readings array.
const int numReadings = 15;

float readings[numReadings];    // the readings from the analog input
int readIndex = 0;              // the index of the current reading
float total = 0;                // the running total
float fifteen_min_TWA = 0;      // the average

//******************************************


void setup()
{
  loraSerial.begin(57600);
  debugSerial.begin(9600);

  // Wait a maximum of 10s for Serial Monitor
  while (!debugSerial && millis() < 10000)
```

```
  ;

 debugSerial.println("-- STATUS");
 ttn.showStatus();

 debugSerial.println("-- JOIN");
 ttn.join(appEui, appKey);

//*********************************************

 //Serial.begin(9600); //from Dust1
 pinMode(ledPower,OUTPUT);

 // initialize all moving average readings to 0:
 for (int thisReading = 0; thisReading < numReadings; thisReading++) {
  readings[thisReading] = 0;
 }

}

void loop(){

 sum_voMeasured = 0;
 min_ave_voMeasured = 0;

 for (int i = 1; i <= 59; i++) { //loop to measure voltage once per second and calculate average for 1 min

  digitalWrite(ledPower,LOW); // power on the LED
  delayMicroseconds(samplingTime);

  voMeasured = analogRead(measurePin); // read the dust value

  delayMicroseconds(deltaTime);
```

```
  digitalWrite(ledPower,HIGH); // turn the LED off
  delayMicroseconds(sleepTime);

  // 0 - 5.0V mapped to 0 - 1023 integer values
  // recover voltage
  calcVoltage = voMeasured * (5.0 / 1024.0);
  sum_voMeasured = sum_voMeasured + calcVoltage;
  min_ave_voMeasured = sum_voMeasured / i;

  Serial.println();
  Serial.print("Raw Signal Value (0-1023): ");
  Serial.println(voMeasured);

  Serial.print("Voltage: ");
  Serial.println(calcVoltage);

  Serial.print("Sum vo: ");
  Serial.println(sum_voMeasured);

  Serial.print("Min Ave: ");
  Serial.println(min_ave_voMeasured);

  Serial.print("Counter: ");
  Serial.println(i);

  delay(985);
}

//*****************************************Begin Moving Average Section

// subtract the last reading:
total = total - readings[readIndex];
// read from the sensor:
```

```
readings[readIndex] = min_ave_voMeasured;
// add the reading to the total:
total = total + readings[readIndex];
// advance to the next position in the array:
readIndex = readIndex + 1;

// calculate the average:
if(minute_counter<15){
  fifteen_min_TWA = total / (readIndex);
}
else{
  fifteen_min_TWA = total / numReadings;
}

// send it to the computer as ASCII digits

Serial.println();
Serial.println("----- 15-Min TWA -----");
Serial.print("15-Min Ave: ");
Serial.println(fifteen_min_TWA);

Serial.print("Minute Sum: ");
Serial.println(total);

Serial.print("Min Counter: ");
Serial.println(minute_counter);

Serial.print("Read Index: ");
Serial.println(readIndex);
Serial.println("----- END 15-Min TWA -----");
Serial.println();

// if we're at the end of the array...
```

```
  if (readIndex >= numReadings) {
    // ...wrap around to the beginning:
    readIndex = 0;
  }

//****************************************End Moving Average Section

  debugSerial.println("-- LOOP");

  battvoMeasured = analogRead(battPin); // read the battery voltage from divider (330k / 220k)
  Serial.print("Raw Battery Signal: ");
  Serial.println(battvoMeasured);

  Battery = battvoMeasured * (5.0 / 1024.0);
  Battery = Battery * 2.506 ; // (330 + 219)/219 ==> voltage divider

  Serial.print("Battery Voltage: ");
  Serial.println(Battery);
  Serial.println();

  lpp.reset();
  lpp.addAnalogInput(1,min_ave_voMeasured);
  lpp.addAnalogInput(2,fifteen_min_TWA);
  lpp.addAnalogInput(3,Battery);

  // Send it off
  ttn.sendBytes(lpp.getBuffer(), lpp.getSize());

  minute_counter = minute_counter+1;

  //delay(10000);

}
```

APPENDIX E - Arduino Code for Prototype-2 Dust Sensing Node – 15 min TWA version

```
// Hello LoRa - ABP TTN Packet Sender (Multi-Channel)
// Tutorial Link: https://learn.adafruit.com/the-things-network-for-feather/using-a-feather-32u4
//
// Adafruit invests time and resources providing this open source code.
// Please support Adafruit and open source hardware by purchasing
// products from Adafruit!
//
// Copyright 2015, 2016 Ideetron B.V.
//
// Modified by Brent Rubell for Adafruit Industries, 2018
/************************** Configuration ***********************************/
#include <TinyLoRa.h>
#include <SPI.h>
#include <CayenneLPP.h>

// Network Session Key (MSB) from TTN
uint8_t NwkSkey[16] = { 0x00, 0x00, 0x00, 0x00, 0x00, 0x00, 0x00, 0x00, 0x00, 0x00, 0x00, 0x00, 0x00, 0x00, 0x00, 0x00 };

// Application Session Key (MSB) from TTN
uint8_t AppSkey[16] = { 0x00, 0x00, 0x00, 0x00, 0x00, 0x00, 0x00, 0x00, 0x00, 0x00, 0x00, 0x00, 0x00, 0x00, 0x00, 0x00 };

// Device Address (MSB) from TTN
uint8_t DevAddr[4] = { 0x00, 0x00, 0x00, 0x00 };

/************************** Example Begins Here ***********************************/
// Data Packet to Send to TTN
unsigned char loraData[11] = {"hello LoRa"};

// How often data transfer should occur, in seconds
```

```
const unsigned int sendInterval = 30;

// Pinout for Adafruit Feather M0 LoRa
TinyLoRa lora = TinyLoRa(3,8,4);

CayenneLPP lpp(51);

//**********************************************************************
/*
 Standalone Sketch to use with a Adafruit Feather M0 LoRa and a
 Sharp Optical Dust Sensor GP2Y1010AU0F
*/
int measurePin = 0; //Connect dust sensor to Feather M0 A0 pin
int ledPower = 5;   //Connect 3 led driver pins of dust sensor to Feather M0 LoRa D5
int battPin = 7;   //measuring battery voltage from onboard voltage divider at Feather M0 LoRa A7 pin (aka D9)

int samplingTime = 280;
int deltaTime = 40;
int sleepTime = 9680;

int minute_counter =1;

float voMeasured = 0;
float sum_voMeasured = 0;
float min_ave_voMeasured = 0;
float calcVoltage = 0;
float battvoMeasured=0;
float Battery=0;

//*******************************************************Moving Average
// Define the number of samples to keep track of. The higher the number, the
// more the readings will be smoothed, but the slower the output will respond to
// the input. Using a constant rather than a normal variable lets us use this
```

```
// value to determine the size of the readings array.
const int numReadings = 15;

float readings[numReadings];    // the readings from the analog input
int readIndex = 0;              // the index of the current reading
float total = 0;                // the running total
float fifteen_min_TWA = 0;              // the average

//******************************************

void setup()
{
  delay(2000);
  Serial.begin(9600);
 // while (! Serial);

  // Initialize pin LED_BUILTIN as an output
  pinMode(LED_BUILTIN, OUTPUT);
  digitalWrite(LED_BUILTIN, LOW);

  // Initialize LoRa
  Serial.print("Starting LoRa...");
  // define multi-channel sending
  lora.setChannel(MULTI);
  // set datarate
  lora.setDatarate(SF9BW125);
  if (!lora.begin())
  {
    Serial.println("Failed");
    Serial.println("Check your radio");  // if this happens need to look at version check line in library cpp file
    while (true);
  }
  Serial.println("OK");
```

```
  pinMode(ledPower,OUTPUT);


  // initialize all moving average readings to 0:
  for (int thisReading = 0; thisReading < numReadings; thisReading++) {
    readings[thisReading] = 0;
  }

}

//*********************************************

void loop()
{
  sum_voMeasured = 0;
  min_ave_voMeasured = 0;

  for (int i = 1; i <= 59; i++) { //loop to measure voltage once per second and calculate average for 1 min

    digitalWrite(ledPower,LOW); // power on the dust sensor LED
    delayMicroseconds(samplingTime); //delaying 280 microseconds = 0.28 milliseconds

    voMeasured = analogRead(measurePin); // read the dust value

    delayMicroseconds(deltaTime); //delaying for 40 microseconds - this achieves 320 us pulse width specified in application note
(280+40=320)
    digitalWrite(ledPower,HIGH); // turn the dust sensor LED off
    delayMicroseconds(sleepTime); //delay for 9680 microseconds

    // 0 - 3.3V mapped to 0 - 1023 integer values, ave 10 count offset subtracted from read below
    // recover voltage
    calcVoltage = voMeasured * (3.3 / 1024.0);
```

```
    sum_voMeasured = sum_voMeasured + calcVoltage;
    min_ave_voMeasured = sum_voMeasured / i;

    Serial.println();
    Serial.print("Raw Signal Value (0-1023): ");
    Serial.println(voMeasured);

    Serial.print("Voltage: ");
    Serial.println(calcVoltage);

    Serial.print("Sum vo: ");
    Serial.println(sum_voMeasured);

    Serial.print("Min Ave: ");
    Serial.println(min_ave_voMeasured);

    Serial.print("Counter: ");
    Serial.println(i);

    delay(985); //delay in milliseconds: 1000 ms = 1 s
    //delayMicroseconds(400);
  }

//*****************************************Begin Moving Average Section

  // subtract the last reading:
  total = total - readings[readIndex];
  // read from the sensor:
  readings[readIndex] = min_ave_voMeasured;
  // add the reading to the total:
  total = total + readings[readIndex];
  // advance to the next position in the array:
  readIndex = readIndex + 1;
```

```
// calculate the average:
if(minute_counter<15){
  fifteen_min_TWA = total / (readIndex);
}
else{
  fifteen_min_TWA = total / numReadings;
}

// send it to the computer as ASCII digits

Serial.println();
Serial.println("----- 15-Min TWA -----");
Serial.print("15-Min Ave: ");
Serial.println(fifteen_min_TWA);

Serial.print("Minute Sum: ");
Serial.println(total);

Serial.print("Min Counter: ");
Serial.println(minute_counter);

Serial.print("Read Index: ");
Serial.println(readIndex);
 Serial.println("----- END 15-Min TWA -----");
Serial.println();

// if we're at the end of the array...
if (readIndex >= numReadings) {
  // ...wrap around to the beginning:
  readIndex = 0;
}
```

```
//*****************************************End Moving Average Section

  battvoMeasured = analogRead(battPin); // read the battery voltage from divider (100k / 100k)
  Serial.print("Raw Battery Signal: ");
  Serial.println(battvoMeasured);

  Battery = battvoMeasured * (3.3 / 1024.0);
  Battery = Battery * 2; // Feather M0 uses 100k 100k divider connected at A7

  Serial.print("Battery Voltage: ");
  Serial.println(Battery);
  Serial.println();

  lpp.reset();
  lpp.addAnalogInput(1,min_ave_voMeasured);
  lpp.addAnalogInput(2,fifteen_min_TWA);
  lpp.addAnalogInput(3,Battery);

  Serial.println("Sending LoRa Data...");
  lora.sendData(lpp.getBuffer(), lpp.getSize(), lora.frameCounter);
  Serial.print("Frame Counter: "); Serial.println(lora.frameCounter);
  lora.frameCounter++;

  // blink LED to indicate packet sent
  digitalWrite(LED_BUILTIN, HIGH);
  delay(1000);
  digitalWrite(LED_BUILTIN, LOW);

  minute_counter = minute_counter+1;

}
```

APPENDIX F – Google App Script for TTN Webhook to Store Data in Google Sheets

```
var SHEET_NAME = "Sheet1";

function doGet(e){
  return HtmlService.createHtmlOutput("Google Sheets Webhook v0.1");
}

function doPost(e){

  var theJSON = JSON.parse(e.postData.contents);

  var theSheet = SpreadsheetApp.getActiveSpreadsheet().getSheetByName(SHEET_NAME);

  var data = [];

  data.push(theJSON.end_device_ids.device_id);

  var theDate = Utilities.formatDate(new Date(), 'GMT-5', 'MM/dd/yyyy HH:mm:ss');
  data.push(theDate);

  data.push(theJSON.received_at);

  data.push(theJSON.uplink_message.f_cnt);
  data.push(theJSON.uplink_message.frm_payload);

  var decoded = Utilities.base64Decode(theJSON.uplink_message.frm_payload);
  var bytesToHex = decoded.reduce(function(str, chr) {
    chr = (chr < 0 ? chr + 256 : chr).toString(16);
    return str + (chr.length==1?'0':'') + chr;
  },'');
  data.push(bytesToHex);
```

```
  data.push(theJSON.uplink_message.decoded_payload.analog_in_1);
  data.push(theJSON.uplink_message.decoded_payload.analog_in_2);
  data.push(theJSON.uplink_message.decoded_payload.analog_in_3);

  data.push(theJSON.uplink_message.rx_metadata[0].rssi);
  data.push(theJSON.uplink_message.rx_metadata[0].snr);


  theSheet.appendRow(data);

}
```